



The
University
Of
Sheffield.

**SEISMIC VULNERABILITY ASSESSMENT OF
SUBSTANDARD REINFORCED CONCRETE BUILDINGS.
CASE STUDY: MARMARA REGION**

By

Soheil Khoshkholghi

(BSc, MSc)

A thesis submitted for the degree of Doctor of Philosophy in the Faculty of
Engineering of the University of Sheffield.

Department of Civil & Structural Engineering

The University of Sheffield

August 2021

I would like to dedicate this thesis to my loving family.

DECLARATION

I, the author, confirm that the Thesis is my own work. I am aware of the University's Guidance on the Use of Unfair Means (www.sheffield.ac.uk/ssid/unfair-means). This work has not been previously been presented for an award at this, or any other, university.

Soheil Khoshkholghi

03/08/2021

ACKNOWLEDGEMENTS

Firstly, I would like to express my gratitude and appreciation to my supervisor Prof. Kypros Pilakoutas for his continuous support, encouragement and guidance during my PhD research. I learned a lot by working with him which helped me grow personally and professionally.

Secondly, this research would not have been possible without the help and support of my co-supervisors Dr. Zuhail Ozdemir and Dr. Iman Hajirasouliha. Their vast knowledge and priceless advice helped me to successfully overcome any difficulties during this project. I would like to also say, I am extremely grateful to my second supervisor Dr. Zuhail Ozdemir for her invaluable advice, continuous support, and patience during my PhD study.

I would like to thank Dr. Reyes Garcia, who has provided me with a lot of support and motivation in the early stages of my research.

I am also grateful for the help and support of Dr. Matteo Di Benedetti. It was a great experience working in your lab under your supervision.

I appreciate the financial assistance provided by the RCUK-TUBITAK Research Partnerships Newton Fund Awards and the British Council Newton Fund.

Special thanks to my friend Dr. Panos Papastergiou for his support and help especially during the tough Pandemic period and at the final stage of my PhD research.

Most of all I am thankful to my family, without their unconditional love, support and encouragement, I would not have had the opportunity to undertake doctoral research.

ABSTRACT

Rapid urbanisation and population growth in developing countries have increased seismic risk regardless of the advances in our knowledge on the seismic behaviour of structures. The need to cover the demand for a low-cost building stock has led a large proportion of residential buildings to be constructed with substandard materials, insufficient designs and poor construction practices. These are the reasons that developing countries have exhibited considerably higher death rates compared to the developed world. Extensive losses and mortality rates observed during recent major earthquakes in developing countries highlight the high seismic vulnerability of existing substandard RC buildings.

This research aims to develop a vulnerability framework (for substandard RC buildings) which can produce advanced adaptive vulnerability curves. For this, an analytical modelling procedure was proposed and validated against field and large-scale tests data.

OpenSees is employed for modelling full-scale substandard RC columns and shake-table RC frames and the analytical model is verified against the experimental results, at both local and global level. An advanced probabilistic seismic vulnerability framework is developed using Matlab code linked with OpenSees.

General vulnerability curves are derived (using an improved CSM) for substandard RC columns as well as an existing 4-storey substandard RC building (case study for Marmara region). The general fragility curves are then disaggregated to derive adaptive fragility curves based on various considered parameters e.g. steel grade, concrete strength, transverse rebar spacing, axial load level. Upgraded fragility curves are obtained by considering external retrofitting with FRP sheets on the case study building. Finally, vulnerability curves are derived for the RC columns and the case study building, using an existing conversion matrix for the case study region.

The developed framework showed that the use of advanced adaptive vulnerability curves can improve the accuracy by up to 20% compared to general vulnerability curves. The study on the upgraded vulnerability analysis using 3 layers of CFRP (for the case study building), revealed that seismic vulnerability can be reduced up to 85% and 45% for slight and collapse damage limit states, respectively.

TABLE OF CONTENTS

Declaration.....	i
Acknowledgements.....	i
Abstract.....	ii
Table of Contents.....	iv
List of Figures.....	ix
List of Tables.....	xiii
Abbreviations.....	xv
Notations.....	xviii
Chapter 1 Introduction.....	1
1.1 Background.....	1
1.1.1 Case study: Marmara region.....	3
1.1.2 Vulnerability assessment.....	4
1.2 Research Aim and Objectives.....	6
1.3 Thesis Layout.....	7
Chapter 2 Literature review.....	9
2.1 Seismic Vulnerability Assessment Methodologies.....	9
2.1.1 Introduction.....	9
2.1.2 Empirical vulnerability assessment: Overview.....	12
2.1.3 Expert judgment fragility approaches: Overview.....	16
2.1.4 Analytical vulnerability approaches: Overview.....	17
2.1.5 Analytical approaches: Analyses methods.....	21
2.1.6 Hybrid Fragility Approaches: Overview.....	23
2.2 Common Deficiencies of Substandard RC Buildings.....	24
2.3 Retrofitting of RC Structures Using FRP and PTMS.....	29
2.3.1 Introduction.....	29
2.3.2 Background.....	29

2.3.3	External jacketing using FRP	30
2.3.4	External jacketing using PTMS.....	31
2.3.5	Analytical modelling approach	32
2.4	Discussion on plasticity element types in OpenSees	35
Chapter 3	Description of tests.....	38
3.1	Introduction	38
3.2	Full-Scale Cantilever RC Column Experiments	38
3.2.1	Specimens and material properties.....	39
3.2.2	Test setup and instrumentation.....	40
3.3	Full-Scale Shaking Table Experiments	41
3.3.1	Specimens and material properties.....	41
3.3.2	Test setup and instrumentation.....	44
3.4	Existing Substandard RC Building: Case Study	45
Chapter 4	Methodology	48
4.1	Introduction	48
4.2	Analytical FE modelling and validation	49
4.2.1	Introduction	49
4.2.2	Finite element modelling of substandard RC columns	50
4.2.3	Finite element modelling of substandard RC frames	59
4.2.4	Finite element modelling of the substandard 4-storey RC building (case study) 62	
4.3	Development of advanced probabilistic seismic vulnerability framework.....	63
4.3.1	Introduction	63
4.3.2	Analytical Vulnerability Assessment	64
4.3.3	Deriving vulnerability curve using OpenSees and Matlab.....	69
4.3.4	Conducting analytical vulnerability assessment using CSM method	70
4.3.5	Probabilistic vulnerability analysis	75
4.3.6	Derivation of advanced adaptive fragility/vulnerability curves	78
4.3.7	Derivation of upgraded vulnerability curves.....	79
4.4	Advanced probabilistic seismic vulnerability analysis for the case study RC building.....	81
Chapter 5	results and discussion	82
5.1	Substandard RC columns	82
5.1.1	Mesh-sensitivity analysis.....	82
5.1.2	Reversed cyclic pushover analysis (RCPA).....	83

5.1.3	TH analysis versus RCPA.....	84
5.1.4	Element-based fragility analysis.....	86
5.2	Shaking table tests.....	96
5.2.1	ECOLEADER frame.....	96
5.2.2	BANDIT shaking table test.....	99
5.3	Case study: 4-storey substandard RC building.....	99
5.3.1	Probabilistic seismic vulnerability analysis.....	100
5.3.2	Comparison of fragility results with literature.....	107
5.4	Proposed Vulnerability assessment framework.....	116
Chapter 6	Conclusions and future work.....	118
6.1	Introduction.....	118
6.2	Conclusions and observations.....	118
6.2.1	Analytical FE modelling practices using OpenSees.....	118
6.2.2	Comparing local and global damage indices.....	119
6.2.3	Performing adaptive probabilistic seismic fragility analysis on substandard RC column/building:.....	119
6.2.4	Upgraded fragility curves for substandard RC column/building:.....	120
6.2.5	Vulnerability analysis of substandard RC building:.....	120
6.2.6	Comparison of derived general fragility curves (4-storey substandard RC building) with fragility curves available in the literature:.....	121
6.3	Recommendations for Future Work.....	123
Appendix A	Literature review on seismic vulnerability assessment of RC buildings. 125	
A.1	Rapid Seismic Vulnerability Assessments:.....	125
A.2	Empirical Methods.....	126
A.2.1	Existing empirical vulnerability assessment studies.....	128
A.3	Existing judgmental vulnerability assessment studies.....	133
A.4	Analytical/Mechanical Methods.....	134
A.4.1	Displacement based vulnerability assessment studies.....	135
A.4.2	Vulnerability assessment studies with detailed modelling consideration 140	
A.5	Hybrid methods.....	152
Appendix B	test results.....	154
B.1	RC columns.....	154
B.2	ECOLEADER frame.....	155

B.3 BANDIT frame.....	159
References	162

LIST OF FIGURES

Figure 1-1: Common deficiencies of substandard RC buildings. A) improper hooking and use of plain bars, B) pull-out failure and C & D) low concrete quality.	2
Figure 2-1: General procedure for analytical vulnerability assessment (adapted from (Dumova-Jovanoska, 2004)).	18
Figure 2-2: Defining the performance point.....	19
Figure 2-3: Comparison of concrete behaviour based on concrete compressive strength (adopted from Mander et al. (1988)).	25
Figure 2-4: Effect of stirrup spacing on concrete core confinement behaviour.	26
Figure 2-5: Effect of stirrup spacing according to Dhakal and Maekawa (2002).	26
Figure 2-6: Observational cyclic behaviour for column with S=180 mm.	28
Figure 2-7: Observational cyclic behaviour for the column with S=60 mm.	28
Figure 2-8: Application of external jacketing using FRP (Mosallam et al., 2014).	31
Figure 2-9: External jacketing with PTMS (Imjai et al., 2018, Garcia et al., 2017).	32
Figure 2-10: Schematic presentation of stress-strain behaviour of actively confined concrete specimens using PTMS (Moghaddam et al., 2010a).	34
Figure 3-1: Column reinforcement details.	39
Figure 3-2: Mechanical characteristics of reinforcing rebars a) 8mm and b) 14mm diameter.....	40
Figure 3-3: (a) Testing setup and LVDTs configuration and (b) strain-gauge location.	41
Figure 3-4: Loading protocol.	41
Figure 3-5: (a) General view and (b) frame geometry and sectional details. (Garcia et al., 2010).....	42
Figure 3-6: General view of BANDIT bare frame (Garcia et al., 2014)	43
Figure 3-7: a) plan b) elevation and c) detailing of the beam and column sections for the 1 st and 2 nd storeys of Bandit frame (Garcia et al., 2014).....	44
Figure 3-8: General view of the building.	45
Figure 3-9: Storey plan.	46
Figure 3-10: Cover removal and checking the columns' detailing.	47

Figure 3-11: Concrete core samples taken from the building.....	47
Figure 4-1: (a) Fibre section approach (b) column's assembly and integration points configuration.....	51
Figure 4-2: Buckling model for plain steel (Dhakal and Maekawa, 2002)	54
Figure 4-3: FEA to take into account the effect of cover on the inelastic buckling of longitudinal rebars.	55
Figure 4-4: The concrete model considered in zero-length section element (Kashani et al., 2016).	58
Figure 4-5: Placement of zero length section element to consider the bond-slip behaviour of longitudinal bars.....	60
Figure 4-6: Loading protocol (ATC-24, 1992).....	64
Figure 4-7: (a) capacity curve (b) capacity spectrum.	65
Figure 4-8: (a) response spectrum (b) demand spectrum.	66
Figure 4-9: CSM (FEMA 440, 2005), procedure B.....	67
Figure 4-10: Site-specific design spectrum for the 4-storey substandard RC building.	77
Figure 4-11: Curve fitting procedure to derive fragility functions.....	78
Figure 5-1: (a) moment-curvature behaviour of the section from section analysis. (b) moment-curvature behaviour of the section recorded after pushover analysis.....	83
Figure 5-2: Comparison of cyclic behaviour for specimen S60	84
Figure 5-3: Maximum curvature profile for S60 specimen (at drift 6%).....	84
Figure 5-4: Selected artificial EQ records versus design spectrum.....	85
Figure 5-5: Element-based derived vulnerability curves for S60 a) based on HRC and T b) rotation-based damage indices.	87
Figure 5-6: Element based derived vulnerability curves for S120.	89
Figure 5-7: General fragility curves for an RC column under 50% axial load.....	92
Figure 5-8: Adaptive fragility curves for axial load level with S220 rebar type.....	92
Figure 5-9: Adaptive fragility curves for steel grade with 20% axial load level.....	93
Figure 5-10: Adapted fragility curves for various stirrup spacing with S220 rebar type and 20% axial load.	93
Figure 5-11: Adaptive fragility curves for concrete strength on a) moderate, b) extensive and c) collapse limit states on the fragility curves for an RC column.	94
Figure 5-12: Upgraded fragility curves for collapse damage state.	94
Figure 5-13: Comparison of section analyses using Xtract and OpenSees.....	96
Figure 5-14: Pushover analysis in OpenSees (Ecoleader bare frame).....	97
Figure 5-15: Input shaking table displacement (mm) histories.	97

Figure 5-16: The strain-gage location used for comparison with analytical results.	98
Figure 5-17: (a) 1 st -floor displacement (mm) histories and (b) strain readings.	98
Figure 5-18: (a) 1 st -floor displacement (mm) histories and (b) strain readings after introducing the bond-slip effect into the model.	99
Figure 5-19: General fragility curve for the 4-storey substandard RC building.....	101
Figure 5-20: Adaptive fragility curves for the 4-storey substandard building based on longitudinal rebar type.	101
Figure 5-21: Adaptive fragility curves for the 4-storey substandard RC building based on concrete strength.	102
Figure 5-22: Comparison of the general fragility curves for the 4-storey substandard RC building with and without retrofitting with S220 steel grade.	104
Figure 5-23: Dynamic upgraded fragility curves for the 4-storey substandard RC building with S220 steel type based on concrete strength.	105
Figure 5-24: Comparison of the adaptive vulnerability curves based on steel type. ...	105
Figure 5-25: Adaptive vulnerability curves based on concrete strength.....	106
Figure 5-26: Comparison of fragility curves for $f_y=220$ MPa and $f_y=320$ MPa.	107
Figure 5-27: Comparison between the derived general fragility curves (PhD) and the fragility curves by Ahmad et al. (2010) for midrise a) ductile b)non-ductile RC buildings.	109
Figure 5-28: The comparison between general fragility curves (PhD) and fragility curves given by Akkar et al., (2005) for a 4-storey RC building.	110
Figure 5-29: Comparison between general fragility curves (PhD) and Erberik's fragility curves for an RC mid-rise bare frame.	111
Figure 5-30: Comparison between general fragility curves (PhD) and fragility curves given by Kirçil and Polat (2006) for a) 3-storey b) 5-storey substandard RC building.	113
Figure 5-31: Comparison between the general fragility curves (PhD) and the fragility curves given by Ozmen et al. (2010) for a 4-storey RC building.	114
Figure 5-32: Comparison between the general fragility curves and fragility curves by (Tsonis et al., 2011) for a) ductile mid-rise low code b) non-ductile mid-rise low code.	115
Figure 5-33: Flowchart of the developed framework.	117
Figure 6-1: Comparison of analytical versus experimental results for RCPC of columns with a) S=60 mm, b) S=90 mm, c) S=120 mm and d) S=180 mm.....	154
Figure 6-2: Comparison between experimental and analytical results of THA with PGA=0.05 g for a)1 st floor and b) 2 nd floor.	155
Figure 6-3: Comparison between experimental and analytical results of THA with PGA=0.1 g for a)1 st floor and b) 2 nd floor.	156

Figure 6-4: Comparison between experimental and analytical results of THA with PGA=0.2 g for a)1 st floor and b) 2 nd floor.	156
Figure 6-5: Comparison between experimental and analytical results of THA with PGA=0.3 g for a)1 st floor and b) 2 nd floor.	157
Figure 6-6: Comparison between experimental and analytical results of THA with PGA=0.4 g for a)1 st floor and b) 2 nd floor.	158
Figure 6-7: Comparison between experimental and analytical results of THA with PGA=0.05 g for a)1 st floor and b) 2 nd floor.	159
Figure 6-8: Comparison between experimental and analytical results of THA with PGA=0.1 g for a)1 st floor and b) 2 nd floor.	160
Figure 6-9: Comparison between experimental and analytical results of THA with PGA=0.15 g for a)1 st floor and b) 2 nd floor.....	161

LIST OF TABLES

Table 4-1: Parameters used for defining concrete.....	52
Table 4-2: Parameters for modelling steel rebars outside the plastic hinge zones.	53
Table 4-3: Hysteretic material parameters for compression to consider buckling.	56
Table 4-4: Hysteretic material parameters for modelling rebar's slip.....	57
Table 4-5: Steel02 parameters.	60
Table 4-6: Hysteretic material parameters for modelling rebar's slip.....	61
Table 4-7: Weight calculation assumptions.....	63
Table 4-8: Threshold values for HRC damage limit states (Rossetto and Elnashai, 2003).	73
Table 4-9: Comparison of damage ratios.	75
Table 4-10: Statistical description of random variables.	75
Table 4-11: Variable parameters considered in probabilistic fragility analyses of a 200 X 300 mm column.	76
Table 4-12: Mechanical properties of FRP sheets.....	80
Table 4-13: Geometric and mechanical characteristics of metal strips for PTMS.	80
Table 5-1: Analytical versus experimental chord rotation for S60.....	84
Table 5-2: THA results for top displacement.	85
Table 5-3: Analytically derived damage versus experimentally observed damage (S60).	87
Table 5-4: analytically derived damage versus experimentally observed damage (S120).	89
Table 5-5: Fragility functions parameters for the 4-storey substandard buildings....	100
Table 5-6: Upgraded fragility functions parameters for the 4-storey substandard building.....	103
Table 5-7: Fragility functions by Ahmad et al. (2010).	108
Table 5-8: Fragility functions by (Akkar et al., 2005).	109
Table 5-9: Fragility functions by Erberik (2008).....	111
Table 5-10: Fragility functions by Kirçil and Polat (2006).....	112

Table 5-11: Fragility functions by Ozmen et al. (2010).....	113
Table 5-12: Fragility functions by Tsionis et al. (2011).....	114
Table B-1: Comparison between experimental and analytical 1 st mode of vibration's period form THA.....	158
Table B-2: Comparison between experimental and analytical 1 st mode of vibration's period from THA.....	161

ABBREVIATIONS

2D or 3D	2 or 3 Dimension
ADRS	Acceleration Displacement Response Spectrum
AFRP	Aramid Fibre Reinforced Polymers
BFRP	Basalt Fibre Reinforced Polymers
CFRP	Carbon Fibre Reinforced Polymers
CSM	Capacity Spectrum Method
DB	Displacement-Based
DBE	Displacement-Based Elements
DCM	Displacement Coefficient Method
DPMs	Damage Probability Matrices
EC8	Eurocode 8
EDP	Engineering Demand Parameters
EQ	Earthquake
ERA	Earthquake Risk Assessment
ERA	Earthquake Risk Assessment
FB	Forced-Based
FBE	Forced-Based Elements
FEA	Finite Element Analysis
FRP	Fibre Reinforced Polymers

GFRP	Glass Fibre Reinforced Polymers
GMPEs	Ground Motion Prediction Equations
IDA	Incremental Dynamic Analysis
IM	Intensity Measure
ITU	Istanbul Technical University
LH	Latin Hypercube
LS	Limit State
LVDTs	Linear Variable Displacement Transducers
MADRS	Modified Acceleration Displacement Response Spectrum
MDR	Mean Damage Ratio
MMI	Modified Mercalli Intensity
MSK	Medvedev Sponheuer Karnik
NLS	Non-Linear Static
NRCPA	Nonlinear reversed cyclic pushover Analysis
NSPA	Nonlinear Static Pushover Analysis
PGA	Peak Ground Acceleration
PGV	Peak Ground Velocity
PP	Performance Point
PTMS	Post-Tensioned Metal Straps
RC	Reinforced Concrete
RCPA	Reversed Cyclic Pushover Analysis
RCUK	Research Councils UK
SD	Standard Deviation
THA	Time History Analysis

TÜBİTAK	Scientific and Technological Research Council of Turkey
UC/C	Unconfined/Confined concrete
UOS	University of Sheffield
URM	Unreinforced Masonry

NOTATIONS

ϕ_{i1}	ith floor's Eigen vector from fundamental mode ϕ_1
$h_{b,i}$	Beam depth at top of the storey i
A_g	gross-sectional area of concrete column
A_s	tension reinforcement area
DI_{HRC}	Homogenised reinforced concrete damage index
DI_T	Period-based damage index
E_s	Elastic modulus of steel
H_i	Storey Height
$ISD_{max\%}$	Maximum inter-storey drift
T_0	Initial period
T_{100}	Ultimate period
T_{sec}	secant period at each SAi-SDi coordinate
U_n	displacement at Nth floor
Z_i	Internal lever arm for a column of storey i
$f_{0t,i}$ and $f_{0b,i}$	The maximum stress that the rebar can develop on top and bottom of column i,
f_{bs}	base shear
f_{cc}	yield stress
f_{cr}	Critical stress
f_l	applied lateral pressure

f_{le}	effective lateral pressure
f_{ult}	ultimate stress
$l_{0,i}$	Lapping of vertical rebars at the base of column i
m_1^*	effective modal mass for the fundamental vibration
m_i	lumped mass at the ith floor
t_f	FRP sheet thickness
Γ_1	fundamental mode participation factor
β_0	Initial damping
ε^*	Intermediate strain
ε_{cc}	yield point strain
ε_{cr}	Critical strain
ε_{fu}	failure strain of FRP
ε_{ult}	ultimate strain
ε_{ult}^*	strip ultimate tensile strain
$\theta_{u,top,i}$ and $\theta_{u,bot,i}$	ultimate rotation at top and bottom of column i,
$\theta_{y,top}$ and $\theta_{y,bot,i}$	Yield rotation at top and bottom of column i,
ρ_f	The geometric ratio of FRP
σ^*	Intermediate point stress
σ_l^*	Corresponding stress for ε^* from the tension side of behaviour
a_{pi}	intersection point spectral acceleration
a_y	yielding point spectral acceleration
b	strain-hardening ratio (ratio between post-yield tangent and initial elastic tangent)
COV	Coefficient of variance
D	Longitudinal bar diameter

d_b	longitudinal rebar diameter
d_{pi}	intersection point's spectral displacement
d_y	yielding point's spectral displacement
E_c	concrete modulus of elasticity
E_s	Initial elastic tangent
E_{sh}	Tangent at initial strain hardening
e_{sh}	Strain corresponding to initial strain hardening
e_u	Strain at peak stress
f_c	concrete compressive strength at 28 days
f_c	concrete compressive strength
f_t	Concrete tensile strength
f_u	ultimate strength of steel reinforcement
f_y	Steel yield strength
f_y	Yield strength of steel reinforcement
f_y	yield strength of longitudinal rebar
h	overall depth of the element
K_e	geometric effectiveness coefficient
L	Stirrup spacing
pinchX	pinching factor for strain during reloading
pinchY	pinching factor for stress during reloading
PP_{pi}	initial assumption of PP
S	Stirrup spacing
$S1n, e1n$	stress and strain at 1st point of the envelope in compression direction
$S1n, e1n$	stress and strain at 1st point of the envelope in compression direction
$S2n, e2n$	stress and strain at 2nd point of the envelope in compression direction

S_{2n}, e_{2n}	stress and strain at 2nd point of the envelope in compression direction
S_{3n}, e_{3n}	stress and strain at 3rd point of the envelope in compression direction
S_a	spectral acceleration
S_d	Spectral displacement
S_u	Ultimate stress of slip rebar
S_y	Yield stress of slip rebar
T	corresponding period of vibration
T_0	Initial period
T_{eff}	effective period
ϵ_0	concrete strain at maximum strength
ϵ_u	concrete strain at crushing
β	The standard deviation of $\ln(IM)$
β_{eff}	effective damping
θ	Median of the fragility function (The IM level which corresponds to 50% probability of collapse)
σ_c	Concrete compressive strength
σ_y	Steel yielding strength
$\Phi()$	Cumulative distribution function
B	Scale factor
$DI(\%)$	Rotation-based damage index
L	distance of critical section
N	number of floor
P	applied axial
$P(C IM = x)$	The probability that ground shaking with $IM = x$ will lead the structure to collapse

α post-yield slope of connecting line between yielding point and ultimate point

μ ductility

CHAPTER 1 INTRODUCTION

1.1 Background

Regardless of advances in our knowledge on the seismic behaviour of structures, urbanisation and population growth have resulted in increased seismic exposure in developing countries. Increased exposure to seismic risk plus rapid growth in the latter part of the previous century, led a large proportion of residential buildings to be built with substandard materials using poor designs/construction practices. Their high vulnerability to seismic actions has been demonstrated on numerous occasions leading to devastating death tolls and economic losses. The global annual earthquake-related economical losses have increased from \$14 billion in 1985 to more than 140 billion in 2014. Earthquakes are currently responsible for almost one-fifth of the annual economic losses due to natural disasters, with an average death toll of 65000 per annum (Fraser et al., 2016).

A large portion of the statistics stated above, is attributed to developing countries which suffer from higher death rates (and economic losses) compared to the developed world. For instance, the 1988 Armenia earthquake (6.8M), which had half the energy released compared to the 1989 Loma Prieta (6.9M) earthquake near San Francisco (the USA), caused 25,000 deaths compared to only 100 in San Francisco. This is also obvious by comparing the 2003 earthquake in Bam (Iran) and the 2003 earthquake in Paso Robles (California), both of the same magnitude (6.6M): The death toll was only 2 in California, while 41,000 in Bam (Kenny, 2009). The 1999 Marmara (Turkey) 7.4 magnitude earthquake caused direct economic losses of over \$5 billion and approximately 18,000 people died due to poorly constructed reinforced concrete

(RC) structures. The majority of these structures were made of low-strength concretes and located close to known fault lines (Escaleras et al., 2007, Anbarci et al., 2005, Özerdem and Barakat, 2000, Kenny, 2009). Another example is the poor performance of around 6000 school buildings in Gujarat, India built in 1999-2000, during the 2001 Bhuj earthquake (6.9M) (Jain, 2005). Around 75% of these buildings were heavily damaged or even collapsed, due to seismically weak, precast construction technology.

The primary action of earthquakes, ground shaking, does not cause loss of life. It is the high vulnerability of the building stock and lack of resilience of the society that turns earthquakes into catastrophes. The high vulnerability of substandard RC buildings characterised by poor construction and low-quality materials as well as deficient detailing in critical locations (such as the use of plain rebars in columns and beam-column joints, sometimes with insufficient anchorage), can lead to weak lateral-load resistant systems with low energy dissipation capacity and rapid strength degradation during reversal loading. Figure 1-1 shows some of the common deficiencies found in substandard RC buildings in developing countries.

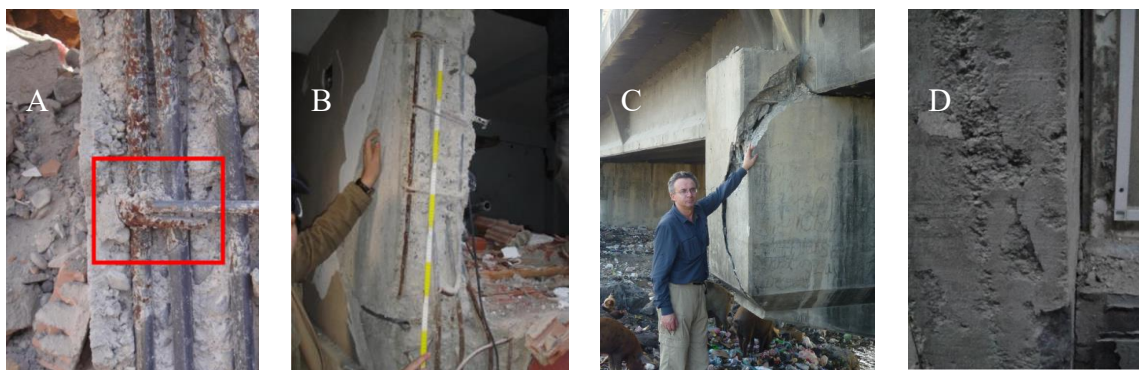


Figure 1-1: Common deficiencies of substandard RC buildings. A) improper hooking and use of plain bars, B) pull-out failure and C & D) low concrete quality.

1.1.1 Case study: Marmara region

To investigate the aforementioned construction issues frequently found in substandard RC buildings, this PhD study analyses in-depth the effect of these deficiencies, by conducting a seismic vulnerability assessment on an existing substandard residential RC building located in Istanbul, Turkey. The main reasons for selecting Istanbul as the case study area are as follows:

a. Istanbul is located in the Marmara region (Turkey), which is one of the most seismically active zones worldwide. For example, the 1999 Kocaeli and Duzce earthquakes have caused extensive structural damage, massive economic losses and high fatality rates. Unfortunately, 18000 people lost their lives after the Kocaeli earthquake (Durukal, 2002) and 1000 fatalities were reported after the Duzce earthquake (Ghasemi et al., 2000).

b. Istanbul is densely populated and according to the available data, a large proportion of RC structures are substandard (66% of the RC buildings built pre-1998). In the Marmara region, many buildings were also constructed without town permission and without following a specific seismic design code (Bal et al., 2008).

c. An earthquake with $M \geq 7.0$ with a 50% probability is expected to hit Istanbul in the next 30 years as reported by Murru et al. (2016).

Bal et al. (2008) conducted a case study for Marmara, which can quantify the extent of the low-quality material issues in this region: Based on 6067 concrete core samples surveyed from 1178 existing RC buildings built during the 80s/90s, the mean compressive strength of concrete was only 17 MPa (and with a high standard deviation of 8 MPa). For 16% of the examined buildings, the compressive strength was equal or even below 8 MPa.

The first design guidelines which set 20 MPa as the lowest acceptable concrete strength, were introduced in early 1998, whilst the use of ready mix concrete in the region started after or even much later than 1998. It is reported that half of the samples taken from ready mixes, did not meet the requirements set by this standard. To tackle this issue, in 2000, the Turkish policymakers introduced strict regulations in concrete manufacturing processes.

1.1.2 Vulnerability assessment

To predict the damage of a catastrophic event caused by an earthquake in terms of economic, societal and human losses, scientists have developed assessment methodologies using empirical or analytical vulnerability curves. Vulnerability curves can be derived for a building/class to calculate the damage in terms of repair-to-replacement cost. To predict the probability of exceedance of a certain damage limit state (e.g. slight, moderate, extensive and collapse), fragility curves are used. The fragility curves can be converted to vulnerability curves for a specific building class, by employing a conversion matrix.

1.1.2.1 Empirical vulnerability

The empirical vulnerability curves are developed based on extensive damage databases from past earthquakes, but their main feature to cover a wide range of damaged buildings is also their weakness: These curves can be representative for generalised building classes, however, they significantly underperform when dealing with sub-classes. When it comes to individual buildings, they are practically of no use.

To compensate for some unknown factors affecting the seismic response of structures, expert opinions can be used to develop judgemental vulnerability curves. This approach is less affected by the lack of data, but it is methodologically subjective and limited to a specific geographic area and time. The accuracy of the derived vulnerability curves, highly depends on the knowledge/experience of the expert panel.

1.1.2.2 Analytical vulnerability

For substandard RC buildings, analytical methods can address their common deficiencies (shear, local buckling, slip-bond failure, beam-column joint failure etc.) to assess their damage potential. The analytical vulnerability assessment methods can overcome the issues regarding empirical and judgemental vulnerability assessment methods. However, the existing analytical vulnerability curves underestimate the damage to substandard RC buildings, due to the following reasons:

- a. The analytical models used in vulnerability assessments are either not validated against the actual building response or do not consider the main deficiencies of substandard buildings. Most of existing analytical vulnerability curves for substandard RC buildings, only consider flexural behaviour, construction materials and geometrical characteristics (e.g. (Cornell et al., 2002, Calvi et al., 2006, Erberik, 2008)) (Objective 2).
- b. The data pool derived after probabilistic sampling process of a building capacity, contain both ductile and brittle behaviours. Although, the results for the ductile behaviour are representative, the damage level for brittle buildings (substandard) is underestimated (Objective 3).

Another critical issue is that currently; literature lacks of vulnerability curves for existing retrofitted substandard RC buildings (Objective 4).

Therefore, based on the above, there is an urgent need to develop more accurate analytical vulnerability curves for substandard buildings (including retrofitted ones) and update existing risk assessment frameworks to achieve more precise damage estimations (Objective 5).

This PhD will investigate the impact of common deficiencies of substandard RC structures on their vulnerability/fragility curves by analytically considering the effect of various brittle failure modes.

1.2 Research Aim and Objectives

This research aims to develop a probabilistic vulnerability framework capable of capturing the actual behaviour of substandard RC buildings. To achieve this, an analytical modelling procedure is proposed and validated against experimental data from existing large-scale tests on both RC column and frames. Advanced adaptive vulnerability curves and upgraded vulnerability curves are derived for a case study existing 4-storey substandard building in Marmara region.

To accomplish this aim, the following objectives are implemented:

1. A critical review on seismic vulnerability assessment methodologies and weaknesses of existing analytical vulnerability curves.
2. Development of an analytical model for substandard RC buildings and validation against full-scale experimental results.
3. Development of advanced adaptive fragility curves for substandard RC buildings.
4. Development of upgraded fragility curves for retrofitted substandard RC buildings.
5. Development of a robust framework for seismic vulnerability assessment of substandard RC columns/buildings using OpenSees and Matlab software.

The main novelties of this research can be highlighted as:

- The proposed analytical model includes various parameters which can accurately capture the actual substandard behaviour of existing RC buildings.
- The developed framework can be easily applied to existing seismic risk frameworks and enhance their accuracy.
- Upgraded (for strengthened RC buildings) and advanced adaptive vulnerability/fragility curves are introduced.

1.3 Thesis Layout

Chapter 2 comprises three main sections: The first section presents a brief literature review of existing seismic vulnerability assessment methods as well as their strengths/weaknesses, followed by a discussion on the key parameters affecting analytical vulnerability assessment (methods of modelling, type of analysis, damage indices, etc.). The second section identifies the most compatible retrofitting techniques using external jacketing applicable for substandard RC buildings in developing countries and also provides the analytical modelling approach based on literature. At the end of this chapter, the available element types of OpenSees software are presented, highlighting their advantages and drawbacks.

Chapter 3 presents the details of four full-scale substandard RC cantilever column tests and two full-scale one-bay two-storey substandard RC frame shaking table tests. The case study, an existing 4-storey substandard RC building located in Turkey, is also described. These results are used to validate the analytical model developed in Chapter 5.

Chapter 4 starts with the analytical modelling approach in OpenSees, proposed to capture the behaviour of substandard RC structures. Then, the verification procedure of the analytical tool follows. Last but not least, the methodology to develop analytical vulnerability curves is presented as well as the probabilistic approach used in fragility analysis. Lastly, the methodology followed to derive the upgraded vulnerability curves is explained.

Chapter 5 analyses, discusses and validates the results of the analytical model for the substandard columns/frames, based on the methodology described in Chapter 4. The local and global damage parameters of the columns are investigated and the adaptive and upgraded fragility curves are produced using the proposed framework. The results of the probabilistic seismic vulnerability assessment of an existing 4-storey substandard RC building (case study) are presented at the end of this chapter, using the developed adaptive vulnerability assessment framework.

Chapter 6 summarises the main conclusions followed by the recommendations for future work.

CHAPTER 2 LITERATURE REVIEW

This chapter presents a brief literature review of the current seismic vulnerability assessment methodologies (more information can be found in Appendix A), followed by a discussion highlighting the advantages and disadvantages of each method. Then, the common deficiencies of substandard RC buildings are summarised. Two retrofitting techniques which are hypothetically used to strengthen the case study RC building are also presented, together with their analytical modelling approach, based on literature: External jacketing using Fibre Reinforced Polymers (FRP) or Post-Tensioned Metal Straps (PTMS). The final section of this chapter discusses the available element types in OpenSees highlighting their advantages and drawbacks.

2.1 Seismic Vulnerability Assessment Methodologies

2.1.1 Introduction

The scope of the vulnerability assessment is to determine the probability of a certain level of damage to a given building type, caused by a scenario earthquake. It estimates the potential structural damage that could affect the building environment as a consequence of a seismic event, in terms of repair-to-replacement cost.

The physical seismic vulnerability is related to the level of exposure and the fragility of elements subjected to the seismic action. Taking the physical aspect on the side, seismic vulnerability has a deeper context and can be envisioned from economic, political or societal points of view. When a catastrophic earthquake strikes, it causes severe damages to the building stock, road infrastructure or even utility networks

(electricity/gas). This physical dimension is the main cause to the social aspects of the vulnerability. The social/economic/political dimensions of the vulnerability make a big impact on the society which may remain (or even grow) over time and is closely associated to the cultural aspects and development of the communities (Cardona, 2013).

The seismic hazard represents such effects of an earthquake as ground motion, liquefaction, landslides, tsunamis, rockslides and surface fault ruptures. However, these hazard sources occur at a smaller size scale; therefore, ground shaking is taken as the main influence factor in seismic risk modelling studies (Bird and Bommer, 2004).

Methods for the seismic vulnerability assessment are fundamental for the identification and delimitation of seismic-prone areas, plan seismic risk reduction and implementation of strategies. They can predict the expected consequences of predetermined event scenarios, generating estimates of the humanitarian impact (injuries/deaths), societal impact (interruption of services, homeless people due to unusable buildings) and damage (actual damage cost as well as repair-to-replacement cost of the impacted structures). Seismic vulnerability assessment analyses allow the authorities to plan an operational response and a model of intervention, constituted by a series of actions aimed at emergency management.

2.1.1.1 Types of assessment approaches

Before the main methods of vulnerability assessment are described, it is essential to present the two main approaches that an assessment can be based on: The probabilistic approach and the deterministic approach.

Probabilistic approach: In general, a probabilistic approach takes into account all possible variabilities in capacity and demand during vulnerability assessment, using the distribution functions fitted to the variability of that considered parameter based on available data. Therefore, a sampling technique is needed to generate sets of data for the probabilistic analysis. While the Monte-Carlo simulation sampling technique is

more popular in seismic hazard analysis, Latin Hypercube (LH) sampling method is widely used in seismic vulnerability analysis. The LH method is efficient, since it needs less sampling size than the minimum sampling size normally required to achieve an acceptable level of accuracy. In case of analytical probabilistic seismic vulnerability analysis, the LH sampling method has an advantage over Monte-Carlo as it is computationally more time-efficient.

Due to the random nature of seismic events and variability in the properties of a structure, the probabilistic approach is essential for developing vulnerability curves to assess the vulnerability and the consequence of seismic damage for a building category.

Deterministic approach: On the other hand, deterministic approaches could be used to assess the seismic performance of a specific building for a certain scenario earthquake. This is a common approach for the performance-based design of a new RC building.

2.1.1.2 Seismic vulnerability assessment methods

Regarding seismic vulnerability assessment, several methods have been proposed in the literature, which can be generally classified into four main categories: Empirical, expert judgment, analytical and hybrid vulnerability assessment methods.

a. Empirical vulnerability assessment methods use actual damage data collected after a seismic event, coupled with statistical procedures to derive vulnerability functions (**See** section 2.1.2).

b. In expert judgment methods, a panel of experts estimates the potential damage to a certain type of building category, based on their experience and knowledge (**See** section 2.1.3).

c. In analytical methods, damage distribution is obtained from an analytical model of the structure subjected to increasing earthquake loads (**See** section 2.1.5).

d. Hybrid methods combine the abovementioned methods attempting to utilise the strong points of each method (See section 2.1.6).

There is also a special category that contains straightforward procedures for conducting quick evaluations which cannot be considered as proper assessment methods, although they have some common characteristics with empirical methods: This category contains procedures called rapid/preliminary procedures (walk-down or street surveys) and only require superficial data, collected after a brief external inspection of the building after the earthquake incident (no internal inspection is allowed). The purpose of rapid evaluation techniques is to identify/rank highly vulnerable buildings that deserve further investigation, and also inform residents and authorities whether a building is safe to be occupied after the earthquake event. Some of the collected data are the number of stories, vertical and plan irregularities, location, age and structural system of the building, and apparent material and workmanship quality. FEMA 154 (154–ATC-21, 1988) and FEMA 310 Tier 1 (310, 1998) fall into this category.

2.1.2 Empirical vulnerability assessment: Overview

The main advantage of empirical vulnerability assessments is the use of post-earthquake damage surveys which can provide a precise image of the damage. Therefore, they can account not only for the strong ground motion but also, other site-specific parameters (soil type, soil-structure interaction, directivity effect, source path, liquefaction, etc.) and the effect of non-structural components (Rossetto et al., 2014). Nevertheless, these assessments have major issues in their predictions due to the methods used to process the damage surveys or even built-in limitations from the initial design of the model.

The main assumption for deriving empirical fragility curves is that the recorded damage for a building class after an earthquake event, is representative of the damage that might happen in the future to this specific building class when a similar earthquake strikes. This brings a limitation to the applicability of empirical fragility curves since the

empirically derived fragility functions are only applicable to buildings in an area very similar to the geographical area where the data was collected. This limits the use of empirically derived fragility functions as the majority of empirical fragility assessment has been performed only for a few countries e.g. Greece, Italy, Japan, Turkey and the USA, where the most observational data after an earthquake was recorded (Rossetto et al., 2013).

Apart from the main limitation mentioned above, empirical vulnerability assessments can be categorised into the following groups according to their weaknesses:

- a. Inconsistency in the methodology of how the damage data is collected and processed
- b. Use of large inaccurate damage databases obtained by rapid post-earthquake surveys or satellite images
- c. Damage observations are linked with ground motion intensity levels obtained by non-accurate motion prediction equations
- d. Lack of a unified and widely accepted empirical method
- e. Process of empirical data using unreliable statistical distribution functions

2.1.2.1 Inconsistency in collected data and processes

The literature highlights that the empirical vulnerability assessment methods exhibit several dissimilarities to each other, due to the data of the observed damage, the type of selected ground motion intensity measure, the variation of functions used to fit the data and the type of statistical technique used (Rossetto et al., 2013).

Empirical fragility functions are generally derived from damage data recorded after one or more earthquake events. The reliability of the results depends on the quality and completeness of the database and is usually affected by the data collection method (Rossetto et al., 2014). If the data are based only on the damage recorded after a single earthquake then, the ground motion intensity values in the database may be limited. Furthermore, the fragility functions may not account for the variability of the

structural response that can be introduced by ground motion e.g. frequency content of the ground shaking, number of cycles, mainshock and aftershock (Rossetto et al., 2014). However, most of the empirical fragility curves are derived based only on single-event damage observation databases (e.g. (Karababa and Pomonis, 2011, Liel and Lynch, 2012)).

Some studies developed fragility curves by combining post-earthquake damage surveys from various events that have affected the same building class to increase the quality of damage database and cover a larger range of ground motion intensity levels (e.g. (Rota et al., 2008, Giilkan et al., 1992)). However, the combined database is highly clustered in the low ground motion intensity level because of the rarity of large magnitude earthquakes in urban areas (Rossetto et al., 2014).

2.1.2.2 Rapid post-earthquake surveys and satellite images

Large damage databases from rapid post-earthquake surveys and satellite images (remotely sensed) have also been used for derivation of damage in the fragility analysis process (e.g. (Hancilar et al., 2012, Estrada et al., 2000, Yusuf et al., 2002)). These techniques are quick and inexpensive if compared to comprehensive field surveys but, these databases are not accurate and are linked with very general building classes. Therefore, there is a high probability that buildings are assigned the wrong level of damage and this can seriously affect the results (Ioannou et al., 2012).

2.1.2.3 Prediction of ground motion using mathematical equations or data collected from similar sites

Empirical fragility curves link damage observations with ground motion intensity levels. Therefore, both post-earthquake damage and ground motion intensity level should be recorded for each building. However, recordings for ground motion are not easily available across the observation area, since this requires ground motion recording instrumentation. Therefore, the majority of empirical studies use Ground Motion Prediction Equations (GMPEs) or macro-seismic intensity measures to evaluate their

intensity levels (Rossetto et al., 2014). Modern attenuation equations or GMPEs are derived based on several ground motion recordings, considering the effect of focal mechanisms and soil types. However, reliable and modern GMPEs may not always be available for the region of interest therefore, adopted GMPEs from similar tectonic locations can be used (Ioannou et al., 2012). The most commonly used intensity measures are the Peak Ground Acceleration (PGA) and Peak Ground Velocity (PGV). Since GMPEs are recently developed for spectral values, there are only a few empirical fragility curves developed using spectral acceleration and velocities (e.g. (Rossetto and Elnashai, 2003, Ghodrati Amiri et al., 2007, Colombi et al., 2008)).

2.1.2.4 Lack of unified empirical method

Empirical seismic vulnerability analysis studies initially started by expressing the probability of attaining specific damage levels for discrete macro-seismic intensity levels, with the so-called Damage Probability Matrices (DPMs). Two of the first pioneer studies conducted by Whitman (1973) and Braga et al. (1982), in which the Modified Mercalli Intensity (MMI) and Medvedev Sponheuer Karnik (MSK) macro intensity measures were used, respectively. Later studies (Sabetta et al., 1998, Orsini, 1999, Rossetto and Elnashai, 2003, Lagomarsino and Giovinazzi, 2006, Colombi et al., 2008, Rota et al., 2008, Rosti et al., 2018, Del Gaudio et al., 2020) introduced various statistical methods which allowed researchers to fit smoothed curves to the observed data and DPMs were upgraded to vulnerability functions as continuous vulnerability curves. However, there is no unified and widely accepted empirical method for deriving empirical fragility curves (Del Gaudio et al., 2020). The main reason is the recorded post-earthquake damage data. The main parameters that cause these differences are, the type of fitted functions, recorded damage, intensity measure, categorisation or typology of the buildings, vulnerability classes, etc.

2.1.2.5 Process of empirical data using statistical distribution functions

Various functions were used by researchers to fit the empirical data using statistical methods. Most of the existing empirical fragility functions are derived based on a cumulative log-normal distribution function. Limited research adopts the cumulative normal distribution (e.g.(Spence et al., 1992)) and only a minority an exponential function (e.g.(Rossetto and Elnashai, 2003)). The three main statistical approaches which fit these parametric functions are the: nonlinear (e.g.(Rota et al., 2008, Rossetto and Elnashai, 2003)), linear (e.g.(Liel and Lynch, 2012)) and generalised linear (e.g.(Ioannou et al., 2012, Shinozuka et al., 2000, Basoz et al., 1999)).

2.1.2.6 Conclusions

It can be concluded that using only empirical vulnerability curves for seismic risk assessment purposes may not give accurate results, as the reliability of results is directly related to the completeness of the database. Damage observation data from various sources cannot be easily compared to each other, since the recorded ground motion intensity parameters may vary as well as the recorded damage scale. Damage data are mostly clustered in low ground motion and low damage level region which limits the use of empirical vulnerability curves for higher levels of intensity. The empirical database can be easily become outdated due to the infrequency of large earthquakes in urban areas and the lack of updates of the building inventory over time. Rossetto and Elnashai (2003), reported that for substandard buildings, vulnerability curves can underestimate the damage level even if the database contains damage data of similar buildings from other regions.

2.1.3 Expert judgment fragility approaches: Overview

This method is not affected by the lack of damage data as empirical approaches. Compared to analytical methods, expert judgment fragility approaches are not affected by the reliability of the numerical model. The expert judgment method can

derive approximate vulnerability curves and account for various parameters considered by the expert panel. However, this technique lacks a robust scientific foundation and has several limitations.

The experience level of each expert can affect the reliability of the outcome. If the panel has expertise with a particular type of structures, then their predictions cannot be applied to a different class of structures. Two of the main rehabilitation codes of the USA (ATC-40, 1996, ATC-13, 1985) are heavily based on expert judgmental vulnerability curves derived after only two seismic events in the USA: (the 1971 San Fernando earthquake and the 1994 Northridge earthquake). The judgmental DPM, developed for typical building classes in California in ATC-13 (Council, 1985), cannot be applied to other continents such as Europe or Asia, due to differences in construction and design practices.

Regarding substandard RC structures, things are getting even more vague, since their structural behaviour is not very well known, hence, it can be difficult for an expert to assess the performance of a specific building class in a specific region at various ground motion levels.

2.1.4 Analytical vulnerability approaches: Overview

In this method, a Finite Element Analysis (FEA) of the structural model is performed to determine damage distributions. This involves the use of simulated response parameters corresponding to different building performance levels with increasing demand. The accuracy of these vulnerability curves is governed by the ground motion parameter, material models, response parameter, analysis type, damage index and structural idealisation. This approach has recently received a lot of attention from the scientific community (e.g. Mosalam et al., 1997; Calvi*, 1999; Lang, 2002; Kyriakides, 2007).

To derive analytical vulnerability curves, a general procedure can be followed as shown in Figure 2-1.

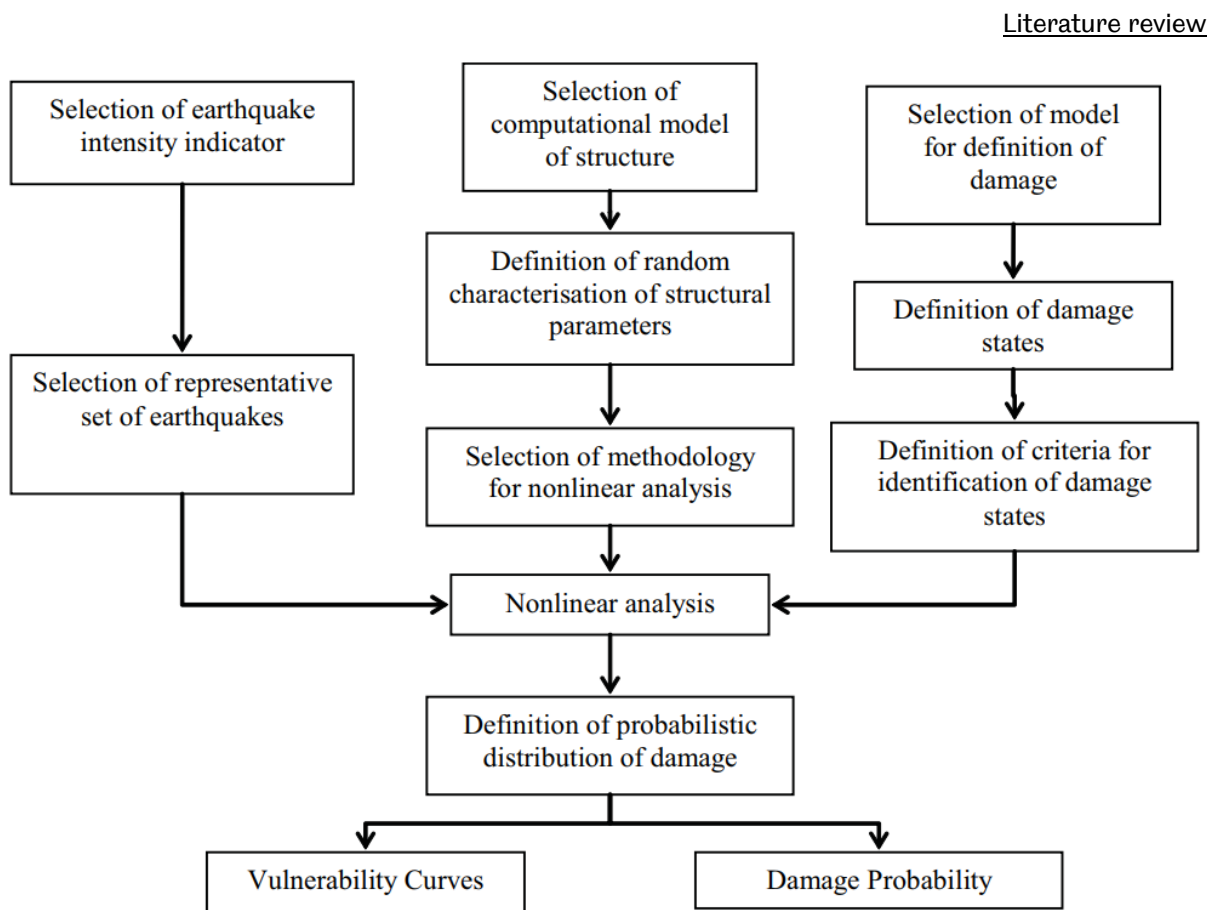


Figure 2-1: General procedure for analytical vulnerability assessment (adapted from (Dumova-Jovanoska, 2004)).

Currently, there are three main approaches for deriving analytical vulnerability curves:

1. Correlation between damage index and damage states.
2. Correlation between capacity curves (for buildings) and spectral response curves (capacity spectrum method).
3. Correlation between capacity curves (for buildings) and acceleration time histories.

2.1.4.1 Correlation between damage index and damage states

This approach was quite popular in the past decade and its accuracy of analytically-derived fragility curves depends on the damage model, level of accuracy on the structural modelling approach and the type of analysis (Rossetto et al., 2014). The

damage indices can be either global (structural level), local (element level) or a combination of both (Rossetto et al., 2014). The most commonly used local damage index (Park and Ang, 1985) is defined by linearly combining dissipated energy of an element at its maximum displacement. The major drawback of this approach is the use of indices which needs to be validated with experimental tests (preferably full-size ones), however, only a few of these tests exist and they do not cover all building types. For instance, the aforementioned damage index (Park and Ang, 1985) requires a model (2D or 3D) of the structure to be built and is more suitable for use in damage evaluation obtained from non-linear time-history analyses than pushover analyses, because of the dissipated energy component of the index.

2.1.4.2 Capacity spectrum approach

For a given structure, the capacity spectrum approach is based on a monotonic static nonlinear pushover analysis, producing a pushover curve (base shear versus roof displacement). This curve describes the global behaviour of the structure subjected to a combination of gravity loads and monotonically increasing lateral forces, to statically simulate the seismic action. Pushover curves are usually idealised as series of linear branches of constant stiffness and expressed in the pseudo-acceleration/displacement spectral graphs, called capacity curves. The capacity curve is then intersected with a spectral demand curve to determine the Performance Point (PP) (Figure 2-2).

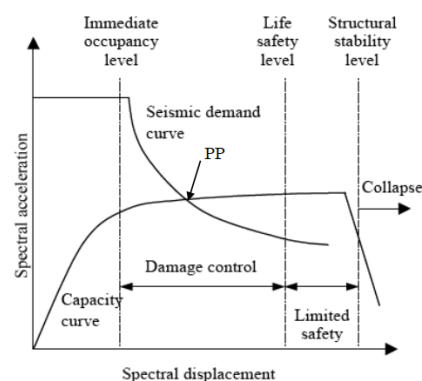


Figure 2-2: Defining the performance point.

There are several methods for deriving performance points in the literature. The five well-known methods are the: Capacity Spectrum Method (CSM) (ATC-40, 1996), Displacement Coefficient Method (DCM) (FEMA 356, 2000), N2 method (Fajfar, 2000), Improved CSM (FEMA 440, 2005) and non-iterative equivalent linearisation method (Lin and Lin, 2009).

A performance point for a structure can be calculated for different intensity levels, from which fragility curves can be constructed. This method is favoured by many seismic codes and researchers (e.g. Fajfar, 2000; Agency, 2003; FEMA 356, 2000; Council, 1996; Lin and Lin, 2009) due to its simplicity and prompt application especially for a large population of structures.

2.1.4.3 Incremental dynamic analysis

This approach follows a simplified version of incremental dynamic analysis proposed by Vamvatsikos and Cornell (2002) and Rossetto and Elnashai (2005). Both procedures allow the performance and hence, damage of a structure, to be calculated for a set of earthquake ground motion records. In this approach, a performance function, rather than a performance point, is defined.

The 2nd (Capacity spectrum) and 3rd (Incremental dynamic analysis) methods follow the same framework as the performance-based design used for new buildings or for seismic assessment of existing buildings if applied deterministically ((Standardization, 2005, FEMA 356, 2000, ATC-58, 2009, Agency, 2008), etc.). By applying the 2nd and 3rd approaches to large sets of buildings, fragility curves and damage levels can be derived for given sites and scenario earthquake.

Generally, for approaches (2) and (3), the basic required analysis steps are:

- (a) Classification of buildings by typology and seismic design.
- (b) Definition of damage states.
- (c) Assignment of capacity curves or backbone curves (for dynamic analysis).

(d) Choice of response spectra (associated with return periods and performance targets) or choice of a set of ground motion records to perform dynamic response time history analysis.

(e) Evaluation of building response in terms of performance points.

2.1.4.4 Discussion

The accuracy of the fragility curves derived by analytical approaches depends on the level of detail considered in the modelling procedure and the type of analysis (IDA or Pushover, etc.) used for deriving the vulnerability curves. To derive vulnerability curves for a specific class of buildings probabilistically, it is required to perform various types of analyses which need different processing times and detailing demands. Therefore, one of the desired characteristics regarding analytical fragility analysis is, to define a relatively simple but accurate modelling procedure that can be executed quickly.

2.1.5 Analytical approaches: Analyses methods

The three most dominant methods of structural analyses used in the literature to obtain the Engineering Demand Parameters (EDP) and damage state thresholds are as follows:

1. Incremental Dynamic Analysis (IDA).
2. Nonlinear static analysis based on simplified mechanism approaches.
3. Nonlinear Static Procedures (NLS).

When using the 1st and 3rd methods to derive EDP, the accuracy of the response depends mostly on the precision and appropriate level of complexity of the analytical model. The 1st method has the most accurate results in comparison to the other two methods, with the advantage of accounting for uncertainties related to record variability (frequency content, soil amplification, near-field and far-field effects). The sections below provide more details about the methods and determine which of these is more suitable for the needs of this PhD study.

2.1.5.1 Incremental dynamic analysis

This method requires performing a nonlinear time-history analysis where the dynamic characteristics of the building (e.g. damping) are unknown and need to be estimated. IDA's output is a backbone or envelope capacity curve using large numbers of nonlinear response history simulations. This method is most suitable when dealing with a specific structure due to the computational effort required. Since in this PhD research, the main aim is to perform vulnerability analysis on a building class covering all possible material and geometrical variabilities, this method cannot be efficient due to high computational demand.

2.1.5.2 Nonlinear static analysis based on simplified mechanism approaches

The second method is also not an option for this PhD study, because the simplified mechanism approaches are not capable of taking into account the degrading behaviours of substandard RC buildings suffering from a series of seismic excitations. Literature also mentions that this type of approach is mostly suitable for unreinforced masonry (URM), and adobe buildings (D'ayala et al., 2014).

2.1.5.3 NLS method

In the literature, the following well-known NLS procedures are very suitable for vulnerability/fragility analysis due to their sufficient accuracy and trustworthy results (D'ayala et al., 2014).

1. Capacity Spectrum Method (CSM), (ATC-40, 1996)
2. Displacement Coefficient Method (DCM), (FEMA 356, 2000)
3. N2 method, (Fajfar, 2000)
4. Improved CSM, (FEMA 440, 2005)
5. Non-iterative equivalent linearization method, (Lin and Lin, 2009)

After an evaluation of the above procedures, it was decided that the most suitable approach to conduct the vulnerability/fragility analysis for this PhD work, would be the NLS method using the improved CSM. Although the drawbacks of IDA are overcome, the NLS method suffers from two major limitations:

- a. The current NLS approaches tend to neglect the cyclic degradation of the material performance by deriving the capacity curve using monotonic pushover analysis (Calvi et al., 2006).
- b. The pinching effect originated by the buckling behaviour also needs to be accounted for an acceptable structural response estimation during numerical analysis.

To solve the above limitations, a new approach was adapted in this PhD and explained more in section 2.1.2.5.

2.1.5.4 NLS method preferred for this PhD

The NLS method is appropriate for this PhD study, since the structural response of the substandard building stock (for the case study region) is dominated by the first mode of vibration. The same applies to degrading behaviours such as buckling and bond-slip. The pushover analysis used in the NLS approach, is ideal for these behaviours, since it forces the building to be excited in the first mode of vibration. To include the effects of cyclic degradation which cannot be captured by a monotonic pushover analysis (section 2.1.5.3 (a,b)), nonlinear reversed cyclic pushover analysis was employed.

2.1.6 Hybrid Fragility Approaches: Overview

This method is a combination of post-earthquake damage statistics and analytical damage statistics obtained from a mathematical model. Various types of uncertainties exist in the vulnerability curves derived from the above-mentioned techniques due to limited post-earthquake damage data, judgemental data subjectivity and modelling issues in analytical vulnerability. To reduce these uncertainties, hybrid vulnerability

curves have been derived by several researchers (e.g. (Jalalian, Kappos et al., 1998, Singhal and Kiremidjian, 1997)) which use data from various sources.

In hybrid curves, the deficiency of the observational data at a particular intensity level can be eliminated by conducting nonlinear static or time history analysis, and the judgemental or analytical curves can be modified by utilising the observational data. Experimental test data can also be used to reduce the deficiencies in observational, judgemental or analytical vulnerability curves.

An alternate way of performing hybrid vulnerability assessment is by using laboratory testing (Pinho and Elnashai, 2000). The benefit of this method is that it gives the freedom to produce needed data for any building type. The limitations are related to the scale of the model, loading type and laboratory equipment capacity. Experimental data are costly and allow only a few parameters to be investigated at a time, so they are mostly used for verification purposes rather than as an additional source.

2.2 Common Deficiencies of Substandard RC Buildings

Substandard RC buildings are constructed using poor construction practices and low-strength/quality materials. This leads to deficiencies which cause high vulnerability in the case study region and force buildings to exhibit softening behaviours due to: a. slippage of rebars in joints and b. buckling of longitudinal rebars.

It should be mentioned that there are also other issues reported during past earthquakes with substandard RC buildings (e.g. shear failure of short columns, joint failures, etc.). This research focuses on failure modes a and b, mentioned above.

Low material quality concrete translates into a low compressive strength concrete, reinforced with plain rebars of low steel grade (e.g. S220). The lower the compressive strength of the concrete, the more ductile the behaviour of concrete will be (Figure 2-3). The low compressive strength of concrete in these buildings can also lead to low initial stiffness and poor lateral/axial load capacity. However, the behaviour of concrete after reaching to the peak strength can be affected by other parameters e.g. loading

rate and sectional size. The comparison in Figure 2-3 is for the same section size and rate of loading to represent a general stress-strain behaviour with various concrete strengths.

The use of plain rebar will adversely affect the bond between the rebar and surrounding concrete, leading to higher yield and ultimate slip. This behaviour also reduces the initial stiffness of the structure since the structure is exposed to higher yield/ultimate slip.

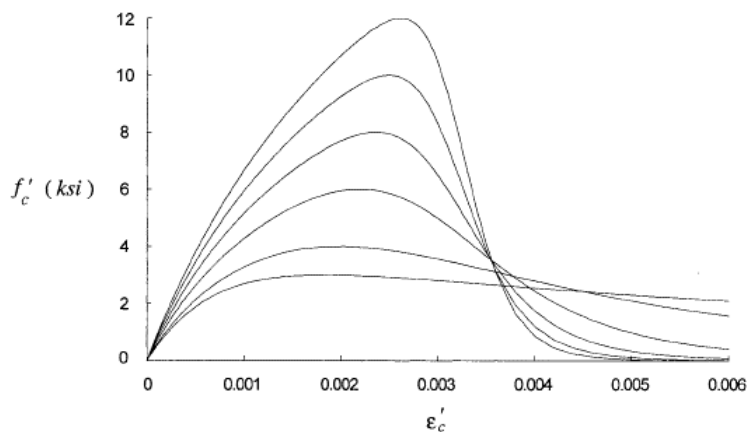


Figure 2-3: Comparison of concrete behaviour based on concrete compressive strength (adopted from Mander et al. (1988)).

Poor detailing refers to large stirrup spacing, low longitudinal reinforcement ratio, inadequate lap splice length, thin concrete cover, etc. Stirrup spacing can be considered the most critical parameter for a substandard building. The large stirrup spacing reduces the effectiveness of confinement, ductility and concrete compressive strength. To visualise this, Figure 2-4 shows a comparison of a confined concrete model, based on Mander et al. (1988), for a typical 200 mm X 300 mm concrete section with 4 longitudinal 14 mm diameter rebars and 10 mm diameter stirrups. The concrete compressive strength is assumed to be $f'_c=20$ MPa and the yielding strength of steel rebars to be $f_y=320$ MPa, at 60 mm and 200 mm stirrup spacing.

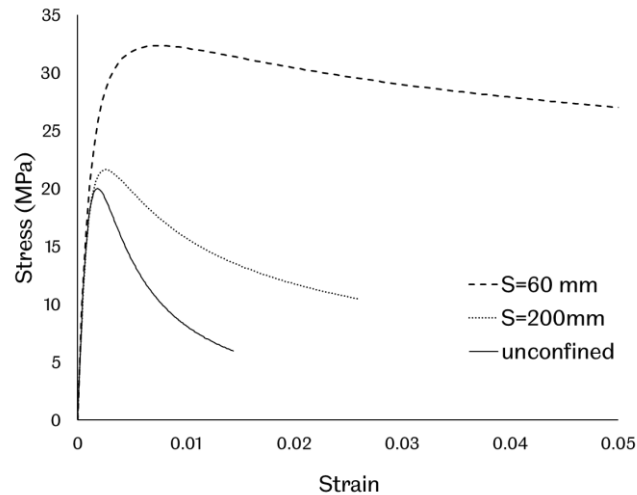


Figure 2-4: Effect of stirrup spacing on concrete core confinement behaviour.

Large stirrup spacing also leads to the most critical degrading behaviour: longitudinal rebar buckling. Buckling is adversely affected by stirrup spacing, as mentioned in various research works in the literature (Bae et al., 2005, Dhakal and Maekawa, 2002). Figure 2-5 presents the effect of stirrup spacing in buckling for longitudinal rebars of S220 steel grade.

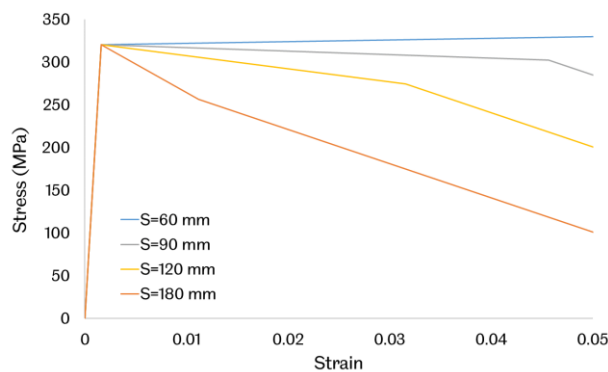


Figure 2-5: Effect of stirrup spacing according to Dhakal and Maekawa (2002).

In case of a strong earthquake, these deficiencies can rapidly deteriorate the structural integrity of a substandard building, which can be described as a weak lateral-load resistant system with insufficient energy dissipation capacity.

The above theory can be also validated by using experimental results from this PhD study, as described in the section below.

2.2.1.1 Experimental verification of theory on typical failure mechanisms of substandard RC frames/columns tests

This section discusses the failure mechanism observed during the experiments presented in sections 03.2 and 03.3. Figure 2-6 and Figure 2-7 (columns with stirrup spacing $S=180\text{mm}$ and $S=60\text{mm}$, respectively) illustrate the general progressive failure mechanism observed during reversed cyclic experiments of substandard RC cantilever columns (section 3.2). Although these figures reveal a tiny part of the actual PhD experimental results, they are shown here to validate the existing theory and visualise in-depth, a typical example of rebar buckling.

After yielding the longitudinal rebars in tension, the existence of high slip from the longitudinal bars enforce more stress and strain on the compression side of the section, and this activates the buckling earlier compared to non-bond-slip behaviour. By initiation of buckling, the cover spalls and the cross-sectional area is reduced, exposing the compression bars to higher stress levels and finally, crushing the concrete in compression. The delay between the initiation of buckling and losing lateral load capacity of the system (ductility) depends mainly on stirrup spacing. This can be seen in Figure 2-6 and Figure 2-7 by comparing the cyclic behaviour of the two cantilever columns with identical properties but different stirrup spacing. The column with the stirrup spacing of $S=60\text{ mm}$ shows a much better cyclic behaviour in terms of ductility (failed at 6% drift), energy dissipation and plastic deformation capacity. Whereas, the cyclic behaviour of the column with $S=180$ shows a brittle behaviour (failed at 3% drift). This is the main reason that makes this flexural dominant failure mode to be brittle and the system lacks of energy dissipation capacity and plastic deformation compared to a seismic code-compliant RC structure.

The same failure mechanism was observed during the shaking table tests described in section 3.3. The deficiencies discussed in this section are all taken into consideration in the analytical modelling procedure.

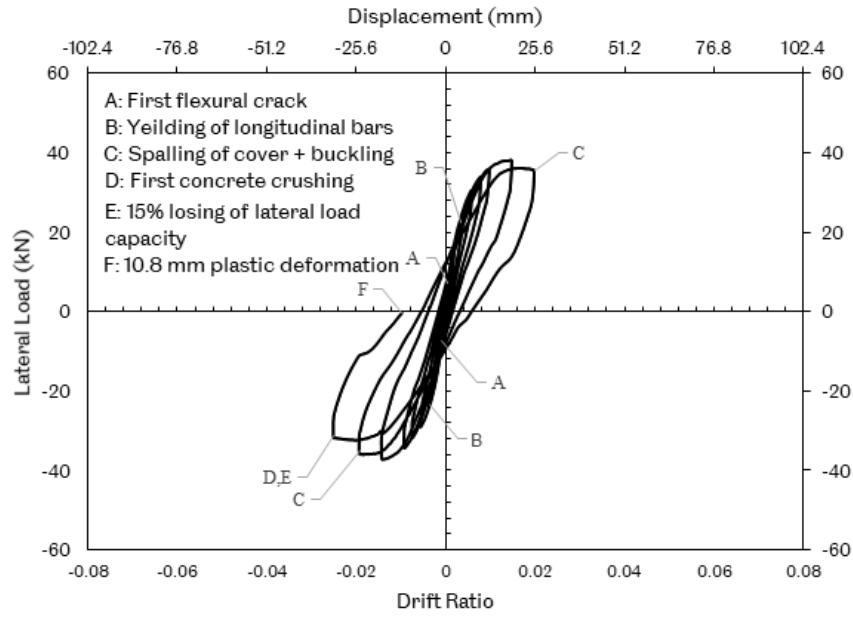


Figure 2-6: Observational cyclic behaviour for column with $S=180$ mm.

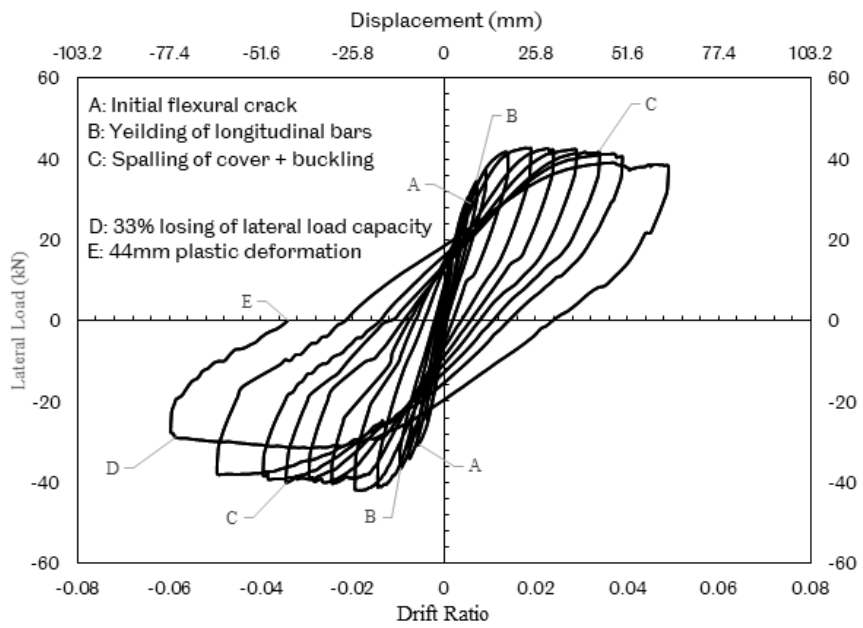


Figure 2-7: Observational cyclic behaviour for the column with $S=60$ mm.

2.3 Retrofitting of RC Structures Using FRP and PTMS

2.3.1 Introduction

To reduce the seismic vulnerability of substandard RC structures and enhance their local and global ductility level, it is crucial to locally strengthen columns and beam-column joints to improve their seismic performance. The seismic behaviour of substandard RC buildings can be improved by using popular external jacketing techniques; these confinement methods are more socioeconomically friendly compared to demolishing or reconstructing the whole RC structure (Mukherjee and Joshi, 2005, Al-Salloum et al., 2011). This PhD analytically processes the effect of the FRP and Post-Tensioned Metal Straps (PTMS) external jacketing techniques to investigate the enhanced seismic behaviour of upgraded substandard RC buildings (retrofitted with FRP/PTMS) and to derive upgraded fragility curves. Both external jacketing techniques reduce the bond-slip of the longitudinal rebars plus delaying the occurrence of longitudinal rebar buckling since both softening behaviours are affected by confined concrete properties.

2.3.2 Background

Two of the main conventional external jacketing retrofitting techniques for substandard RC buildings are: a. jacketing with steel plates and b. concrete/shotcrete jacketing. The seismic performance of substandard RC joints is improved (in terms of strength, ductility and stiffness) after being retrofitted with concrete/shotcrete jacketing based on numerous experimental studies (Corazao and Durrani, 1989, Tsonos, 2010, Karayannis et al., 2008, Alcocer and Jirsa, 1993, Shannag et al., 2002). Steel jacketing also proved to be effective by enhancing the seismic behaviour of RC columns and joints (especially ductility) (Corazao and Durrani, 1989, Ghobarah et al., 1996, Biddah et al., 1997).

The popularity of using concrete/steel jacketing methods has dropped during the past decades due to their disadvantages compared to innovative recently developed

jacketing techniques (e.g. jacketing with FRP or Post Tensioned Metal Straps (PMTS)). In general, retrofitting with concrete/steel jackets are highly invasive, time-consuming, labour intensive and also can disrupt the functionality of the building during retrofitting. For steel jacketing, heavy equipment is needed as in-situ welding is required by specialised welders. The effectiveness of the steel/concrete jacketing highly depends on the full contact of the jacket to the concrete surface which makes the confinement procedure difficult to assess during application and modelling. Both retrofitting techniques (steel/concrete jacketing) will considerably increase the mass of the building, forcing the structural members to be exposed to higher levels of seismic forces.

External jacketing can be split into two main categories: Active and passive confinement. Active confinement allows the lateral pressure from the jacket to be applied to the concrete from the initial stage (e.g. PTMS jacketing). While in passive confinement (e.g. FRP jacketing) the lateral pressure will be engaged after lateral expansion of the RC confined section (Moghaddam et al., 2010b).

The sections below describe the aforementioned external jacketing strengthening techniques using FRP and PTMS with a highlight on their advantages.

2.3.3 External jacketing using FRP

To enhance the seismic performance of an RC member, external jacketing with FRP sheets is employed using the lay-up procedure: the sheets are impregnated with resin and then wrapped around the areas of the element that need strengthening. The strengthening area can be confined entirely (full jacket) or partially in the form of strips (Figure 2-8). There are four main types of FRP used in construction as confining materials: Carbon Fibre Reinforced Polymers (CFRP), Glass Fibre Reinforced Polymers (GFRP), Aramid Fibre-Reinforced Polymers (AFRP) and Basalt Fibre-Reinforced Polymers (BFRP).



Figure 2-8: Application of external jacketing using FRP (Mosallam et al., 2014).

The advantages of FRP jackets compared to traditional steel/concrete jacketing methods are the high strength-to-weight ratio, high resistance to corrosion, high durability, prompt in-situ application, flexibility to confine different shapes of structural members and minimal change in cross-sectional geometry. FRP jacketing techniques are usually less invasive/labour-intensive than traditional techniques such as concrete or steel jacketing.

2.3.4 External jacketing using PTMS

External jacketing with PTMS technique was developed by Frangou et al. (1995). This method fastens high-strength ductile steel straps around the RC member by applying post-tensioning using strapping tools similar to these used in the packaging industry (Figure 2-9). The post-tensioning force is then maintained with metal seals acting as the mechanical fastening method. The application of post-tensioning makes the technique to be characterised as active confinement, thus the ductility and the capacity of the structure increases before applying axial load.

PTMS retrofitting has advantages compared to other external jacketing confinement methods (steel, concrete and FRP jacketing), such as prompt application, low material

cost and ease of maintenance (removing/replacing damaged straps and seals is easy, since no adhesive or sophisticated equipment are needed).



Figure 2-9: External jacketing with PTMS (Imjai et al., 2018, Garcia et al., 2017).

2.3.5 Analytical modelling approach

The effect of external jacketing with FRP/PTMS can be taken into consideration by modifying the constitutive relationship of externally confined concrete in the plastic hinge zones (Binici and Mosalam, 2007). The effect of different parameters on the confinement effect of FRP (effect of pre-damage, cyclic loading, fibre orientation, corner radius, anchorage length, etc) has already been investigated experimentally, whilst stress-strain relationships have been developed for the FRP confined RC sections (e.g. (Ilki et al., 2008, Lam and Teng, 2003, Samaan et al., 1998)).

Similar to FRP retrofitting, various stress-strain relationships for the PTMS confined RC sections have been also proposed (e.g. (Moghaddam et al., 2010a, Ma et al., 2016)).

The following subsections present representative confinement models which can be used in analytical analyses for substandard RC buildings, to consider the confinement effect of external retrofitting using FRP or PTMS on concrete.

2.3.5.1 FRP-confined concrete

Biskinis and Fardis (2013) developed a numerical model to predict FRP confinement in concrete. The effect of FRP retrofitting was modelled by changing the confined concrete properties according to using Equation 2-1, Equation 2-2 and Equation 2-3.

$$f_{cc} = f_c \left[1 + 3.5(\alpha_f \rho_f f_f / f_c)^{0.75} \right] \quad \text{Equation 2-1}$$

$$\varepsilon_{cc} = 0.002 \left[1 + 5 \left(\frac{f_{cc}}{f_c} - 1 \right) \right] \quad \text{Equation 2-2}$$

$$\varepsilon_{cu,c} = 0.0035 + \left(\frac{10}{h} \right)^2 + 0.4 \alpha_f \alpha_{eff,j} \min \left(0.5, \frac{\rho_f f_f}{f_c} \right) \quad \text{Equation 2-3}$$

Where;

ρ_f The geometric ratio of FRP, $\rho_f = \frac{2t_f}{b}$

$f_f = E_f (K_{eff} \varepsilon_{fu})$; ε_{fu} is the failure strain of FRP and $K_{eff}=0.6$ for FRP

h depth of cross-section in the loading direction in mm

$\alpha_{eff,j} = 0.5 \left[1 - \min \left(0.5, \frac{\rho_f f_f}{f_c} \right) \right]$ for CFRP and GFRP

$\alpha_f = 0.5$ for rectangular cross-section and continues jacketing

2.3.5.2 PTMS-confined concrete

A robust model which can predict the confined concrete properties using metal straps, was developed by Moghaddam et al., 2010a. To model the confined concrete core properties, Equation 2-4 to Equation 2-9 can be used. Figure 2-10 illustrates the confinement model as well as the critical/yield points.

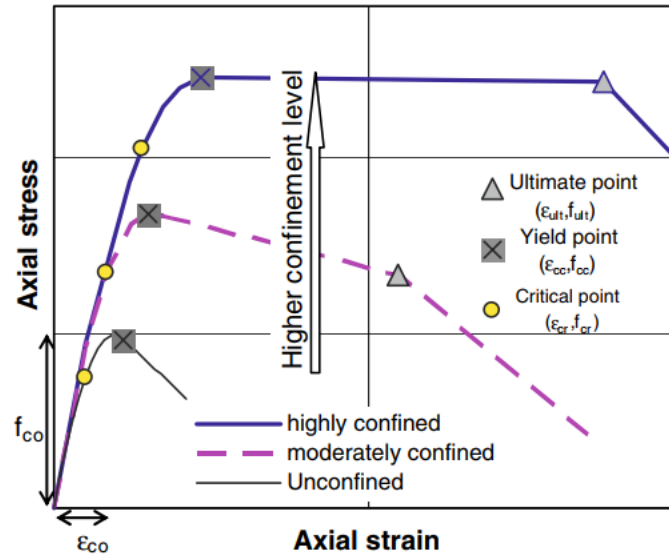


Figure 2-10: Schematic presentation of stress-strain behaviour of actively confined concrete specimens using PTMS (Moghaddam et al., 2010a).

$$f_{cr} = 0.85f_{cc} \quad \text{Equation 2-4}$$

$$\varepsilon_{cr} = 3.1 \times 10^{-4} \frac{f_{cr}}{\sqrt{f_{co}}} \quad \text{Equation 2-5}$$

$$\frac{f_{cc}}{f_{co}} = 1 + 8 \frac{f_{le}}{f_{co}} - 4 \left(\frac{f_{le}}{f_{co}} \right)^{1.2} \quad \text{Equation 2-6}$$

$$\varepsilon_{cc} = \varepsilon_{co} \left(\frac{f_{cc}}{f_{co}} \right)^{1.1} \quad \text{Equation 2-7}$$

$$\varepsilon_{ult} = 0.003 e^{(160 \frac{f_{le}}{f_{co}} \varepsilon_{ult}^*)} + 1.3 \frac{f_{le}}{f_{co}} \varepsilon_{ult}^* \quad \text{Equation 2-8}$$

$$\alpha = -62300 \left(\frac{f_{le}}{f_{co}} \right)^2 + 31150 \left(\frac{f_{le}}{f_{co}} \right) - 3900 \quad \text{Equation 2-9}$$

Where;

$f_{le} = K_e \times f_l$; effective lateral pressure

K_e ; is geometric effectiveness coefficient calculated according to Razvi and Saatcioglu (1999)

f_l ; applied lateral pressure

α ; the post-yield slope of connecting line between yielding point and ultimate point.

$f_{cr} , \varepsilon_{cr}$; critical point's stress and strain

$f_{cc} , \varepsilon_{cc}$; yield point's stress and strain

$f_{ult} , \varepsilon_{ult}$; ultimate point's stress and strain

ε_{ult}^* ; strap ultimate tensile strain

2.4 Discussion on plasticity element types in OpenSees

This section presents a critical review of two types of plasticity elements available in OpenSees: Lumped/concentrated plasticity and distributed plasticity element types. Plasticity is a crucial parameter in analyses of substandard RC buildings, hence, the chosen OpenSees element must accurately capture this important material characteristic.

2.4.1.1 Lumped-Plasticity element type

Lumped-plasticity models are essentially elastic elements with rotational springs at element ends to simulate inelastic deformations. The behaviour of the rotational springs is empirically derived, and as a result, the element behaviour has to be known a-priori, which makes this approach unsuitable for determining element based vulnerability but can be useful to determine overall structural level behaviour.

2.4.1.2 Distributed-Plasticity element type

Forced-based Elements (FBEs) and Displacement-Based Elements (DBEs) allow the plasticity to spread along the member. The fibre section method allows higher characterisation detailing of the nonlinearity distribution along with RC elements by

considering various behaviour of material constituting the RC cross-section (D'ayala et al., 2014).

In distributed plasticity, element yielding is allowed to happen at any location along the member, which is especially important in elements with distributed loading such as gravity loads and infill walls. The disadvantages of using DBE over FBE for nonlinear analysis of RC structures are well known and discussed by many researchers: The DBE approach unrealistically overestimates the stiffness and the strength of the element compared to the FBE formulation (Calabrese et al., 2010, Coleman and Spacone, 2001, Neuenhofer and Filippou, 1997). The main issues with DBE are the constraints on the deformation fields imposed by DBE yield to exact solution only in the case of linear elastic material and nodal loads. Furthermore, equilibrium in FB formulations is verified pointwise along the element length, whereas in DBE the internal forces are in equilibrium with the nodal forces in an average sense (Calabrese et al., 2010). This leads to two main drawbacks for DBE. Since the general equilibrium is not verified, the combination of forces acting on each section can be unrealistically off, therefore unreliable results (such as curvature or strains) can be given by the DBE, at the sectional level.

If the fibre discretisation model is used with the DBE which considers the interaction between axial force and bending moment, the sectional level behaviour of each element is dependent on the number of elements used to model the frame (Calabrese et al., 2010). To overcome the localisation issues arising from using the FBE, different approaches were proposed by many FE researchers focusing on regularisation techniques of FBE (Coleman and Spacone, 2001, Scott and Ryan, 2013, Lee and Filippou, 2009, Scott and Hamutçuoğlu, 2008, Kashani et al., 2016).

2.4.1.3 Conclusion

Since DBE are not suitable for seismic analysis for the above-mentioned reasons and to avoid the localisation issues of FBE, the element type "forceBeamColumn" element by Scott and Ryan (2013) can be used in analytical models for substandard RC

buildings. This element type allows the plasticity to spread along the member length and it is reported to have a good agreement with experimental results, without suffering from localisation issues as the integration points are modified (Scott and Ryan, 2013).

CHAPTER 3 DESCRIPTION OF TESTS

3.1 Introduction

This chapter presents a detailed description (including testing set-up and instrumentation) of tests previously performed by researchers of The University of Sheffield (UOS) and Istanbul Technical University (ITU). These experimental results were used to validate the proposed FE modelling approach in capturing the actual structural response of substandard RC elements/buildings. The case study building is also described in detail, an existing 4-storey substandard RC building located in Istanbul, Turkey, which is used to derive adaptive and upgraded vulnerability/fragility curves for seismic vulnerability assessment.

The tests comprised four reversed cyclic tests on substandard full-scale substandard cantilever RC columns (¹ITU research group) and two full-scale shaking table tests of one-bay two-storey substandard RC frames (ECOLEADER and BANDIT projects, UOS) (Garcia et al., 2017).

3.2 Full-Scale Cantilever RC Column Experiments

The experimental study described in this section, was conducted at the Structural and Earthquake Engineering Laboratory of Istanbul Technical University (ITU).

¹ The data is provided by ITU group as part of a RCUK-TÜBİTAK Research Partnership Project entitled “Rapid Earthquake Risk Assessment and Post-Earthquake Disaster Management Framework for Substandard Buildings in Turkey”

3.2.1 Specimens and material properties

Four cantilever RC columns were tested with a cross-sectional size of 200 mm x 300 mm, representing typical substandard RC columns in developing earthquake-prone countries, made with low concrete strength and plain longitudinal rebars of low-strength steel grade. All columns were designed to have a flexural failure, hence, they were well anchored in the base. The spacing between transverse links varied for each column (60, 90, 120 and 180 mm), to examine buckling of the longitudinal rebars. Figure 3-1 shows a typical example of a column with transverse reinforcement spacing of 90 mm (the other three columns had the same geometrical and mechanical characteristics varying only in spacing of transverse links). A single batch of ready-mix low-strength concrete (compressive strength 10 MPa, concrete cover 15 mm) was used to cast the columns (mix materials in kg/m^3 , Portland cement 215, crushed aggregates 923, sand 1104, water 232) and superplasticiser 2.75 lt/m^3 .

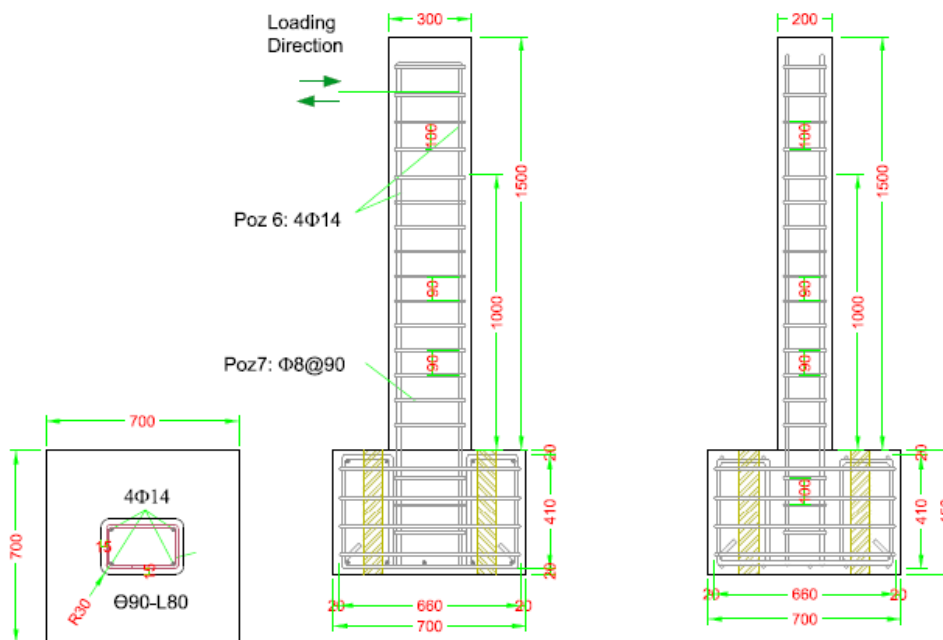


Figure 3-1: Column reinforcement details.

The column height above the base footing, was 1500 mm. The footing, used for restraining the rotation of the column, was 700 mm x 700 mm (cross-section) x 450 mm (height). Four 14mm diameter plain rebars of $f_y=320$ MPa were used, providing an

approximate longitudinal rebar reinforcement ratio of 1% while, 8mm deformed stirrups of $f_y=510$ MPa were used, as transverse reinforcement. The mechanical characteristics of the reinforcement were evaluated by direct tensile tests according to TS EN ISO 6892-1 (see Figure 3-2).

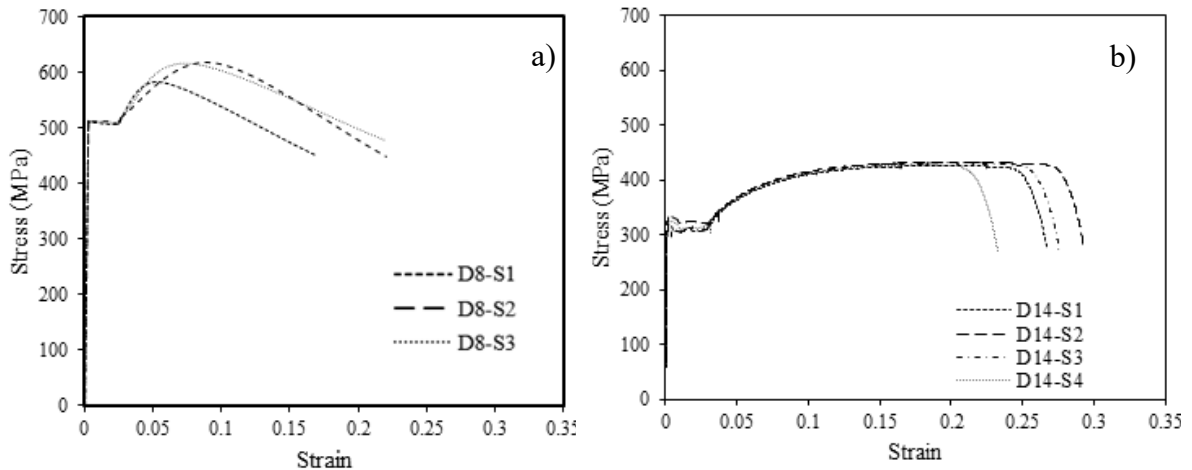


Figure 3-2: Mechanical characteristics of reinforcing rebars a) 8mm and b) 14mm diameter.

3.2.2 Test setup and instrumentation

The columns were subjected to both axial and reversed cyclic lateral loading. The axial force was applied by a 50kN capacity hydraulic jack reacting against a rigid steel beam tied to the strong floor with steel rods. The axial force was measured by a 100kN capacity load cell, placed on the top face of each column using a special capping arrangement. The lateral load was applied at the top of the columns using a 250kN capacity stroke (displacement stroke capacity of ± 300 mm) at 1280 mm above the column footing, reacting against a strong reaction wall (Figure 3-3 (a)). The lateral load was applied in displacement control following the loading protocol (see Figure 3-4).

Twelve Linear Variable Displacement Transducers (LVDTs) were used to capture displacements and rotations at critical sections of each column (plastic hinge region). Sixteen electrical strain-gauges were attached to the longitudinal and transverse reinforcement to monitor strain in various locations (Figure 3-3(b)).

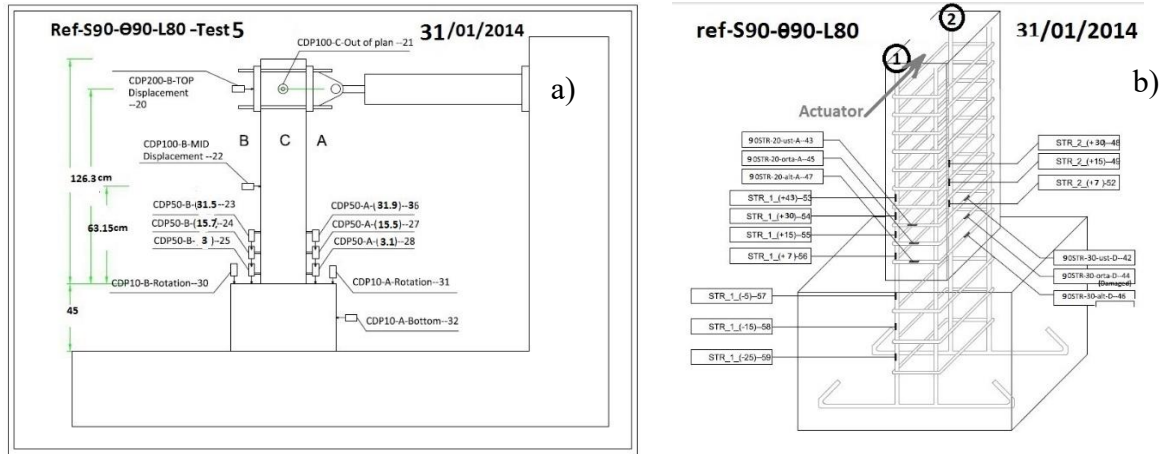


Figure 3-3: (a) Testing setup and LVDTs configuration and (b) strain-gauge location.

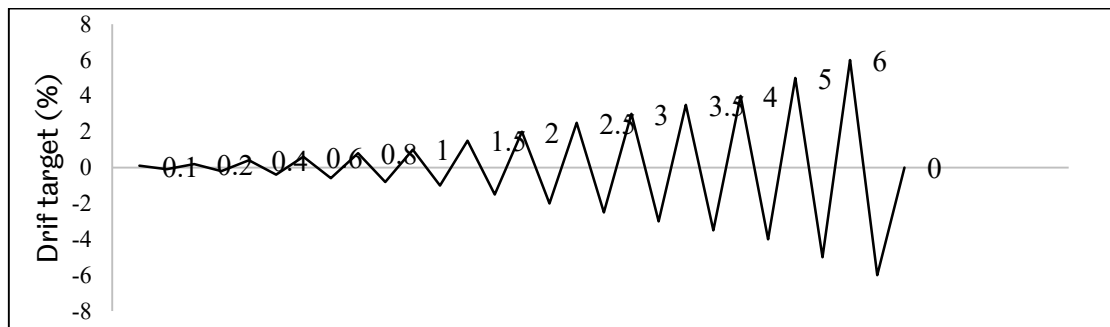


Figure 3-4: Loading protocol.

3.3 Full-Scale Shaking Table Experiments

The experimental data from the shaking table tests of two full-scale one-bay two-storey substandard RC frames was used to verify the analytical model of this PhD study.

3.3.1 Specimens and material properties

The first frame (ECOLEADER project) was designed and built according to a typical outdated pre-seismic construction European practice from the 60s (Garcia et al., 2010). The tested structure was a symmetric two-storey one-bay RC frame which, had

dimensions of 4.26 x 4.26 m in plan and a height of 3.3 m for both stories. Figure 3-5 (a, b) show the general view of the frame and details of the structural elements, respectively.

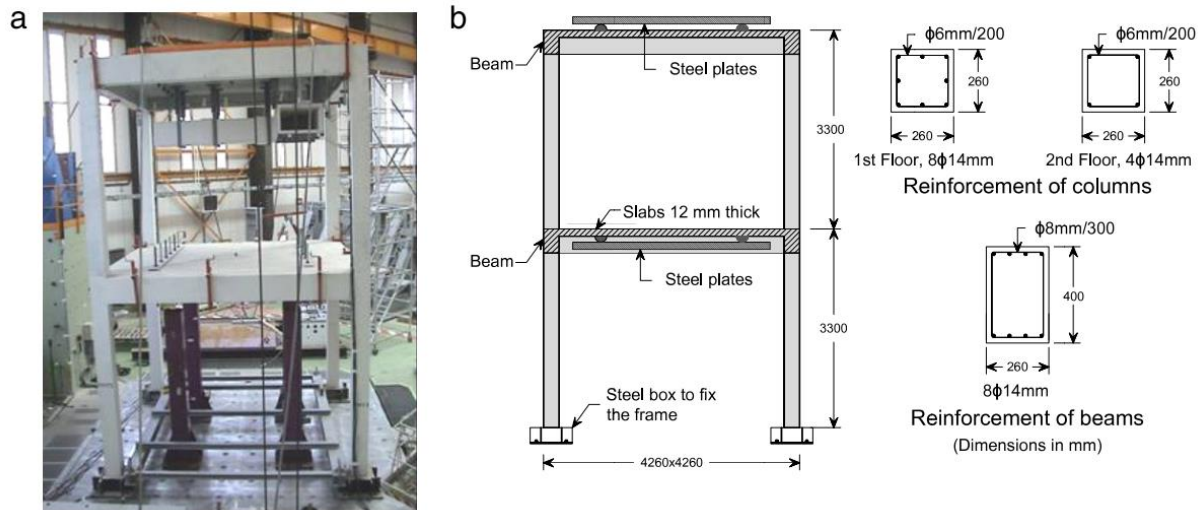


Figure 3-5: (a) General view and (b) frame geometry and sectional details. (Garcia et al., 2010)

The average material properties obtained based on tests were as follows: Yield and ultimate strength of steel reinforcement were $f_y=551$ MPa and $f_u=656$ MPa, and concrete compressive strength and modulus of elasticity were $f_c=20$ MPa and $E_c=25,5$ GPa, respectively. An additional mass of 9.0 tonnes (steel plates) was secured to each floor as dead loading (Figure 3-5 (b)).

The second frame (BANDIT project) was also a one-bay two-storey substandard RC frame and its geometry is identical to the ECOLEADER building. While the column sections are the same as the ECOLEADER frame, the beam sections are different. Figure 3-6 presents the general view of the frame, whilst Figure 3-7 gives the geometry and reinforcement detailing for beams and columns.



Figure 3-6: General view of BANDIT bare frame (Garcia et al., 2014)

The average mechanical properties of $\Phi 14$ mm longitudinal reinforcement obtained from direct tensile tests were $f_y=526$ MPa and $f_u=616$ MPa. Separate batches of concrete were used for each storey with properties of $f_c=30.8$ MPa, $E_c=23.9$ GPa and $f_c=25.5$ MPa, $E_c=21.7$ GPa for the 1st and 2nd floor, respectively.

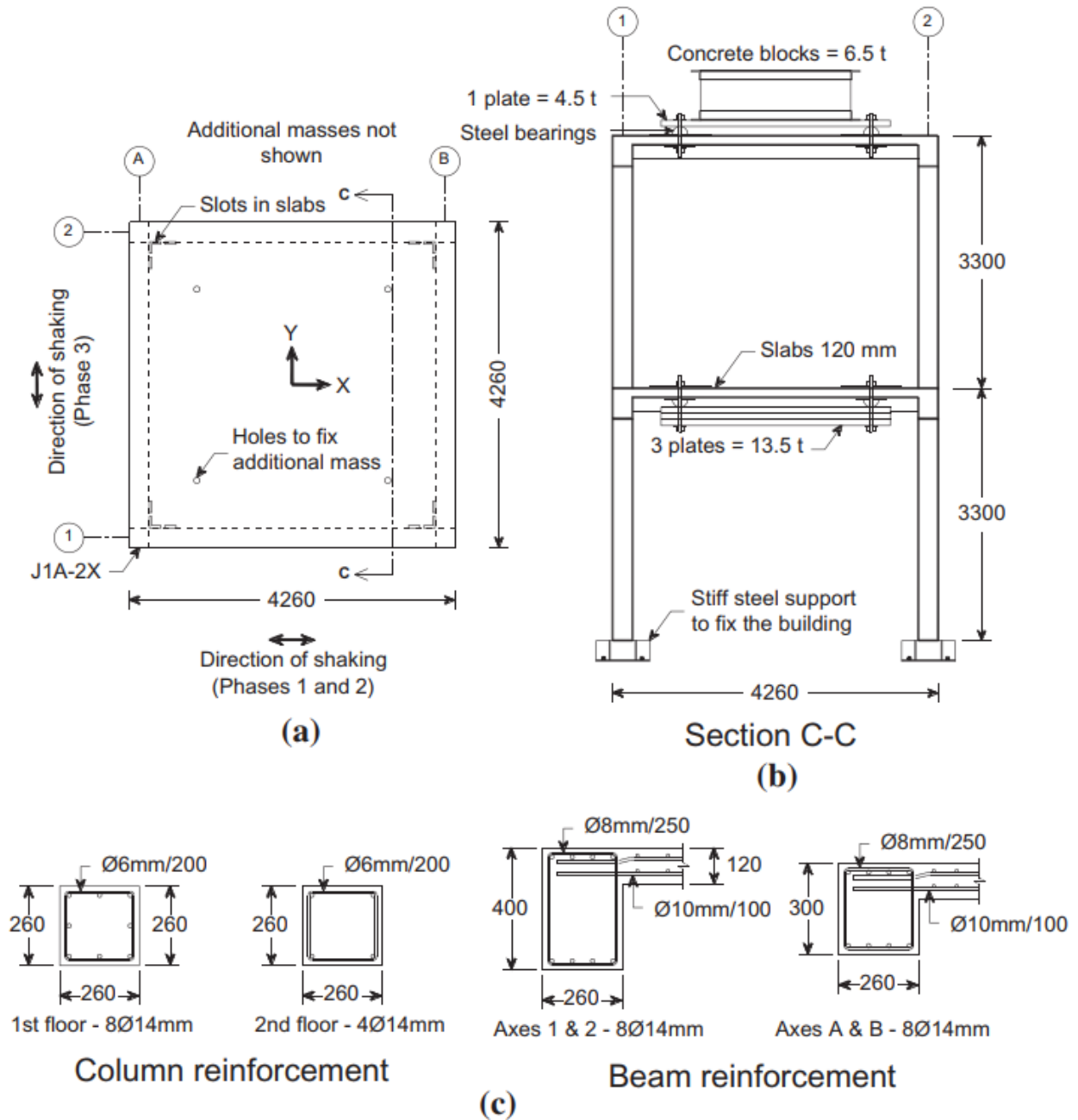


Figure 3-7: a) plan b) elevation and c) detailing of the beam and column sections for the 1st and 2nd storeys of Bandit frame (Garcia et al., 2014).

3.3.2 Test setup and instrumentation

The experimental programme consisted of unidirectional horizontal input shaking using incremental peak ground accelerations (PGA) levels ranging from 0.05g to 0.4g

for the ECOLEADER frame and from 0.025g to 0.15g for the BANDIT frame. For each frame, a single artificial ground motion record was used, based on Eurocode 8 (EC8) soil profile type C spectrum (Chaudat et al., 2005, Garcia et al., 2012).

Both structures were instrumented with acceleration and displacement transducers at each floor plus strain gauges attached to longitudinal and transverse reinforcement in various locations. The natural frequencies of the structure were obtained by executing white noise as an input signal, before the start and after the end of each test.

3.4 Existing Substandard RC Building: Case Study

The building selected for this PhD study, is a typical substandard residential 4-storey RC building located in Istanbul (Turkey) with an average 2.9m storey height and 11.6m total height. Figure 3-8 shows the general view of the building.



Figure 3-8: General view of the building.

The plan dimensions of the building are 10.1m X 10.4m. Figure 3-9 shows the storey plan, column arrangement and column section sizes.

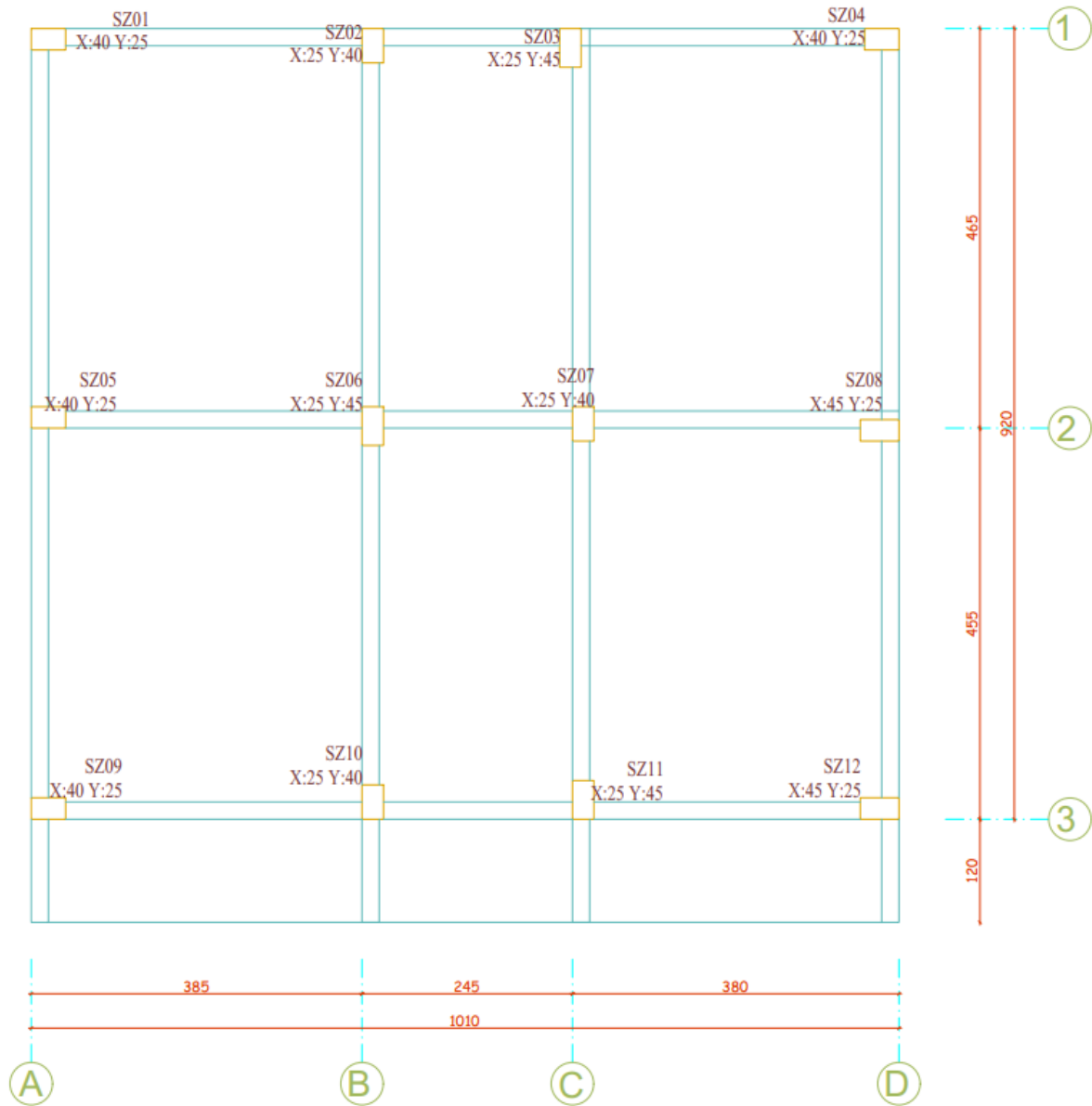


Figure 3-9: Storey plan.

The building was built in 1994, with plain S220 steel rebars for both longitudinal (14 mm diameter) and transverse reinforcement (10 mm diameter). The condition of reinforcement and construction quality as well as the detailing of the columns were checked, by removing the concrete cover from several columns in various locations of the building. Pachometer surveys were carried out on columns in several locations. The transverse reinforcement spacing of the columns was observed to be 200 mm (see Figure 3-10).



Figure 3-10: Cover removal and checking the columns' detailing.

The compressive concrete strength was 9.44 MPa, as the average of five uniaxial compressive tests performed on core samples extracted from various locations of the building (see Figure 3-11). The beams have a section of 250mm X 500mm with four 14 mm rebars and the two types of columns, 250 mm X 400 mm and 250 mm X 450 mm with four and six longitudinal 14 mm rebars, respectively. The columns longitudinal reinforcement ratio is 0.62% (section 250mm X 400mm) and 0.82% (section 250mm X 450m).



Figure 3-11: Concrete core samples taken from the building.

CHAPTER 4 METHODOLOGY

4.1 Introduction

This chapter describes the methodology followed to develop a novel advanced analytical seismic vulnerability framework. The main aim of the framework is to derive advanced adaptive vulnerability/fragility functions for substandard RC columns/buildings in developing countries.

The main methodology steps can be summarised as follows:

1. Data collection from various research projects conducted in the past from researchers of The University of Sheffield (UOS) and Istanbul Technical University (ITU) (See Chapter 3).
2. Developing an analytical FE modelling approach using OpenSees (Mazzoni et al., 2007) capable of capturing the behaviour of substandard RC columns/frames considering degrading behaviours (slippage of longitudinal rebars, buckling of longitudinal rebars and pinching effect (introduced by buckling)) at both local (strain, curvature and rotation) and global levels (inter-storey drift, lateral force and global displacement).
3. Validating the analytical FE modelling approach with the collected experimental data (Step 1).
4. Developing a seismic vulnerability assessment framework by linking proprietary Matlab code with OpenSees to automate the analysis procedure and conduct advanced seismic vulnerability assessments. This framework is capable of deriving adaptive fragility/vulnerability functions considering various parameters (e.g.

transverse bar spacing, storey height, steel grade, concrete compressive strength, external jacketing with FRP/PTMS).

5. Conducting advanced probabilistic seismic fragility analysis for the ITU column and substandard existing 4-storey building. Upgraded fragility curves are also obtained using hypothetical FRP retrofitting (1-layer of CFRP for column scenario, 3 layers of CFRP for 4th -storey substandard building – case study).
6. Comparing the derived adaptive fragility curves with several well-known existing fragility curves available in the literature (4-storey substandard building – case study).

4.2 Analytical FE modelling and validation

4.2.1 Introduction

To determine the vulnerability of structures using a numerical approach, accurate numerical models are required to capture the behaviour of substandard elements. The Opensees package (Mazzoni et al., 2007) offers several material models that can simulate material nonlinearities, longitudinal rebar buckling and bond-slip behaviour which are the most critical parameters in a structural response analysis of substandard RC buildings/columns.

To verify the analytical tool, a comparison was made between the analytical and experimental results using global and local parameters, such as: change of structural period, inter-storey drift (global damage indices) and rotation-based damage index (local).

The following sections discuss in detail the analytical modelling approach proposed for capturing the behaviour of substandard RC columns and buildings.

4.2.2 Finite element modelling of substandard RC columns

This section presents the proposed FE modelling approach, considering the common deficiencies in substandard RC columns. Buckling of longitudinal reinforcement and bond-slip behaviour, are the two main identified degrading behaviours for substandard RC columns and they were taken into account in the analytical modelling procedure.

4.2.2.1 The finite element modelling approach

The columns were modelled using two main elements. A “zerolengthSection” element and a “forcebeamcolumn” element. After critical evaluation of DBE and FBE (section 2.4), for the analyses conducted in this PhD study, it was decided “forcebeamcolumn” element is the most suitable one. A “zerolengthSection” element at the base of the columns uses duplicate nodes to model rebar slip at the foundation interface (Mazzoni et al., 2006). The column itself was modelled by using a “forcebeamcolumn” element. To account for buckling, the stress-strain characteristics of steel were introduced in compression only, within the anticipated plastic hinge zone.

4.2.2.1.1 Finite element model of substandard RC columns

A fibre-based structural modelling technique was used for modelling the structural elements. This method divides a structural element into a two-end frame element and links each boundary to a discrete cross-section with grids of fibres. The material’s nonlinear stress-strain behaviour in each fibre is integrated to obtain force and stiffness parameters over the length using finite element interpolation functions which must meet the compatibility and equilibrium conditions.

In fibre-based analytical models, materials have only unidirectional strength and stiffness and their behaviour is defined in terms of stress-strain. OpenSees provides several predefined constitutive models for each material type. During the analysis, fibre sections are assumed to remain plane. In RC structures, the fibre section is modelled with predefined concrete and steel materials. The section is divided into a

number of concrete segments where the steel fibres will be located. Strain compatibility between reinforcement and surrounding concrete is assumed. The sectional reactions under force and moment are in terms of axial strain at mid-section and curvature. A unique solution of this deformation combination will be obtained based on the moment-curvature analysis of the section.

The forceBeamColumn element (Scott and Ryan, 2013) with HingeRadauTwo integration configuration is used to model the columns. Figure 4-1(a) shows the detail of the fibre section approach to model the RC section and Figure 4-1(b) presents a typical column configuration. In this element type two-point, Gauss integrations are assigned over plastic hinge zones at each end, plus two integration points on the element interior (points 3-4). Material nonlinearity is considered with a fibre discretisation cross-section at each integration point. Since during the experiment, the direction of axial load during the reversed cyclic experiment was maintained parallel to the member (to eliminate any secondary moment effect), a linear geometric transformation formula was used to get the global response of the system.

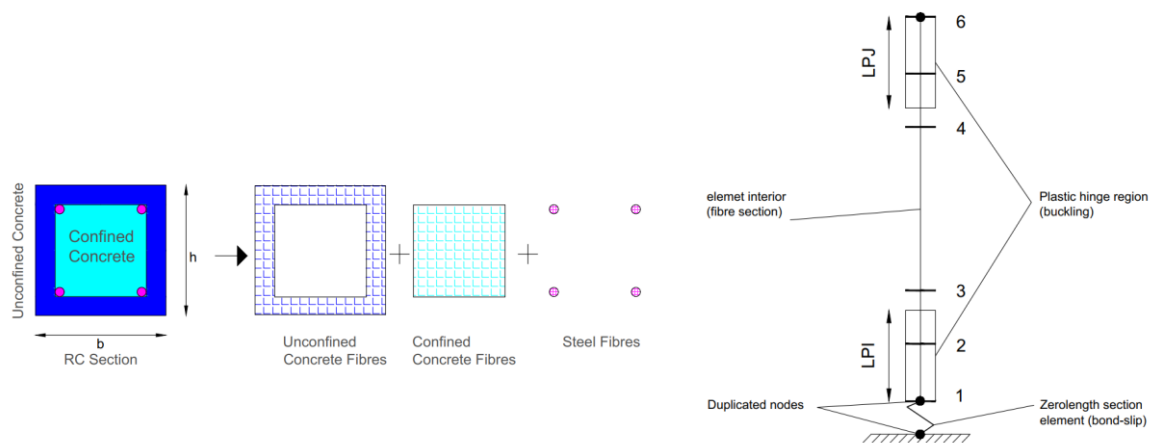


Figure 4-1: (a) Fibre section approach (b) column's assembly and integration points configuration.

4.2.2.2 Uniaxial material behaviour including the bond-slip and inelastic buckling behaviour

The following sections present the material models used to model the substandard RC columns.

4.2.2.2.1 Concrete model

Concrete02 material model is used to represent the uniaxial monotonic and cyclic behaviour of confined and unconfined concrete. The results of concrete core tests were used to provide the key parameters for the unconfined concrete. The confinement effect due to stirrups was taken into account using the Mander confinement model (Mander et al., 1988). Whilst the unconfined concrete model remained the same for all columns, the confinement model was different for each column since the spacing of stirrups varied. Table 4-1 gives the parameters used in the analysis for both confined and unconfined concrete.

Table 4-1: Parameters used for defining concrete.

Type	S (mm)	f_c (MPa)	ϵ_0	f_u (MPa)	ϵ_u
UC	All	10.00	0.0015	5.00	0.005
C	60	17.30	0.007	13.80	0.02
C	90	14.62	0.005	11.70	0.02
C	120	13.10	0.0036	11.09	0.02
C	180	11.60	0.0035	8.00	0.02

Where:

- UC/C Unconfined/Confined concrete
- S Stirrup spacing
- f_c concrete compressive strength at 28 days

ϵ_0	concrete strain at maximum strength
f_u	concrete crushing strength
ϵ_u	concrete strain at crushing

4.2.2.2 Reinforcing steel model including the effect of inelastic buckling

The direct uniaxial tensile tests on plain longitudinal steel rebars showed a typical behaviour for this type of mild steel after yielding, exhibiting a large plateau before strain hardening (Figure 3-2 (b)). To simulate this behaviour, the uniaxial “Reinforcing Steel material” model was used which is based on work conducted by Chang and Mander (1994). This model was used for parts of the column outside the plastic hinge region. Table 4-2 gives details of the parameters used for the reinforcing longitudinal steel rebars. All yield strength values for both longitudinal and transverse rebars are taken directly from the experimental results as mentioned in section 3.2.

Table 4-2: Parameters for modelling steel rebars outside the plastic hinge zones.

f_y (MPa)	f_u (MPa)	E_s (MPa)	E_{sh} (MPa)	e_{sh}	e_u
320	430	$2.0e^5$	5000	0.03	0.2

Where:

f_y	Yield stress in tension
f_u	Ultimate stress in tension
E_s	Initial elastic tangent
E_{sh}	Tangent at initial strain hardening
e_{sh}	Strain corresponding to initial strain hardening
e_u	Strain at peak stress

Buckling behaviour of longitudinal rebars: To consider the buckling behaviour of longitudinal rebars in the plastic hinge region, the post-yield compressive behaviour of steel was modified using the buckling model developed by Dhakal and Maekawa (2002) (Figure 4-2, Equation 4-1 and Equation 4-2). This model was developed using tests on plain rebars only (ignoring the effect of concrete cover on the buckling behaviour). Previous studies on the nonlinear cyclic response using such rebars revealed that buckling led to a more severe pinching effect than expected (Kashani et al., 2013).

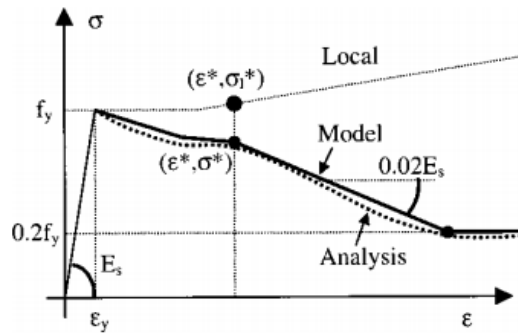


Figure 4-2: Buckling model for plain steel (Dhakal and Maekawa, 2002)

$$\frac{\varepsilon^*}{\varepsilon_y} = 55 - 2.3 \sqrt{\frac{f_y}{100} \frac{L}{D}}; \varepsilon^*/\varepsilon_y \geq 7$$

Equation 4-1

$$\frac{\sigma^*}{\sigma_l} = \alpha \left(1.1 - 0.016 \sqrt{\frac{f_y}{100} \frac{L}{D}} \right); \sigma^* \geq 0.2f_y$$

Equation 4-2

Where:

- f_y Yield stress in tension
- L Stirrup spacing
- D Longitudinal bar diameter
- E_s Initial elastic tangent
- ε^* Intermediate point strain
- σ^* Intermediate point stress

- σ_l^* Corresponding stress for ε^* from the tension side of behaviour
- α Constant considered 1 for linear hardening bars

Effect of concrete cover and stirrup spacing on buckling: To examine the effect of concrete cover and stirrup spacing on buckling, a short FEA study was conducted using Abaqus (Figure 4-3).

The effect of concrete cover was modelled using lateral pressure in one direction on the rebar from 1ft (concrete cover times the tensile strength of concrete (ft)) up to 5ft. To trigger buckling, an initial imperfection of 0.1 mm was introduced. The results of the analysis show that concrete cover can substantially prevent buckling but only at higher L/D ratios (Figure 4-3) (Note: in these models, L varied but D was kept constant D=14 mm).

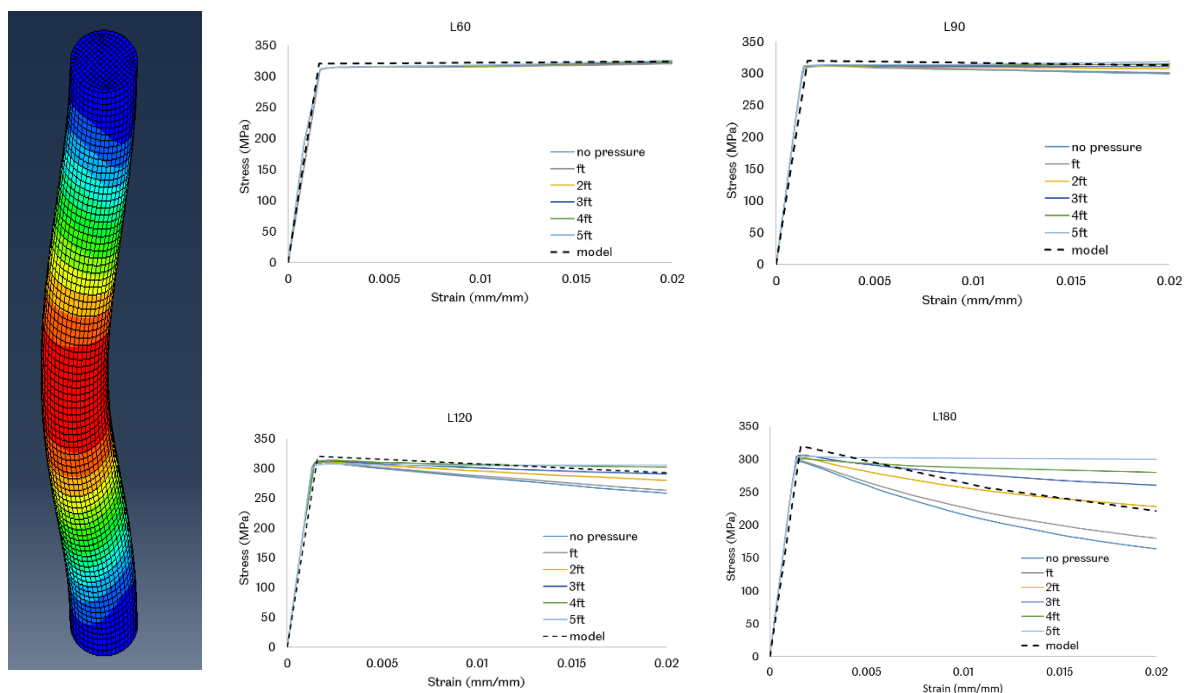


Figure 4-3: FEA to take into account the effect of cover on the inelastic buckling of longitudinal rebars.

Uniaxial material behaviour of steel rebars: The Hysteretic material model in OpenSees was used to represent the uniaxial material behaviour of steel rebars over

the plastic hinge region. This model allows the definition of different behaviours in compression and tension and has two predefined parameters to control the pinching effect of the cyclic rule. Table 4-3 shows the calculated parameters used for buckling of longitudinal steel rebars for the compression zone, while the direct tensile experimental result (Figure 3-2 (b)) was used to define the tension side.

Table 4-3: Hysteretic material parameters for compression to consider buckling.

s1n (MPa)	e1n	s2n (MPa)	e2n	s3n	e3n	Pinch X	Pinch Y
320	0.0016	331.6	0.06	64	0.127	0.8	0.8
320	0.0016	302.4	0.046	64	0.105	0.8	0.8
320	0.0016	274.4	0.032	64	0.084	0.8	0.8
320	0.0016	256.2	0.012	64	0.059	0.8	0.8

Where:

S1n , e1n	stress and strain at 1 st point of the envelope in compression direction
S2n , e2n	stress and strain at 2 nd point of the envelope in compression direction
S3n , e3n	stress and strain at 3 rd point of the envelope in compression direction
pinchX	pinching factor for strain during reloading
pinchY	pinching factor for stress during reloading

4.2.2.2.3 Slip model for zero-length section element

Since the zero-length section element in OpenSees has a unit length, the uniaxial stress-strain material behaviour of both steel and concrete needs to be modified to simulate stress-slip. The longitudinal steel rebars are considered to be fully anchored into the foundation. To model slip on longitudinal bars, the stress-slip constitutive model by Zhao and Sritharan (2007), was used, derived from pull-out tests performed on fully anchored steel reinforcing rebars. The two important parameters in this

model are the rebar slip at member interface at yield, S_y , and ultimate stress, S_u (Equation 4-3).

$$s_y(mm) = 2.54 \left(\frac{d_b(mm)}{8437} \frac{f_y(MPa)}{\sqrt{f'_c(MPa)}} (2\alpha + 1) \right)^{\frac{1}{\alpha}} + 0.34 \quad \text{Equation 4-3}$$

Where:

- d_b longitudinal rebar diameter
- f_y yield strength of longitudinal rebar
- α Constant taken as 0.4 (CEB-FIP, 1993)
- S_u pinching factor for strain during reloading
 S_u is suggested to be 30–40 times S_y . In this study, S_u is taken as 35 times S_y .

The hysteretic uniaxial material model from the OpenSees library was used to assign the slip model to the steel fibres in the zero-length section element. Since most of the pinching is expected to develop during buckling of the longitudinal rebars, zero pinching was assigned to the slip model. Because the slip model is symmetric, the parameters considered for hysteretic material for the tension side are given in Table 4-4.

Table 4-4: Hysteretic material parameters for modelling rebar's slip.

s_{1n} (MPa)	e_{1n} (mm)	s_{2n} (MPa)	e_{2n} (mm)
320	0.5	430	16.4

Where:

- s_{1n} , e_{1n} stress and strain at 1st point of the envelope in compression direction
- s_{2n} , e_{2n} stress and strain at 2nd point of the envelope in compression direction

The slip of the longitudinal rebars on the tension side of the section, in combination with the high axial force and flexural compressive force, results in highly localised compressive stress at the extreme compressive fibre. This can cause localised damage, over a depth d_{comp} (Berry and Eberhard, 2006). In this study, $\frac{1}{3}$ of the length of the section was used as d_{comp} to convert the strain values of the concrete to slip.

The uniaxial material Concrete01 with zero tension was used to model the concrete in the zero-length section element (see Figure 4-4).

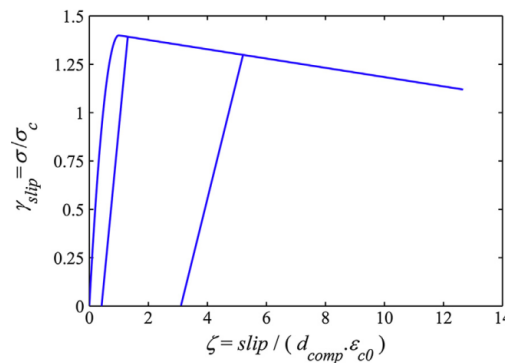


Figure 4-4: The concrete model considered in zero-length section element (Kashani et al., 2016).

4.2.2.2.4 Plastic hinge length calculation

To calculate and assign the plastic hinge length, the widely-used plastic hinge length formula developed by Bae and Bayrak (2008), was used (Equation 4-4).

$$\frac{l_p}{h} = \left[0.3 \left(\frac{P}{P_o} \right) + 3 \left(\frac{A_s}{A_g} \right) - 0.1 \right] \left(\frac{L}{h} \right) + 0.25 \geq 0.25 \quad \text{Equation 4-4}$$

Where;

h overall depth of the element

P applied axial load

$$P_o = 0.85f'_c(A_g - A_s) + f_yf_s$$

A_s tension reinforcement's area

A_g gross-sectional area of concrete column

L distance of critical section from point of contra flexure

Note: This approach was used to calculate the plastic hinge length for all RC models in this research.

4.2.2.3 Conducted analysis on column models

Since the distributed plasticity element model was used to model columns, a mesh sensitivity analysis was performed to ensure that the sectional response, in terms of moment-curvature, is correctly captured by OpenSees.

Reversed cyclic pushover analysis was conducted and the local structural response parameters (chord rotation, contribution of slip of reinforcement to the total rotation and maximum curvature from the most critical section of the column), as well as global parameters (global forces, drift), were compared with the experimental data.

4.2.3 Finite element modelling of substandard RC frames

The experimental results of two substandard shaking table RC frames (Ecoleader and Bandit projects) were used to validate the accuracy of the numerical model using local and global structural response parameters.

4.2.3.1 The finite element modelling approach

3D finite element models of both frames were developed in OpenSees following the same approach (fibre-based structural modelling) as described in Section 4.2.2. The only difference in the parameters is the sectional geometry and material mechanical characteristics. The p-delta effect is considered in the analytical model. The zero-length section element which was used to represent the bond-slip behaviour, is introduced to the model only for the columns' reinforcement. The zero-length element is assigned to the model for the column-to-joint connections (Figure 4-5). Concrete02 from the OpenSees library was used to represent the hysteretic concrete material behaviour. The use of Concrete02 material model was chosen over other available concrete models (e.g. Concrete04, Concrete07 and ConcreteCM) for the ease of convergence. Mander et al. (1988) concrete (confined and unconfined) material models were used.

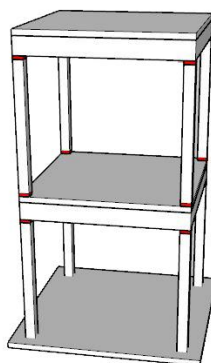


Figure 4-5: Placement of zero length section element to consider the bond-slip behaviour of longitudinal bars.

Columns and beams: The forceBeamColumn element type was used for both columns and beams. This element has three main zones two plastic hinge zones and a middle section. All zones are assigned with fibre sections, however, the main difference is that the plastic hinge zones for both columns and beams, have a hysteretic uniaxial material model assigned for reinforcement, to consider the effect of buckling. For the middle zone of the element steel02, Giuffre-Menegotto-Pinto steel material model (Filippou et al., 1983) was used to represent the hysteretic behaviour of reinforcement which is symmetric in the compression and tension zones without considering buckling effects. Table 4-5 shows the steel stress-strain material models.

Table 4-5: Steel02 parameters.

f_y (MPa)	E_0 (MPa)	b	R0	CR1	CR2
551	2.1e5	0.035	12	0.925	0.15

Where:

- f_y yield strength
- E_0 initial elastic tangent
- b train-hardening ratio (ratio between post-yield tangent and initial elastic tangent)
- R0, CR1, CR2 parameters to control the transition from elastic to plastic branches.
Recommended values: R0=between 10 and 20, cR1=0.925, cR2=0.15

Bond-slip behaviour of longitudinal reinforcement of columns to joints or foundation: To consider the bond-slip behaviour of longitudinal reinforcement of columns to joints or foundation, both ends of all columns have a duplicated node which is used to assign the “zerolengthsection” element. While these sections have the same geometry as the column sections, concrete and steel material characteristics are modified to be able to capture the bond-slip behaviour. Since the “zerolengthsection” element is considered by OpenSees to have the unit length, this means that the stress-strain relationship for steel can be considered as stress-slip. Hysteretic uniaxial material was used to assign the stress-slip behaviour to the longitudinal bars of the “zerolengthsection” element, whilst concrete01 uniaxial material behaviour was selected to model the concrete behaviour. Table 4-6 presents the longitudinal rebar’s material parameters considering the bond-slip behaviour. The same material model (Figure 4-4) is used for concrete fibres in the zero-length section element.

Table 4-6: Hysteretic material parameters for modelling rebar’s slip.

s1n (MPa)	e1n (mm)	s2n (MPa)	e2n (mm)
550	0.55	656	19.3

Where:

S1n , e1n stress and strain at 1st point of the envelope in compression direction

S2n , e2n stress and strain at 2nd point of the envelope in compression direction

4.2.3.2 Performed analysis on the 3d RC frame models

During the gravity analysis, the weight of the fixed steel plates on the slabs (which simulate the live/dead loading on each floor) are distributed evenly on the surrounding beams. Eigenvalue analysis was performed after applying the gravity loads to the model, to compare the frequency response of the structures with the experimental data. Then, a pushover analysis was performed considering the inverse triangular lateral loading, to further investigate the structural response before conducting any

dynamic analysis. Finally, dynamic analysis was performed, using the displacement histories recorded from the shaking table tests. To represent the actual experimental conditions where damage is accumulated after each level of seismic excitation, the same procedure was employed during the dynamic analysis: The capacity state of the structure was not restored to undamaged state after each dynamic analysis. Instead, the analytical output at different PGA levels was introduced from one dynamic analysis to the next one, taking into account the damage accumulation.

The global response of the structures was compared with the experimental data in terms of displacement histories of the first and second floors. The local response of the structures in terms of longitudinal rebar strains was also compared at the location of 13 cm below the first floor's joint.

4.2.4 Finite element modelling of the substandard 4-storey RC building (case study)

The finite element modelling approach (discussed above) showed promising results in terms of capturing the behaviour at both elemental level (substandard columns) and global level (3D shaking table frames). Hence, the same method was used to model the existing substandard 4-storey RC building which is used for the vulnerability/fragility analysis (chapter 3.4 for details of the building). The P-delta effect is considered in the analytical model.

It should be mentioned that this analytical modelling methodology can be applied to any substandard RC building with similar deficiencies and failure mechanism.

Table 4-7 shows the weight assumptions used to calculate the gravity loads.

Table 4-7: Weight calculation assumptions.

Item	Weight (t/m ²)	Item	Weight (t/m ²)
terrace slab	0.195	Openings	0.05
19 cm brick wall	0.32	top roof + slab	0.15
13 cm brick wall	0.25	Storey roof + slab	0.532
9 cm brick wall	0.2	stairs	0.352

4.3 Development of advanced probabilistic seismic vulnerability framework

4.3.1 Introduction

The capacity spectrum method (CSM) uses two main inputs (demand and capacity curves) which are plotted in the same graph (spectral acceleration versus spectral displacement), called Acceleration Displacement Response Spectrum (ADRS). The demand curve either can be a design spectrum or a record specific spectrum, and the capacity curve is the outcome of the Nonlinear Static Pushover Analysis (NSPA). However, firstly, the capacity curve needs to be plotted in a form of a bilinear or multi-linear curve. To take into account the effect of cyclic degradation of structural elements (which comes from cyclic behaviour of the material plus the pinching effect due to the buckling of the longitudinal rebar), the NSPA is replaced with the Reversed Cyclic Pushover Analysis (RCPA), providing two main advantages: The first advantage is that it captures the cyclic degradation which found not to be negligible when dealing with substandard structural elements. The second advantage has to do with the use of the envelope curve of the RCPA which eliminates the need for generating the capacity curve vs NSPA. The use of RCPA instead of monotonic pushover analysis can affect the performance point by up to 10%. After plotting these inputs into ADRS, CSM uses an iterative procedure to determine the maximum inelastic displacement of the analysed structure by defining the Performance Point (PP).

The following section presents the adapted CSM implemented into the novel advanced probabilistic seismic fragility framework developed in this PhD research.

4.3.2 Analytical Vulnerability Assessment

This section gives the methodology and theoretical assumptions behind the developed framework.

4.3.2.1 Capacity curve

The capacity curve, used for this PhD research, is the envelope curve of RCPA. The loading protocol followed for the RCPA, is according to (ATC-24, 1992) up to ductility level 8 (Figure 4-6). The capacity curve is transformed into a capacity spectrum (spectral coordinates) using Equation 4-5 and Equation 4-6 (Figure 4-7).

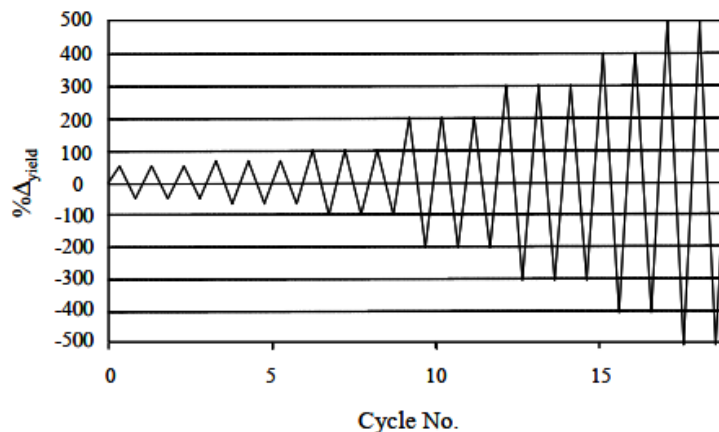


Figure 4-6: Loading protocol (ATC-24, 1992)

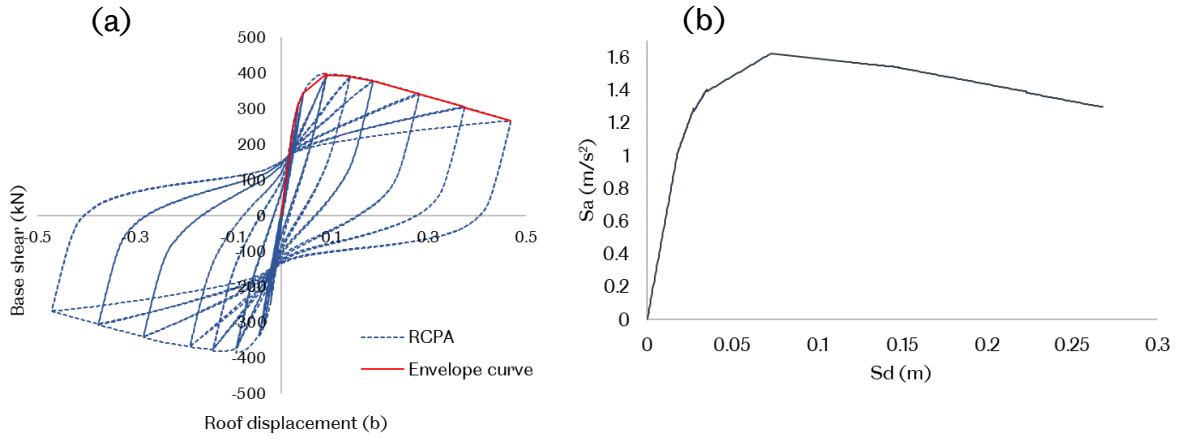


Figure 4-7: (a) capacity curve (b) capacity spectrum.

$$SA = \frac{f_{bs}}{m_1^*} \quad \text{Equation 4-5}$$

$$SD = \frac{U_n}{\Gamma_1 \Phi_{N1}} \quad \text{Equation 4-6}$$

Where;

$$\Gamma_1 = \frac{\sum_{i=1}^N m_i \Phi_{i1}}{\sum_{i=1}^N m_i \Phi_{i1}^2} \quad \text{Equation 4-7}$$

$$m_1^* = \frac{(\sum_{i=1}^N m_i \Phi_{i1})^2}{\sum_{i=1}^N m_i \Phi_{i1}^2} \quad \text{Equation 4-8}$$

Where;

f_{bs} base shear

U_n displacement at N^{th} floor

m_i lumped mass at the i^{th} floor

Φ_{i1} i^{th} floor's Eigenvector from fundamental mode Φ_1

N number of floor

m_1^* effective modal mass for the fundamental vibration

Γ_1 fundamental mode's participation factor

4.3.2.2 Demand curve

As a demand curve, either a site-specific design spectrum (taken from a recent hazard map of the assessed developing country) or, a record specific spectrum can be used. For this PhD research, the demand curve is the elastic response spectrum, specifically derived for the site of the building. Then, the response spectrum is converted to demand spectrum (spectral coordinates) using Equation 4-9 (Figure 4-8).

$$SD = \left(\frac{T}{2\pi}\right)^2 SA \quad \text{Equation 4-9}$$

Where;

SD displacement ordinate of the response spectrum

SA acceleration ordinate of the response spectrum

T corresponding period of vibration

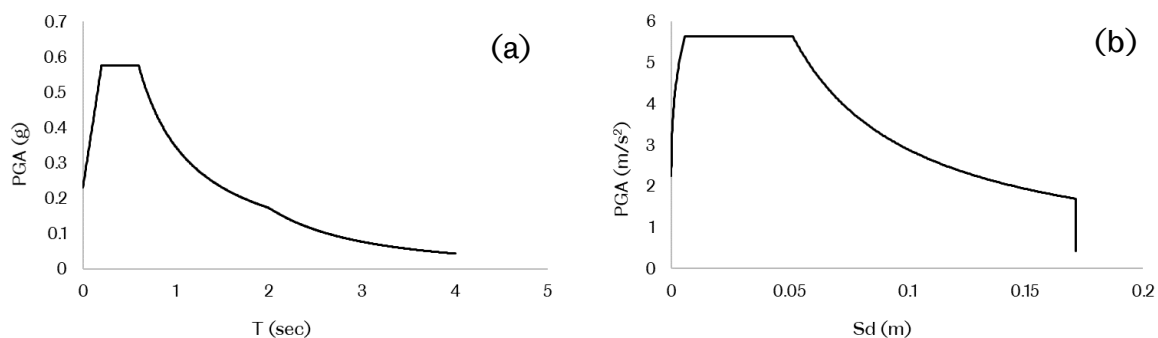


Figure 4-8: (a) response spectrum (b) demand spectrum.

4.3.2.3 Iterative CSM procedure to determine the PP

The main aim of this procedure is to estimate the maximum displacement (PP) of a nonlinear system with an equivalent linear system by using effective damping and effective period. In this procedure, the effective period and effective damping are functions of the ductility ratio. The steps, followed to derive the PP according to FEMA 440 (2005), are as follows (Figure 4-9):

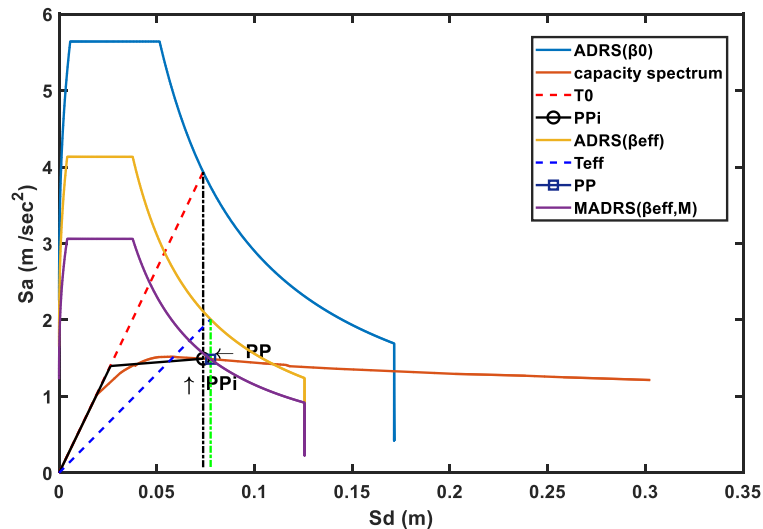


Figure 4-9: CSM (FEMA 440, 2005), procedure B.

1. A suitable elastic response spectrum (with 5% damping) is selected and converted into a demand spectrum which is denoted as $ADRS(\beta_0)$.
2. The demand spectrum is derived from the numerical analysis and plotted in the same graph.
3. An initial performance point is assumed based on equal displacement approximation (a line from the origin with the slope of T_0 is intersected with the demand spectrum. The intersection point's spectral displacement (d_{pi}) and the corresponding spectral acceleration (a_{pi}) from the demand spectrum with the same displacement (d_{pi}) are assumed to be the initial assumption for PP_{pi}).
4. To calculate ductility (μ) and post elastic stiffness (α), the yielding point is assumed for the initial PP. Bi-linearisation Procedure from (ATC-40, 1996) was used to derive the yielding point (d_y and a_y). The initial T_0 line is followed by a post yielding line connecting the yielding point with PP_i in the way that the areas under and above the capacity and bilinear curves are equal (Fig. 3-16).
5. Ductility and post-elastic stiffness are calculated using Equation 4-10 and Equation 4-11.

$$\alpha = \frac{\left(\frac{a_{pi} - a_y}{d_{pi} - d_y}\right)}{\left(\frac{a_y}{d_y}\right)}$$

Equation 4-10

$$\mu = \frac{d_{pi}}{d_y}$$

Equation 4-11

6. Using the calculated ductility and post-elastic stiffness from the previous step, and considering stiffness degrading hysteretic behaviour, the effective period (T_{eff}) and effective damping (β_{eff}) are calculated using Equation 4-12, Equation 4-13, Equation 4-14, Equation 4-15, Equation 4-16 and Equation 4-17. (Note: the constant values in the formulas below are selected from Tables 6-1 and 6-2, chapter 6 of (FEMA 440, 2005).

For $1.0 < \mu < 4.0$:

$$\beta_{eff} = A(\mu - 1)^2 - B(\mu - 1)^3 + \beta_0$$

Equation 4-12

For $4.0 \leq \mu \leq 6.5$:

$$\beta_{eff} = C + D(\mu - 1) + \beta_0$$

Equation 4-13

For $\mu > 6.5$:

$$\beta_{eff} = E \left[\frac{F(\mu - 1) - 1}{[F(\mu - 1)]^2} \right] \left(\frac{T_{eff}}{T_0} \right)^2 + \beta_0$$

Equation 4-14

For $1.0 < \mu < 4.0$:

$$T_{eff} = [G(\mu - 1)^2 + H(\mu - 1)^3 + 1]T_0$$

Equation 4-15

For $4.0 \leq \mu \leq 6.5$:

$$T_{eff} = [I + J(\mu - 1) + 1]T_0$$

Equation 4-16

For $\mu > 6.5$:

$$T_{eff} = \left\{ K \left[\sqrt{\frac{(\mu - 1)}{1 + L(\mu - 2)}} - 1 \right] + 1 \right\} T_0$$

Equation 4-17

7. After calculating the β_{eff} , the $ADRS(\beta_0)$ is rescaled to $ADRS(\beta_{eff})$ using the scale factor B using Equation 4-18 and Equation 4-19 (Note: since S_a and S_d are linked with Equation 4-9, after applying the scale factor B to S_a , S_d also needs to be adjusted (see Figure 4-9).

$$B = \frac{4}{5.6 - \ln \beta_{eff}} \quad \text{Equation 4-18}$$

$$(S_a)_\beta = \frac{(S_a)_0}{B(\beta_{eff})} \quad \text{Equation 4-19}$$

8. $ADRS(\beta_{eff})$ is modified to MADRS by multiplying the acceleration ordinates only by the M factor which is calculated using Equation 4-20 (see Figure 4-9).

$$M = \frac{a_{max}}{a_{eff}} = \left(\frac{T_{eff}}{T_{sec}}\right)^2 \quad \text{Equation 4-20}$$

9. The intersection of the capacity curve with the MADRS is the PP_i (estimated maximum elastic displacement of the structure).
10. A comparison between PP_i and the initial assumed PP_{pi} is needed. If the difference is acceptable (below 5%), P_i is valid and considered as the final PP (the range of acceptance is considered to be 2% for this research). Otherwise, the PP_i is replaced with PP_{pi} (step 3) and steps 4 to 10 are repeated until convergence is achieved.

4.3.3 Deriving vulnerability curve using OpenSees and Matlab

For deriving the performance point (maximum inelastic displacement of the structure/structural element) and the vulnerability curve, a Matlab code was compiled and linked with the OpenSees software to directly obtain necessary input and perform the vulnerability analysis as described below.

1. Performing a gravity analysis with OpenSees and keep the gravity loads constant for the structure.

2. Performing an Eigen-value analysis with OpenSees to derive the Eigenvectors and the Eigenvalue of the fundamental mode of vibration. This is needed to convert the capacity curve to capacity spectrum.
3. Performing NRCPA with OpenSees and record the base shear versus the roof displacement as one of the main inputs for the CSM. To derive the damage parameter used in vulnerability/fragility analysis, the following parameters are also recorded:
 - a. Local and global structural response in terms of sectional parameters (curvature and strain),
 - b. Elemental parameters (global forces and plastic rotation),
 - c. Storey level (storey shear and storey displacement/drift) and,
 - d. Global level (structural period, base shear and roof displacement).
4. Importing necessary data from OpenSees to Matlab code:
 - f. Eigenvectors of the fundamental mode of vibration,
 - g. Capacity curve and,
 - h. Damage parameters.Importing the demand curve into Matlab.
5. Converting the capacity curve to capacity spectrum and demand curve (response spectrum) to demand spectrum.
6. Following the procedure as described in section 4.3.2.3 to derive the PP.
7. Conducting analytical vulnerability assessment using CSM (section 4.3.2).

4.3.4 Conducting analytical vulnerability assessment using CSM method

Both local and global damage indices are calculated and compared with the shaking table tests (Ecoleader and Bandit projects) and the substandard column tests (from ITU) to evaluate their accuracy. PGA was used as the ground motion intensity measure since it is the most commonly used IM in the literature. Additionally, the use of intensity measure needs to be suitable with the type of analysis and method used to derive the vulnerability curves. In CSM the most suitable IM is PGA because of using design/site

specific spectrum with certain PGA. Spectral displacement and spectral acceleration IM are more suitable for IDA method to derive vulnerability curves.

To perform the seismic vulnerability analysis, the previously generated Matlab code for deriving PP was adopted. An additional loop function was added to the code (after step 10 of section 4.3.2.3); inside this loop, two steps are repeated to derive the vulnerability curve. The main aim of this loop is to calculate different PPs and their corresponding damage ratios to the various intensity levels of the selected demand spectrum to cover the damage ratio from 0 to 100%. For each iteration inside the loop, the selected demand capacity $ADRS(\beta_0)$ is scaled from lower to higher and the corresponding PP is derived. The damage parameters are calculated for each PP using the structural performance outputs recorded in NRCPA. The PGA varies from 0.01g to 1.0g with incremental steps of 0.1g. For all 100 PPs, PGA values and damage ratios are calculated and plotted in a graph to form the final vulnerability curve for a specific analysed structure.

4.3.4.1 Local and global damage index considered for vulnerability study.

For columns, the plastic hinge rotation, θ , is used as the local damage parameter. The ultimate and yield rotation of columns with plain bars, considering the bond-slip behaviour and cyclic behaviour with flexural-controlled failure, is calculated based on Grammatikou et al. (2018) using Equation 4-21 and Equation 4-22.

$$\theta_{y,top,i} = \frac{H_i(f_{y,i} + f_{0b,i}) + h_{b,i}(f_{0t,i} - f_{0b,i}) + l_{0,i+1}(f_{y,i} + f_{0t,i})}{2E_s Z_i} \quad \text{Equation 4-21}$$

$$\theta_{y,bot,i} = \frac{H_{i-1}(f_{y,i-1} + f_{0b,i-1}) + l_{0,i}(f_{y,i-1} + f_{0t,i-1})}{2E_s Z_i} \quad \text{Equation 4-22}$$

Where:

H_i Storey Height

$h_{b,i}$	Beam depth at top of storey i
Z_i	Internal lever arm for a column of storey i
$l_{0,i}$	Lapping of vertical rebars at the base of column i
E_s	Elastic modulus of steel
$f_{0t,i}$ and $f_{0b,i}$	The maximum stress that the rebar can develop on top and bottom of column i, $f_0 = 22\sqrt{f_c}$

$$\theta_{u,top,i} = \theta_{y,top,i}$$

$$\begin{aligned} & + (\phi_{u,i} - \phi_{y,i}) \left(a_{max} \frac{H_i - h_{b,i}}{2} \right. \\ & \left. + a_{min}(l_{0,i+1} + h_{b,i}) \right) \\ & + \frac{\phi_{u,i} \xi_{u,i} d_i}{2} \left(\frac{H_i - h_{b,i}}{Z_i} + \frac{Z_i}{H_i - h_{b,i}} \right) \end{aligned} \quad \text{Equation 4-23}$$

$$\begin{aligned} \theta_{u,bot,i} = \theta_{y,bot,i} + a_{lap,i} & \left((\phi_{u,i-1} - \phi_{y,i-1}) \left(a_{max} \frac{H_{i-1} - h_{b,i-1}}{2} + a_{min} l_{0,i} \right) \right. \\ & \left. + \frac{\phi_{u,i-1} \xi_{u,i-1} d_i}{2} \left(\frac{H_i - h_{b,i}}{Z_i} + \frac{Z_i}{H_i - h_{b,i}} \right) \right) \end{aligned} \quad \text{Equation 4-24}$$

$$\text{End with hooks } a_{lap,i} = \min \left(1; \frac{l_{0,i}}{50d_{b,i-1}} \right) \quad \text{Equation 4-25}$$

$$\text{Straight ends } a_{lap,i} = \max(0; \min \left(1; \frac{l_{0,i}}{25d_{b,i-1}} - 1 \right)) \quad \text{Equation 4-26}$$

Two global damage indices, based on inter-storey drift and change of structural period, were considered in fragility analysis. The homogenised reinforced concrete (HRC) damage index was used for non-ductile moment-resisting frames as well as the

global damage parameter (Equation 4-27) and thresholds for damage states (Table 4-8). This index was developed by Rossetto and Elnashai (2003), based on the maximum inter-storey drift ratio.

$$DI_{HRC} = 34.89 \ln(ISD_{max\%}) + 39.39 \quad \text{Equation 4-27}$$

Table 4-8: Threshold values for HRC damage limit states (Rossetto and Elnashai, 2003).

ISD _{max} (%) limits for HRC-scale	
HRC damage state	ND MRF
Slight	0.32
Moderate	1.02
Extensive	2.41
collapse	>5.68

For the damage index considering the change in the structural period, Kyriakides et al. (2014) was used (Equation 4-28).

$$DI_T = 100 \times \left(\frac{T_{sec} - T_0}{T_{100} - T_0} \right) \quad \text{Equation 4-28}$$

$$T_{sec} = 2\pi \sqrt{\frac{SD_i}{SA_i}} \quad \text{Equation 4-29}$$

Where:

- T_{sec} secant period at each SA_i - SD_i coordinate given by Equation 4-29
- T_0 Initial period
- T_{100} Ultimate period

The threshold values considered for DIT according to Kyriakides N (2007) are; 2% for slight, 20% for moderate, 70% for extensive and 100% for collapse damage limit states.

The damage states considered for this PhD research, are as follows:

- **Slight damage:** corresponds to the limit of elastic behaviour of the components.
- **Moderate damage:** corresponds to the peak lateral bearing capacity.
- **Extensive (near collapse):** corresponds to the initiation of buckling of longitudinal rebars.
- **Complete (collapse):** represents the collapse level triggered by the software when violating the following two fundamental rules:
 - a. if the lateral load capacity drops by 20%
 - b. the inter-story drift limit reaches 5.68, as suggested by the HRC damage index (Rossetto and Elnashai, 2003).

To convert the fragility curves based on the aforementioned global damage indices, the correlation of damage states to the actual cost of the repair/replacement is needed, for the case study region. For the conversion matrix, it was decided to use the one suggested by Bal et al. (2008). Bal et al. based their work on data obtained from 231 damaged buildings after the 1998 Ceyhan and 1999 Kocaeli earthquakes in Turkey (Table 4-9).

Note: Non-structural damage is assumed to be included in this conversion matrix as mentioned by Bal et al. (2008). The reason the assigned values for extensive and collapse damage are more than 100%, is that in Turkey, repair/retrofitting of structures after an earthquake event, is only allowed up to moderate damage. Buildings exceeding moderate damage need to be demolished and reconstructed. Since, these conversion rates contain demolishing cost, re-accommodation of residents and building reconstruction cost.

Table 4-9: Comparison of damage ratios.

Damage state	HRC (Rossetto and Elnashai, 2003)	(HAZUS, 2003)	(Bal et al., 2008)
Slight	0	2	16
moderate	40	10	33
Extensive	70	50	105
Collapse	100	100	104

4.3.5 Probabilistic vulnerability analysis

To perform the probabilistic seismic vulnerability analysis, a Matlab code was implemented and the methodology steps were based on the Latin Hypercube (LH) sampling method, using available published data from a Turkish building database (Bal et al., 2008).

1. The first step is to randomise the chosen variables based on the LH sampling method. The material and geometrical properties were taken from the Turkish building stock (Bal et al., 2008) (Table 4-10).

Table 4-10: Statistical description of random variables.

Parameter	Mean	COV (%)	Upper/lower limit	Distribution
$\bar{\sigma}_c$ (MPa)	16.73	51	35/8	Gamma
$\bar{\sigma}_y$ (MPa)	371.13	24	200/500	Normal
Storey Height (m)	2.84	8	3.3/2.5	Log-normal

Where:

$\bar{\sigma}_c$ Concrete compressive strength

$\bar{\sigma}_y$ Steel yielding strength

2. Selected variables are imported to OpenSees and concrete, steel, buckling and bond-slip behaviours are recalculated for each step, using the pre-defined corresponding characteristics for each behaviour.
3. Repeating steps 1-8 of section 4.3.3 for LH sampling size of 100 for building (256 for column). (Note: the LH sampling size of 100 was selected as sufficient, based on recent research work in the seismic vulnerability analysis (Dizaj et al., 2018) and (Ahmad, 2011)).
4. Performing statistical analysis using the output of step 3 to determine the probability of exceeding a damage state threshold related to the corresponding PGA levels.
5. Curve-fitting of results of step 4, based on a Log-normal cumulative distribution function, to derive the general vulnerability curve related to ground shaking intensity level (PGA) to the probability of exceeding a certain damage state (The maximum likelihood method was used with a lognormal cumulative distribution function to define the fragility functions (Baker, 2015)).
6. Converting fragility functions to vulnerability curves using the conversion matrix proposed by Bal et al. (2008) and shown in Table 4-9.

4.3.5.1 Probabilistic fragility assessment of RC column

A total of 256 probabilistic fragility analyses of a 200 X 300 mm column were performed as part of a large parametric study where several variable parameters were considered (Table 4-11).

Table 4-11: Variable parameters considered in probabilistic fragility analyses of a 200 X 300 mm column.

Concrete Strength (MPa)	Steel grade	Stirrup spacing (mm)	Axial load (%)	Upgraded with
8 to 35	S220	60	20	1 Layer of CFRP
	S420	90	50	
		120		
		180		

4.3.5.2 Probabilistic vulnerability assessment of the 4-storey RC building (case study)

To perform the probabilistic seismic vulnerability analysis, a Matlab code was implemented and the methodology steps were based on the Latin Hypercube (LH) sampling method, using available published data from a Turkish building database (Bal et al., 2008).

7. The first step is to randomise the chosen variables based on the LH sampling method. The material and geometrical properties were taken from the Turkish building stock (Bal et al., 2008) (Table 4-10).

100 LH samples were produced and analysed using RCPA to collect the damage data related to each level of ground shaking intensity measure (IM) for each building sample. After performing statistical analysis (section 4.3.4), the adaptive fragility curves were derived and the effects of the considered parameters are also discussed. Finally, the upgraded fragility curves are derived considering a hypothetical external 3-layer CFRP column retrofitting of the substandard 4-storey RC building.

In the probabilistic fragility analysis, a site-specific design spectrum (Figure 4-10) according to TBEC (2018) and the most recent Turkish seismic hazard map (AFAD, 2018) were used.

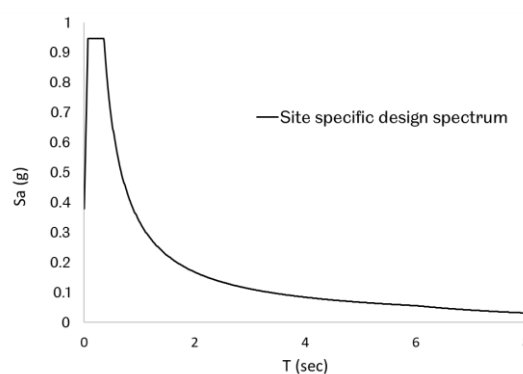


Figure 4-10: Site-specific design spectrum for the 4-storey substandard RC building.

A lognormal cumulative distribution function (Equation 4-30) is used to define the fragility curves.

$$P(C | IM = x) = \Phi\left(\frac{\ln(x/\theta)}{\beta}\right)$$

Where;

$P(C | IM = x)$ The probability that ground shaking with $IM = x$ will lead the structure to collapse

$\Phi()$ Cumulative distribution function

θ Median of the fragility function (The IM level which corresponds to 50% probability of collapse)

β The standard deviation of $\ln(IM)$

This assumption that intensity measure (IM) values of ground shaking causing structure collapse are log-normally distributed, is commonly accepted by various researchers (Ibarra and Krawinkler, 2005, Porter et al., 2007, Bradley and Dhakal, 2008, Ghafory-Ashtiany et al., 2011, Eads et al., 2013). Figure 4-11 shows the statistical procedure for deriving fragility curves using Equation 4-30.

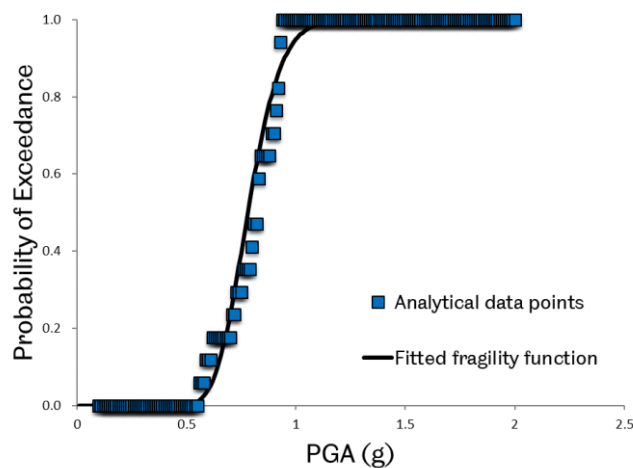


Figure 4-11: Curve fitting procedure to derive fragility functions.

4.3.6 Derivation of advanced adaptive fragility/vulnerability curves

This step is a novel additional step after deriving the general fragility curves (general fragility curves in this PhD study refers to the fragility curves derived through

probabilistic fragility analysis as described in chapter 4.3.5). The main aim of this step is to provide more flexibility to the user to:

- a. choose the most accurate set of fragility curves for a building, based on the available input (e.g. material quality, detailing of the structural components, etc.)
- b. improve the accuracy of the seismic risk assessment studies.

The statistical analysis procedure (steps 4 to 6 sections 4.3.5) was coded in Matlab. The procedure followed for deriving adaptive fragility curves is as follows:

- 1- Collecting all damage data from the probabilistic fragility analysis (section 4.3.5).
- 2- Disaggregating damage data based on the selected parameter (concrete quality, steel grade, stirrup spacing, axial load level, etc.).
- 3- Deriving parameter specific (adaptive) fragility curves for the considered substandard RC building.

4.3.7 Derivation of upgraded vulnerability curves

Upgraded vulnerability/fragility curves in this PhD study, refer to the fragility/vulnerability curves derived for the case study building but hypothetically strengthened. Two well-known external jacketing techniques are considered to derive the upgraded vulnerability curves and implemented in the developed framework: The first is the Fibre-reinforced polymer (FRP) jacketing and the second is external jacketing using post-tensioned metal straps (PTMS) (Section 2.3).

Only columns were considered to be hypothetically externally jacketed using 3 layers of CFRP in the plastic hinge regions of the bottom and top of the columns assuming the jacket length to be 50 cm.

The upgraded vulnerability curves come with two main advantages:

- a. They provide an overall idea to decision-makers to see if a high vulnerability building class can be upgraded to a safe level of response (acceptable level of vulnerability).
- b. They enhance the accuracy of risk analysis for developing countries like Turkey which has lots of retrofitted buildings in its building inventory.

The upgraded vulnerability curves are produced for the substandard RC column (retrofitted with 1 layer of CFRP) and the 4-storey case study building (retrofitted with 3 layers of CFRP) following the same method used for the bare frames (section 4.3.5). To model the confinement effects of external jacketing with FRP or PTMS the models from Biskinis and Fardis (2013) and Moghaddam et al. (2010b) were used (Sections 2.3.5.1 and 2.3.5.2).

Table 4-12 shows the mechanical properties of FRP used based on Garcia et al. (2010) for the analytical modelling of the retrofitted RC buildings.

Table 4-12: Mechanical properties of FRP sheets.

Property (unit)	Nominal Value
Tensile strength (MPa)	2550
Tensile elastic modulus (GPa)	135
Failure tensile strain (%)	1.7
Compressive strength (MPa)	1470

Table 4-13 gives the geometric and mechanical characteristics of metal straps (Garcia et al., 2014) used to calculate the confined concrete based on Equation 2-4 to Equation 2-9.

Table 4-13: Geometric and mechanical characteristics of metal strips for PTMS.

Width (mm)	Thickness (mm)	Tensile strength (MPa)	Yield strength (MPa)	Elongation (%)	Elastic modulus (GPa)
25.0	0.80	1100	982	7	230

4.4 Advanced probabilistic seismic vulnerability analysis for the case study RC building

For the case study 4-storey existing substandard RC building (see chapter 3.4 for the building details), the same methodology is applied following the developed framework (section 4.3). As a result, general, adaptive and upgraded vulnerability curves are derived. The results are then compared with several well-known studies for the case study region from the literature, to ensure the accuracy and applicability of the framework.

CHAPTER 5 RESULTS AND DISCUSSION

Chapter 5 presents the overall results of the analytical work divided as follows:

- Validation of substandard RC columns analytical modelling procedure.
- Probabilistic adaptive/upgraded seismic fragility assessment of substandard RC columns (reversed-cyclic tests - ITU).
- Validation of substandard RC frames (full-scale shaking table tests) analytical modelling procedure.
- Probabilistic adaptive/upgraded seismic fragility assessment of the substandard RC 4-storey building (case study).
- Comparison of the derived fragility functions for the 4-storey substandard RC building with well-known existing fragility curves for the case study region.

5.1 Substandard RC columns

This section presents the results of the substandard RC columns.

5.1.1 Mesh-sensitivity analysis

Mesh-sensitivity analysis was performed to ensure the accuracy of the fibre section's moment-curvature capacity. Firstly, a section analysis with various mesh sizes was conducted using OpenSees and a moment-curvature relationship was derived for the column's section. Secondly, a monotonic pushover analysis was performed to compare the moment-curvature of the most critical section (base of the column) (from the output of the column element) with the section analysis results (Figure 5-1a).

The moment-curvature behaviour of the section of the nonlinear column element is also compared with the section analysis results (Figure 5-1b).

A series of analyses in OpenSees revealed that mesh size practically does not affect section capacity, however, it significantly impacts the convergence of the analysis. The parametric analysis showed that a mesh size of 10 mm² is ideal for simulating accurately the moment-curvature behaviour without compromising convergence. To confirm the accuracy of the fibre section moment-curvature behaviour, the results of section and pushover analysis are compared and match perfectly (Figure 5-1b).

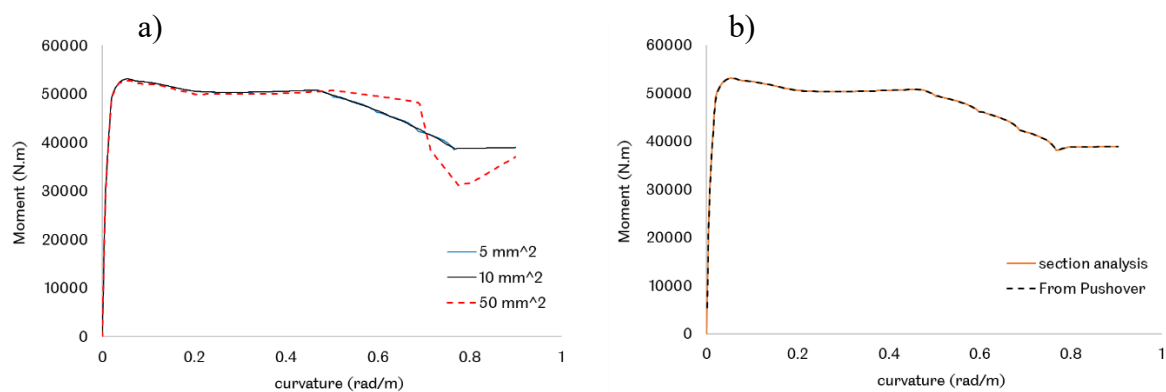


Figure 5-1: (a) moment-curvature behaviour of the section from section analysis. (b) moment-curvature behaviour of the section recorded after pushover analysis.

5.1.2 Reversed cyclic pushover analysis (RCPA)

The reversed cyclic pushover analysis was conducted on the 4 full-scale cantilever columns with various spacing of stirrups and the analytical results are compared with the experimental recordings. This section presents the results of specimen S60 with 60 mm stirrup spacing, considering local and global parameters; Appendix B.1 gives the results of the other three specimens.

Firstly, the cyclic behaviour of the column (lateral load versus drift) was compared with the experimental results (Figure 5-2), showing satisfactory agreement in terms of global response. Secondly, the analytical chord rotation at all drift targets (derived

using the area under the curvature profile of the plastic hinge zone, Figure 5-3), was compared with the experimental recordings and are in good agreement (Table 5-1).

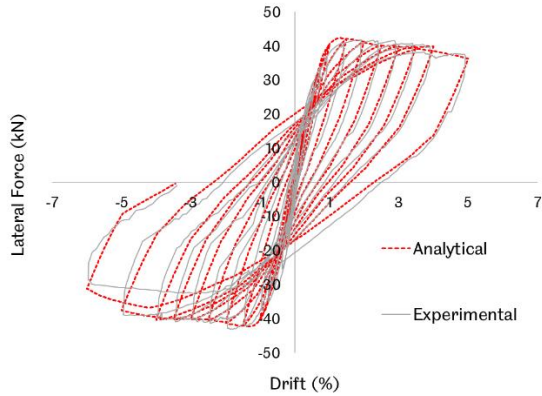


Figure 5-2: Comparison of cyclic behaviour for specimen S60

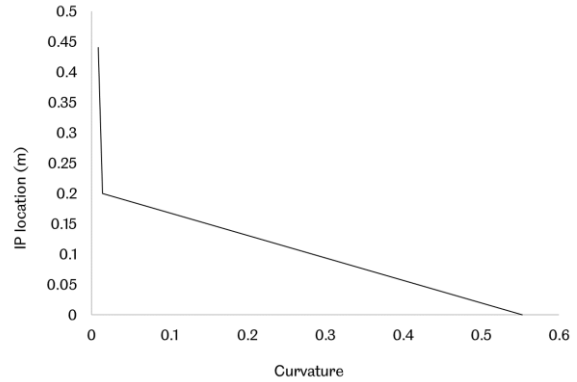


Figure 5-3: Maximum curvature profile for S60 specimen (at drift 6%)

The comparison between analytical and experimental results of RCPA for both local and global response also exhibited promising agreement.

Table 5-1: Analytical versus experimental chord rotation for S60.

drift (%)	Chord rotation (rad)		drift (%)	Chord rotation (rad)	
	Analytical	Experimental		Analytical	Experimental
0.1	0.000	0.001	2.0	0.016	0.017
0.2	0.001	0.001	2.5	0.021	0.022
0.4	0.002	0.002	3.0	0.026	0.028
0.6	0.003	0.004	3.5	0.032	0.035
0.8	0.004	0.006	4.0	0.037	0.041
1.0	0.006	0.008	5.0	0.047	0.047
1.5	0.011	0.012	6.0	0.057	0.053

5.1.3 TH analysis versus RCPA

To assess the performance of structural elements in a simpler, time-efficient and accurate way, CSM is employed and compared with the dynamic TH analysis for a column element. Firstly, a design spectrum was generated based on EC8 soil type C with a PGA level of 0.23g and a set of 7 artificial earthquake excitation records was selected. The SeismoArtif software (Seismo-Artif) was used to generate synthetic

records. Figure 5-4 shows the comparison of the record specific response spectra with the design spectrum. Seven THA were performed selecting compatible EQ records with the design spectrum and the maximum top displacement was recorded for each analysis. The same design spectrum was used to assess the performance of the column element using CSM. Table 5-2 gives the average maximum top displacement of the column from 7 THA. The pp point from CSM was found to be 0.050 (m) and the average ultimate top displacement from THA is 0.053 (m). The comparison shows promising agreement between the results of THA and RCPA.

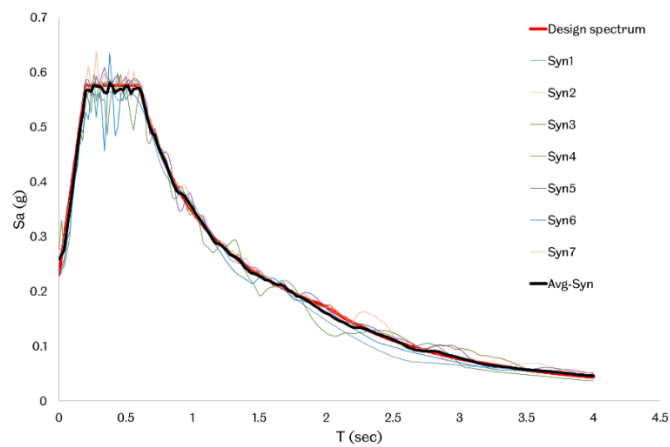


Figure 5-4: Selected artificial EQ records versus design spectrum.

Table 5-2: THA results for top displacement.

Record	Top displacement (m)
Syn1	0.047
Syn2	0.063
Syn3	0.047
Syn4	0.045
Syn5	0.054
Syn6	0.064
Syn7	0.053
AVG	0.053

The developed 3D analytical model showed good agreement with the experimental results using various analytical methods such as TH and RCPA. This indicates that the model is capable of representing the actual behaviour of substandard RC columns.

5.1.4 Element-based fragility analysis

The comparison between the PP derived using both THA and CSM showed promising agreement at elemental level. In this section, the compatibility of three damage parameters for seismic fragility analysis is investigated and their advantages and disadvantages are discussed (Section 5.1.4.1.1). Then, advance probabilistic seismic fragility analysis is performed for a 200 X 300 mm substandard RC column using the developed framework. Section 5.1.4.2 presents the results of the element-based probabilistic fragility analysis.

5.1.4.1 Investigation of local and global damage parameters

Inter-storey drift-based Mean Damage Ratio (MDR) was calculated based on the HRC damage index developed by Rossetto and Elnashai (2003). For the damage index, considering the change in the structural period, the formula from Kyriakides et al. (2014) was used (Equation 4-28) to derive the MDR and for the rotation-based damage index, a similar formula was adopted (Equation 5-1). The difference between the first two aforementioned damage indexes and the rotation based damage index is that the inter-storey drift/structural period-based damage formula represents the MDR (repair-to-replacement cost), while the rotation-based damage index shows the structural damage level at a certain PGA value. Figure 5-5a shows a comparison of these two vulnerability curves using the drift-based and the period-based damage indices. Figure 5-5b presents the derived vulnerability curve based on the rotation-based damage index.

$$DI(\%) = \frac{\theta_c - \theta_y}{\theta_u - \theta_y} \times 100 \geq 0 \quad \text{Equation 5-1}$$

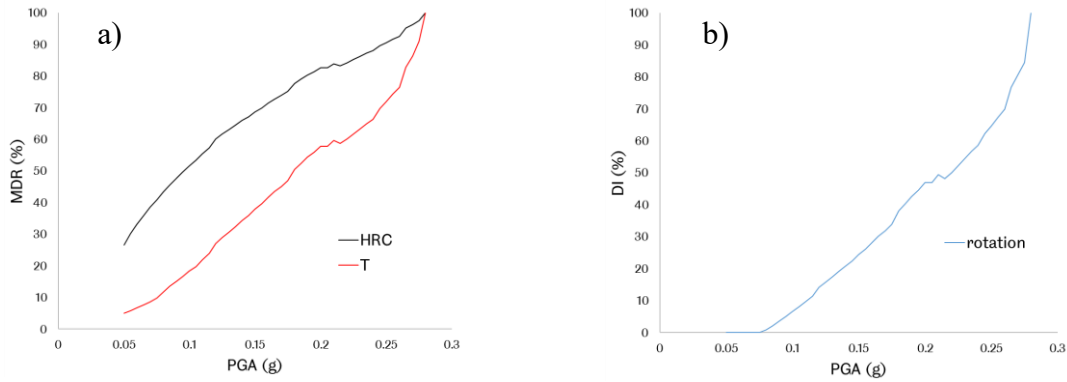
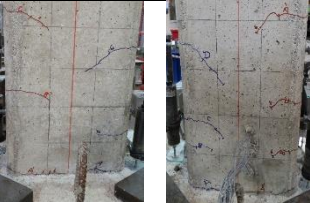


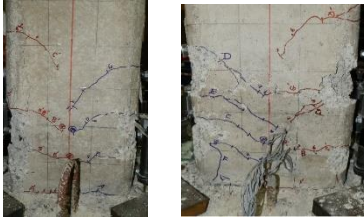




Figure 5-5: Element-based derived vulnerability curves for S60 a) based on HRC and T b) rotation-based damage indices.

Table 5-3 compares the calculated damage indices and recorded damage level for specimen S60.

Table 5-3: Analytically derived damage versus experimentally observed damage (S60).

MDR HRC(%)	MDR T(%)	DI θ (%)	Drift (%)	PGA (g)	Exp. Pic	comments
39.39	8.5	0	1	0.07		Formation of flexural cracks
63.1	30.7	17.5	2	0.13		
77.73	50.5	38	3	0.18		Initiation of cover spalling

88	66.4	58.5	4	0.24		Start of buckling and concrete crushing
92.6	76.5	69.8	5	0.26		Failure of column by losing more than 20% of the lateral load capacity
100	100	100	6	0.28		Failure of column by losing more than 30% of the lateral capacity

The same procedure was followed for another specimen, with stirrup spacing of 120mm (S120) to compare the damage levels captured with the above-mentioned damage parameters. This comparison is of major importance since it shows that stirrup spacing increases as the column ductility decreases; since DI HRC only depends on the maximum inter-storey drift limits, it is obvious that this damage index will not be able to capture the 100% damage level if the specimen fails before the predefined threshold limit. This is why there is a need for a better damage index, especially for element level vulnerability analysis of substandard columns. Figure 5-6 shows that for this substandard RC column, the HRC damage index is not suitable since failure can happen before reaching the target drift limit at 100 % damage as for S120. To overcome this issue, the collapse of the element (or structure) is assumed to take place when lateral force capacity drops by 20% of its maximum value, since this is the most accurate assumption for collapse limit for substandard structures or elements (Goksu, 2021, Cardone, 2016).

shows the comparison between experimental and calculated analytical damage whilst Figure 5-6 presents the element based vulnerability curve.

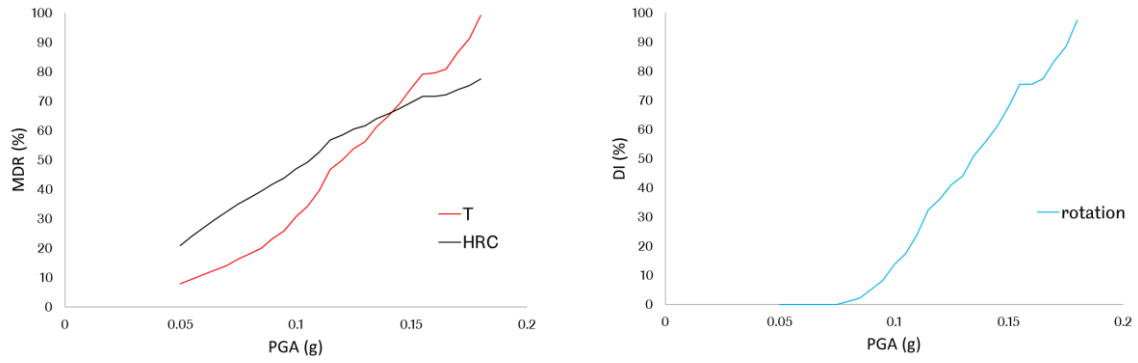







Figure 5-6: Element based derived vulnerability curves for S120.

Figure 5-6 shows that for this substandard RC column, the HRC damage index is not suitable since failure can happen before reaching the target drift limit at 100 % damage as for S120. To overcome this issue, the collapse of the element (or structure) is assumed to take place when lateral force capacity drops by 20% of its maximum value, since this is the most accurate assumption for collapse limit for substandard structures or elements (Goksu, 2021, Cardone, 2016).

Table 5-4: analytically derived damage versus experimentally observed damage (S120).

MDR HRC(%)	MDR T(%)	DI θ (%)	Drift (%)	PGA (g)	Exp. Pic	comments
39.39	20	2.2	1	0.07		Formation of flexural cracks
52.6	39.4	23.8	1.5	0.13		

63.9	61.15	51.1	2	0.18		Start of cover spalling
71.5	79.1	75.4	2.5	0.24		Initiation of buckling and concrete crushing
77.9	100	97.5	3	0.26		Failure of column by losing over 20% lateral force capacity

5.1.4.1.1 Advantages/disadvantages of damage parameters for vulnerability analysis

A rotation-based damage parameter may capture the damage accurately, however, since yielding and ultimate curvatures are used to calculate the ultimate and yield rotation for each column, a prior section analysis needs to be performed before conducting the RCPA. This additional step might be acceptable, since it deterministically assesses the performance of a specific existing building. However, in the probabilistic seismic fragility assessment, this is not practical, since the material and geometric properties of the building will be considered as variables. Unfortunately, until now the formulas for calculating the ultimate rotation has not shown promising accuracy (coefficient of variance is nearly 40%) as reported by Grammatikou et al. (2018), one of the most leading research groups in this area. This

inaccuracy in available prediction formulas for the ultimate rotation capacity of the columns will introduce additional error to damage calculation. In addition, in case of an RC building, the failure in a column on a certain storey level may not necessarily represent the total collapse of the building. Therefore, relating rotation-based damage parameter to the damage limit states will need to be first investigated based on a large experimental data pool. This information is not available in the literature to the best knowledge of the author at the time of this research.

The damage parameter, based on change of structural period, was reported to have a sufficient accuracy in capturing the damage level of the substandard RC buildings (Kyriakides N, 2007, Ahmad, 2011). The results of section 5.1.4 also showed promising agreement between the calculated damage based on change of period and experimental observations. Therefore, the change of structural period is one of the most suitable damage parameters for probabilistic fragility analysis of both RC buildings and elements. Especially while using CSM which is very convenient to find and work with since, the diagonal lines in the Sa-Sd coordinate system represent the structural period in Equation 4-9.

5.1.4.2 Probabilistic seismic vulnerability analysis

This section presents all the results of the probabilistic seismic vulnerability assessment (Section 4.3.5.1) for the substandard RC column (Section 3.2).

5.1.4.2.1 General fragility curves

Figure 5-7 illustrates the general fragility curves for the RC column under 50% axial load.

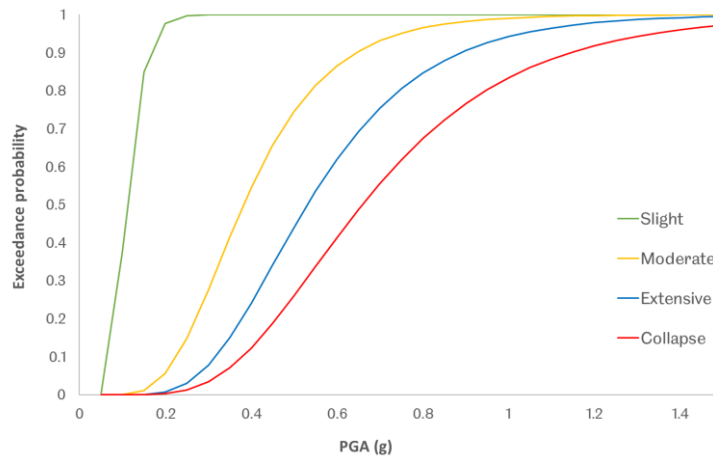


Figure 5-7: General fragility curves for an RC column under 50% axial load.

5.1.4.2.2 Adaptive fragility curves

Figure 5-8 shows the adaptive fragility curves for axial load level with S220 rebar type. Figure 5-9 present the adaptive fragility curves disaggregated from general fragility curves for bar-type. Figure 5-10 illustrates the adapted fragility curves for various stirrup spacing with S220 rebar type and 20% axial load.

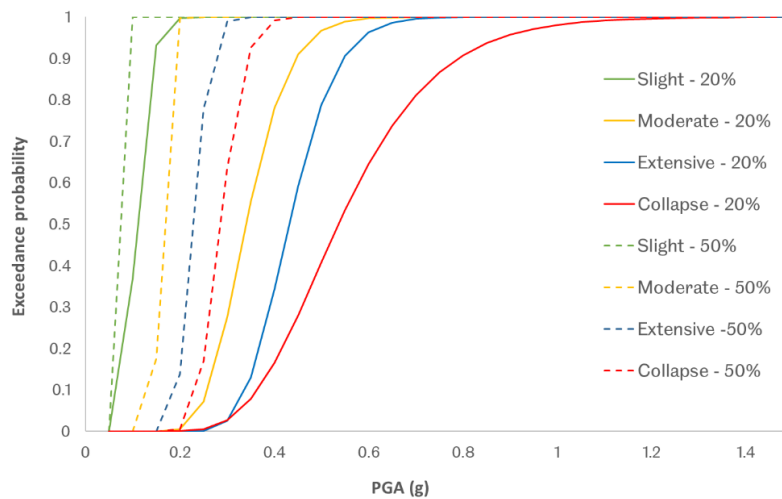


Figure 5-8: Adaptive fragility curves for axial load level with S220 rebar type.

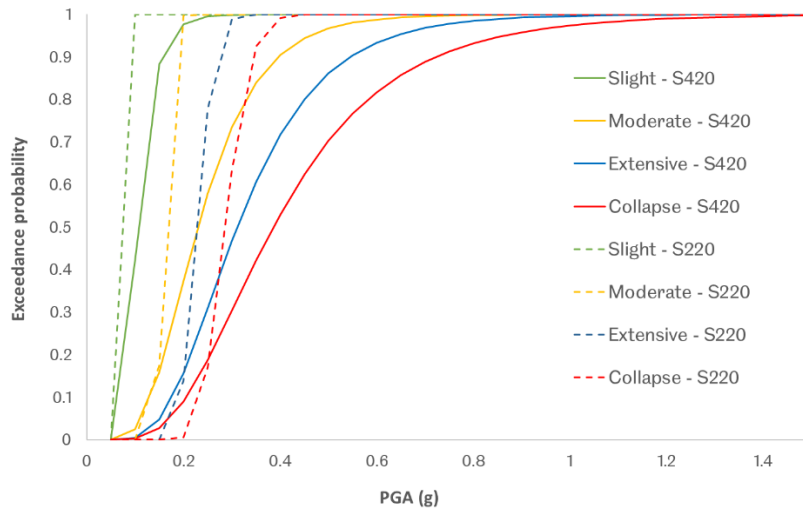


Figure 5-9: Adaptive fragility curves for steel grade with 20% axial load level.

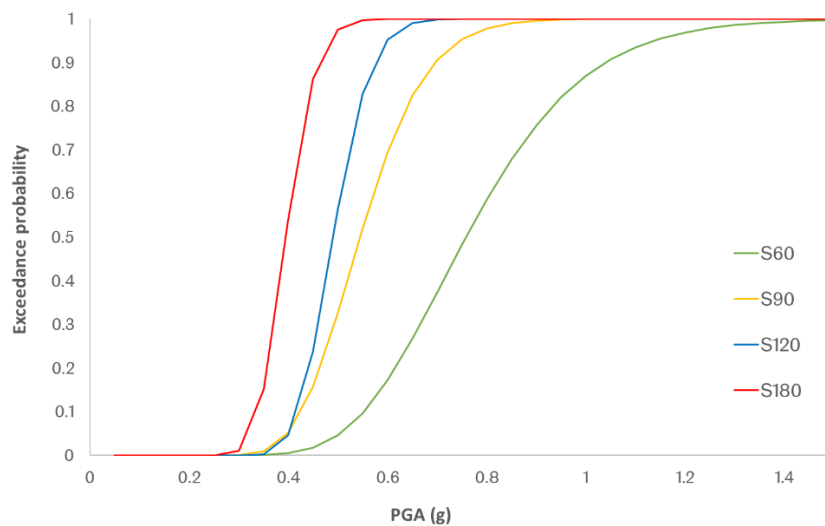


Figure 5-10: Adapted fragility curves for various stirrup spacing with S220 rebar type and 20% axial load.

Figure 5-12 a, b and c presents the adaptive fragility curves for concrete strength of the RC column (divided into three categories; $F_c=8$ to 15 MPa, $F_c=15$ to 25 MPa and $F_c=25$ to 45 MPa) on moderate, extensive and collapse damage limit states of the fragility curves, respectively.

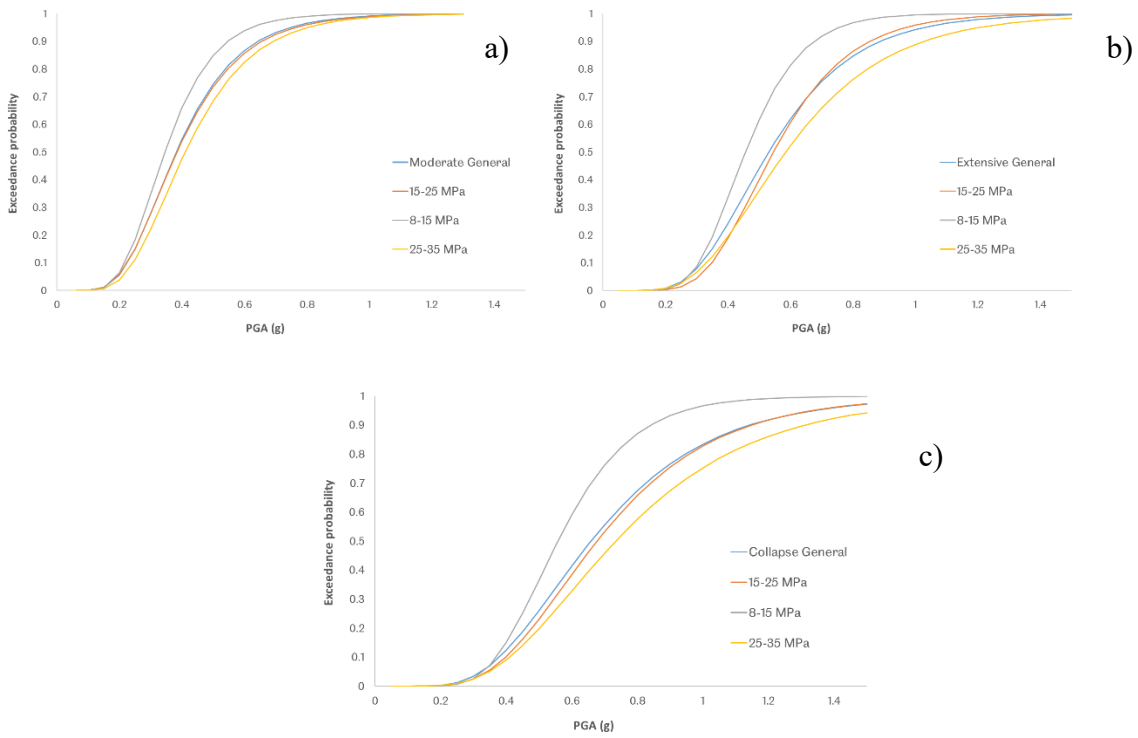


Figure 5-11: Adaptive fragility curves for concrete strength on a) moderate, b) extensive and c) collapse limit states on the fragility curves for an RC column.

5.1.4.2.3 Upgraded fragility curves

Figure 5-12 illustrates the upgraded fragility curve for collapse damage limit state for the column with 50% axial load and 180 mm stirrup spacing with rebar type S220.

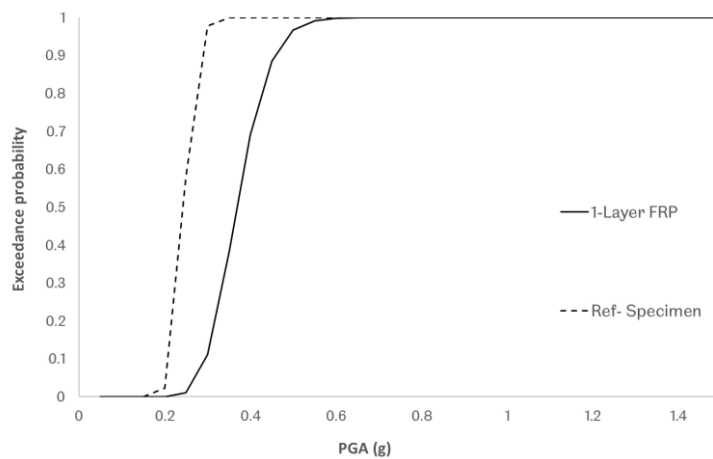


Figure 5-12: Upgraded fragility curves for collapse damage state.

5.1.4.2.4 Discussion and conclusions

From Figure 5-8 and Figure 5-9 it can be concluded that the main two parameters affecting the fragility curves are the transverse stirrup spacing and the level of axial load on the column. For the rebar type S220, the increase of axial load from 20% to 50% can adversely affect the fragility curves by approximately 55% for slight, moderate and extensive damage limit states and 46% for collapse damage limit state. The percentile difference for the PGA values corresponds to 50% probability of exceedance between S220 and S420 rebar types for the column under 20% axial load are; 17%, 30% for slight and moderate while 25% for extensive and collapse damage limit states. However, for the range of probability of exceedance above 70% these reported values are even more severe.

This parametric study can explain why the current analytical fragility curves are underestimating the damage for substandard buildings/elements. The reason is, considering all the capacity variabilities during the probabilistic vulnerability analysis will bring both ductile and brittle building/element samples to the data pool which the fragility curves will be derived based on. That is why there is a considerable deviation between the general fragility curves and derived dynamic fragility curves. This can lead to underestimation of the damage up to 50% for the case of substandard RC column. By availability of adaptive fragility curves this underestimation can be eliminated and the seismic risk studies based on adaptive fragility curves will increase the accuracy of the damage related parameters (possible number of collapsed buildings, number of deaths, financial impact, etc.,) significantly.

Figure 5-10 shows that the effectiveness of the concrete strength on the fragility curves increases towards higher damage state limits. The largest difference between the fragility curves disaggregated from the general fragility curves for the concrete strength, was observed to be at the lowest compressive concrete strength group between 8 to 15 MPa.

Upgraded fragility curve (Figure 5-12) shows promising improvement even with a slight retrofitting of 1 layer of CFRP. The collapse damage limit state fragility curve for the

column with S220 rebar type and 180 mm of stirrup spacing, improved approximately 55% comparing the PGA values corresponding to 50% probability of exceedance.

5.2 Shaking table tests

This section presents the comparison between the dynamic experimental results of the two shaking table tests and the analytical 3D model outputs from THA.

5.2.1 ECOLEADER frame

To ensure the correct moment-curvature relationship, section analysis was performed using OpenSees and Xtract (Chadwell, 2002) (Figure 5-13).

After creating the model in OpenSees, gravity and modal analyses were performed: After conducting a gravity analysis, the reaction forces from the base nodes were compared with gravity loads to ensure that the local and global coordinate system in OpenSees is registered correctly. The initial period of the frame was derived analytically after modal analysis compared with the experimental data. The analytical initial period, T_{an} , for the first mode was estimated to be as 0.52 sec while, the experimental, T_{exp} , was 0.53 sec.

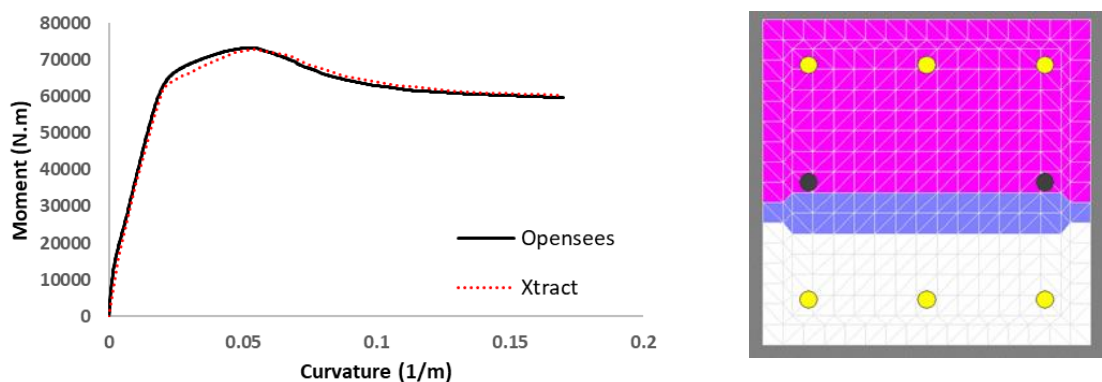


Figure 5-13: Comparison of section analyses using Xtract and OpenSees.

To better understand the potential failure mode of the system, a pushover analysis was performed using the inverse triangular lateral force distribution (Figure 5-14). The dominating failure mode observed was the second-floor column sway mechanism.

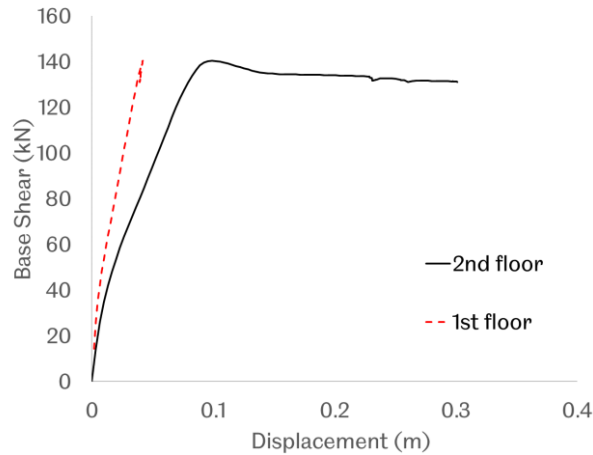


Figure 5-14: Pushover analysis in OpenSees (Ecoleader bare frame)

5.2.1.1 Time History Analysis without considering bond-slip effect of the longitudinal rebars

Then, a time history analysis (THA) was conducted without considering bond-slip effect of the longitudinal rebars. The input motion for THA was the series of shaking table displacement histories (Figure 5-15) recorded during the experiment. These displacements were imposed simultaneously to all four nodes fixed at the ground level using the Multiple Support Pattern in OpenSees.

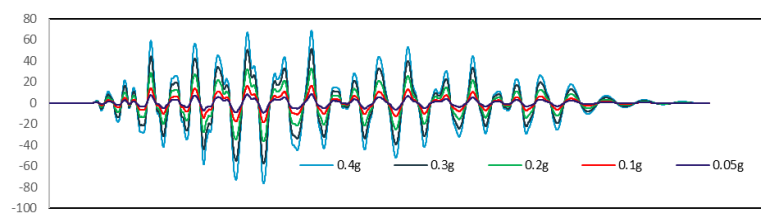


Figure 5-15: Input shaking table displacement (mm) histories.

The THA was performed using five different input records, following the experimental PGA levels which were at 0.05g, 0.1g, 0.2g, 0.3g and 0.4g and accumulating the damage after each analysis.

To monitor the structural behaviour, the displacement at each level plus strains at certain locations along the longitudinal reinforcement were obtained and compared with the experimental results. Figure 5-17 shows the comparison of the 1st floor analytical and experimental displacement histories for 0.05g and 0.3g. Figure 5-16 presents a typical example of strain comparison for a column of the first floor (longitudinal reinforcement, 13cm below the 1st floor joint). Both analytical and experimental displacement and strain-gage readings show an acceptable match at 0.05g. However, at 0.3g while the experimental displacement is larger than the analytical one, the experimental strains are much less than the analytical ones. This can be attributed to softening behaviour due to rebar slippage, something that this numerical model is not able to capture (the initial assumption of the model was that the bond-slip effect of the longitudinal rebars is ignored).

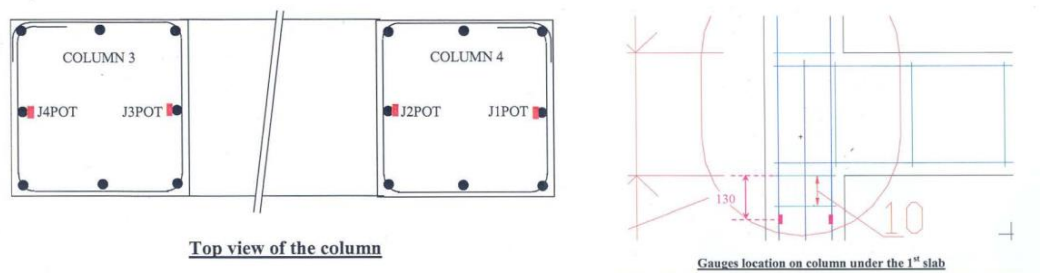


Figure 5-16: The strain-gage location used for comparison with analytical results.

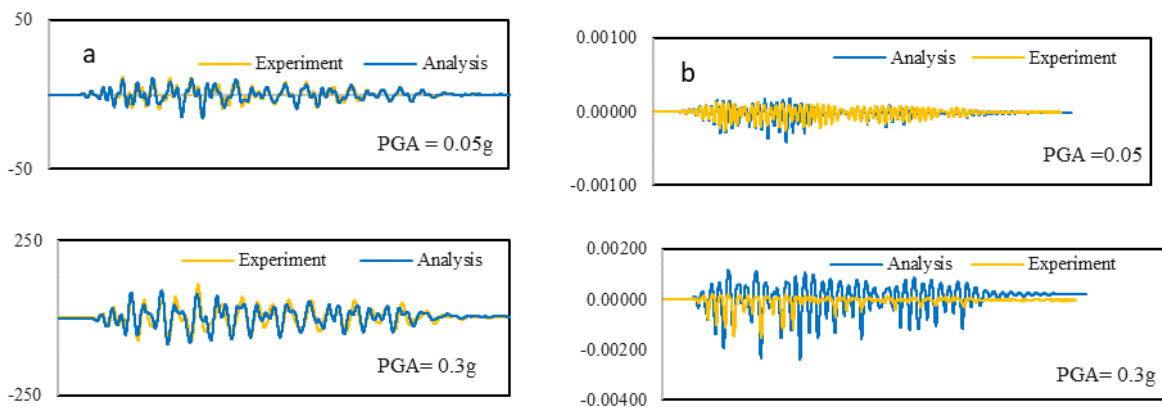


Figure 5-17: (a) 1st-floor displacement (mm) histories and (b) strain readings.

5.2.1.2 Time History Analysis considering bond-slip effect of the longitudinal rebars

A second THA was performed taking into account the rebar slippage and the displacement history and strain-gauge readings showed good agreement for both storeys (Figure 5-18). Both floor displacements for all PGA levels and a comparison of the structural period after each seismic excitation, are presented in Appendix B.2.

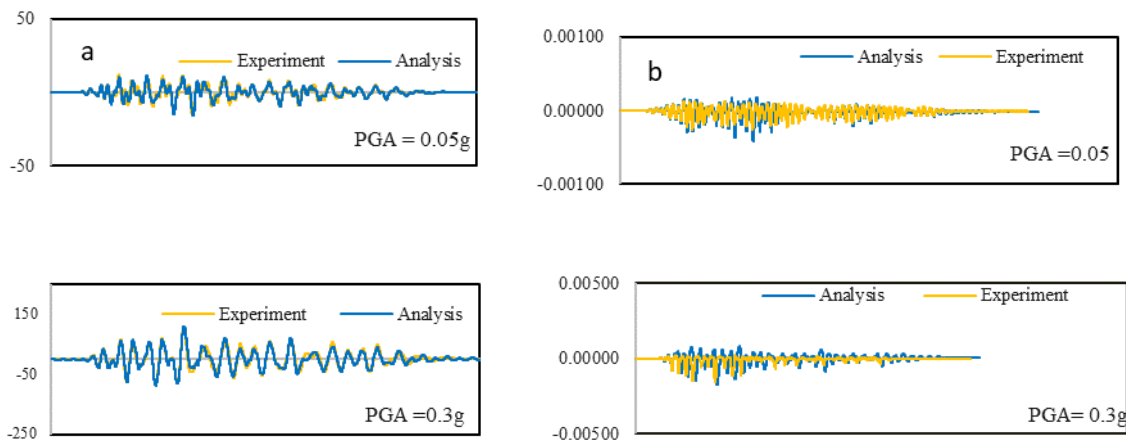


Figure 5-18: (a) 1st-floor displacement (mm) histories and (b) strain readings after introducing the bond-slip effect into the model.

5.2.2 BANDIT shaking table test

To model the BANDIT bare frame, the same methodology was used as for the ECOLEADER frame (see section 4.2.3). The analytical and experimental results for the BANDIT frame are in good agreement and presented in Appendix B.3.

5.3 Case study: 4-storey substandard RC building

To perform advanced probabilistic seismic fragility analysis on the existing 4-storey substandard RC building (Istanbul, Turkey), the following main variable parameters were considered: storey height, as well as concrete and steel material characteristics. This section presents and compares the derived adaptive fragility/vulnerability curves

and upgraded fragility curves with well-known existing fragility curves available in the literature for the case study region.

5.3.1 Probabilistic seismic vulnerability analysis

Table 5-5 gives all the fragility functions derived for the case study building.

Table 5-5: Fragility functions parameters for the 4-storey substandard buildings.

Fragility type		parameter	Slight	Moderate	Extensive	collapse
General		θ	0.13	0.40	0.63	0.78
		β	0.14	0.17	0.18	0.15
Steel grade	S220	θ	0.13	0.36	0.56	0.71
		β	0.12	0.18	0.18	0.15
	S420	θ	0.13	0.44	0.70	0.86
		β	0.16	0.10	0.10	0.10
Concrete strength	8-15	θ	0.11	0.36	0.60	0.73
		β	0.10	0.17	0.15	0.16
	15-25	θ	0.13	0.40	0.65	0.78
		β	0.08	0.16	0.15	0.16
	25-35	θ	0.15	0.47	0.70	0.85
		β	0.10	0.16	0.16	0.16

5.3.1.1 General fragility curves

Figure 5-19 presents the general fragility curves for the 4-storey substandard RC building. The test of goodness of fit is performed for the general fragility curves based on Shinozuka et al. (2000). The significant level is set equal to 0.1 the results of this test confirms that the hypotheses for all general fragility curves cannot be rejected at the significance level of 10%.

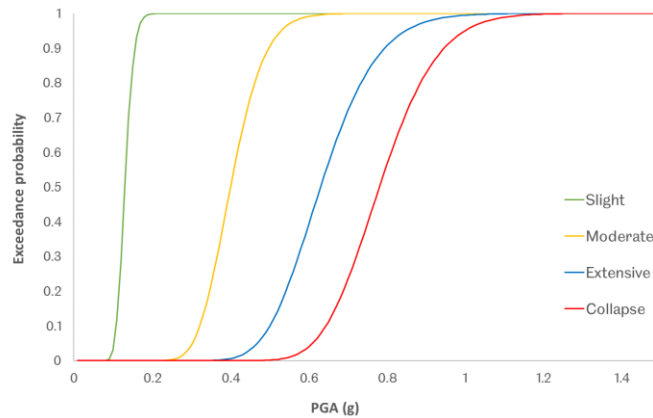


Figure 5-19: General fragility curve for the 4-storey substandard RC building.

5.3.1.2 Adaptive fragility curves

For this study, the geometrical and reinforcement detailing of the existing 4 storey-building were used and the parametric study investigates the effect of concrete strength and type of steel rebars on the fragility curves.

The effect of longitudinal reinforcement type on the fragility curves is investigated and the general fragility curves disaggregated for the two most common steel grades S220 (plain rebar) and S420 (ribbed rebar). Figure 5-20 shows the longitudinal rebar type-specific (adaptive) fragility curves.

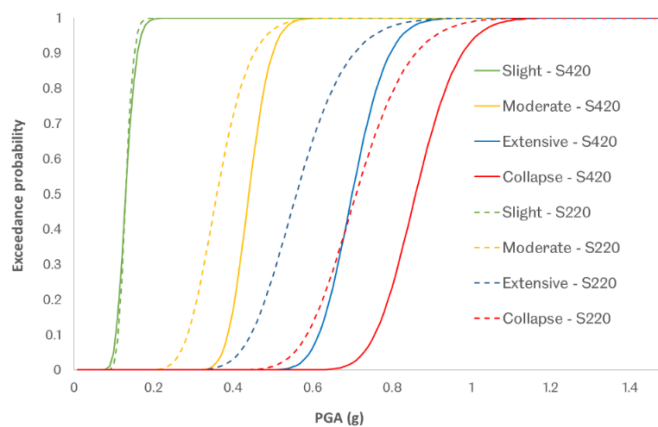


Figure 5-20: Adaptive fragility curves for the 4-storey substandard building based on longitudinal rebar type.

The effect of concrete compressive strength on the adaptive fragility curves is assessed, considering three concrete strength ranges (8 to 15 MPa, 15 to 25 MPa and 25 to 35 MPa) (Figure 5-21). On the slight damage limit state, the effect of concrete strength was found to be negligible. However, it has a considerable effect on higher damage limit states (moderate and extensive).

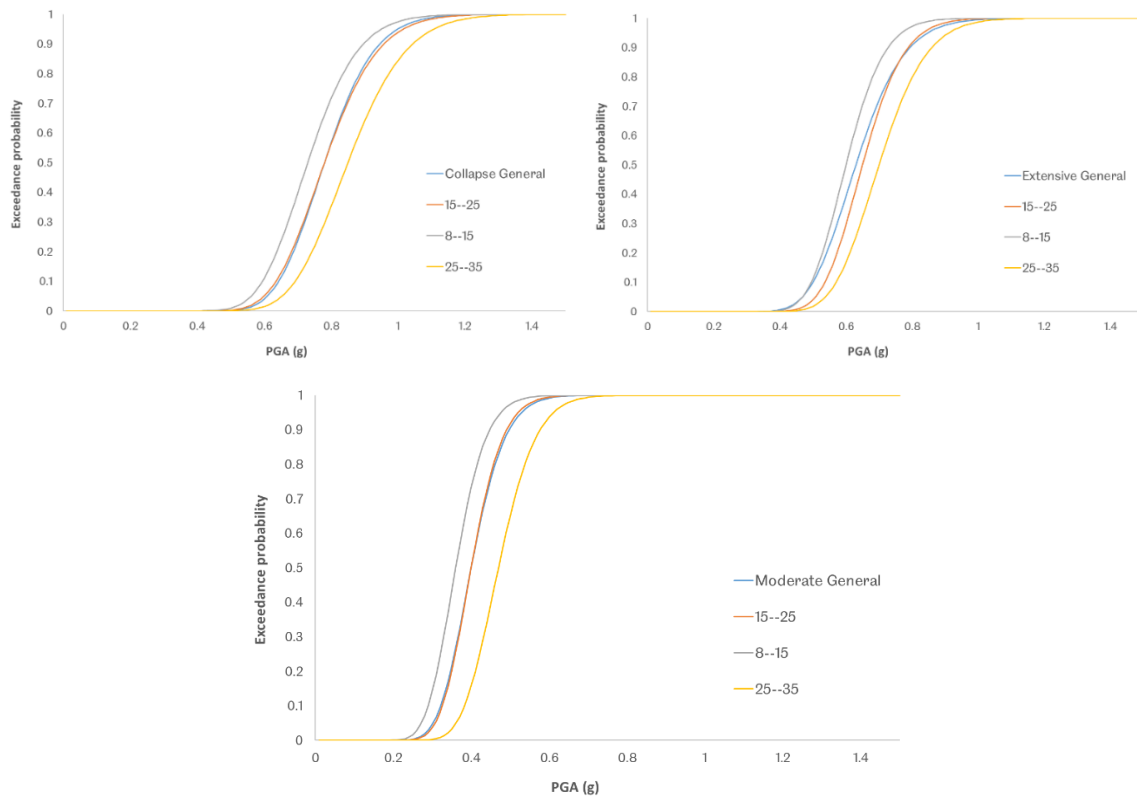


Figure 5-21: Adaptive fragility curves for the 4-storey substandard RC building based on concrete strength.

The percentage difference (that leads to a 50% probability of collapse) in PGA (g) for both steel grades S220 and S420 is around 10% less than the general fragility curve, for moderate, extensive and collapse damage limit states (Table 5-5).

For the concrete parameter, the fragility curves in the range of 15-25 MPa are almost the same as the general fragility curves. For 8-15 MPa, the PGA values are slightly less than the general fragility curves by -10%, -5% and -7% for moderate, extensive and collapse, respectively. For the range of 25-35 MPa, the fragility curves are significantly

higher especially for moderate state (+17.5%) whilst for extensive and collapse the percentage difference is around +10%.

From the results of this parametric study, it was found that both concrete and steel strength parameters can affect the fragility functions of a substandard RC structure. If adaptive fragility curves are used instead of general fragility curves, the accuracy of damage calculations can improve up to approximately 20%.

5.3.1.3 Upgraded fragility curves

This section discusses the probabilistic seismic fragility analysis on the externally retrofitted 4-storey building to derive the advanced dynamic fragility curves with 3 layers of CFRP. In total, 50 RCPA were conducted and the results are discussed in section 4.3.1. During the upgraded seismic probabilistic fragility analysis, the steel grade is assumed to be S220 (as the actual rebar type of the existing building, Section 3.4). Compressive strength of concrete and storey height are considered as the variable parameters. Table 5-6 provides the derived upgraded fragility functions whilst Figure 5-22 presents the general fragility curves compared to the derived upgraded fragility curves.

Table 5-6: Upgraded fragility functions parameters for the 4-storey substandard building.

Fragility type	parameter	Slight	Moderate	Extensive	collapse
S220	Θ	0.24	0.56	0.83	1.02
	β	0.10	0.11	0.08	0.10
8-15	Θ	0.21	0.48	0.72	0.92
	β	0.08	0.05	0.08	0.10
15-25	Θ	0.24	0.58	0.90	1.09
	β	0.10	0.07	0.10	0.10
25-35	Θ	0.26	0.62	0.89	1.10
	β	0.09	0.09	0.08	0.09

As it can be seen from Figure 5-22, there is a dramatic improvement in terms of seismic vulnerability compared with the bare frame. Figure 5-24 shows that the effectiveness of retrofitting decreases towards higher damage states. Comparison between the PGA values of fragility curves for the steel grade of S220 of the bare and retrofitted cases (corresponding to 50% probability of exceedance) for slight, moderate, extensive and collapse limits show 85%, 55%, 48% and 44% improvement, respectively.

The general upgraded fragility curves derived for the 4-storey substandard RC building with S220 steel type and retrofitted with 3 layers of FRP disaggregated to reflect the effectiveness of concrete strength on the probabilistic upgraded seismic fragility analysis (Figure 5-23).

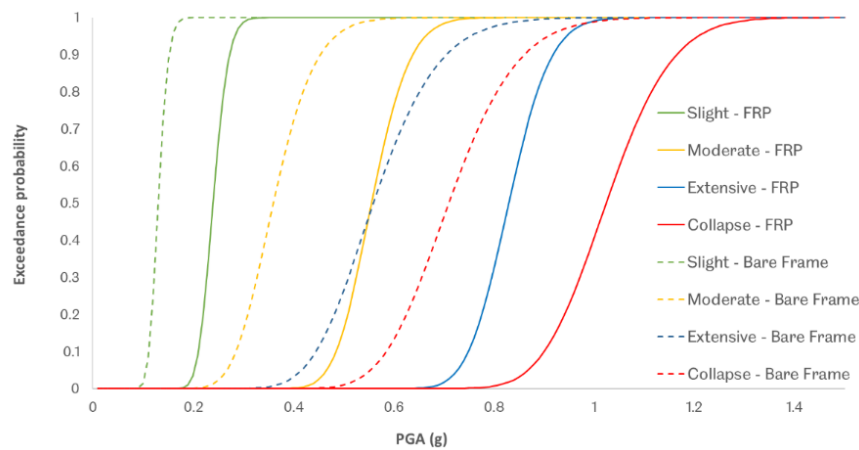
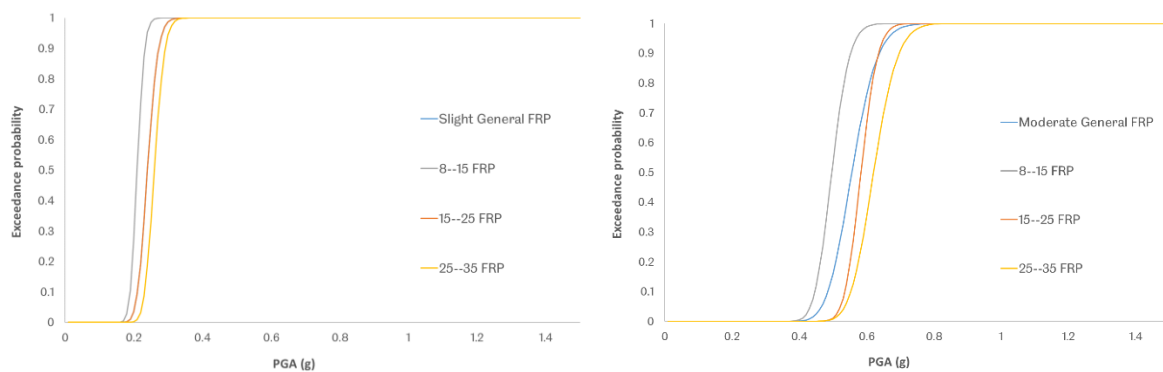


Figure 5-22: Comparison of the general fragility curves for the 4-storey substandard RC building with and without retrofitting with S220 steel grade.



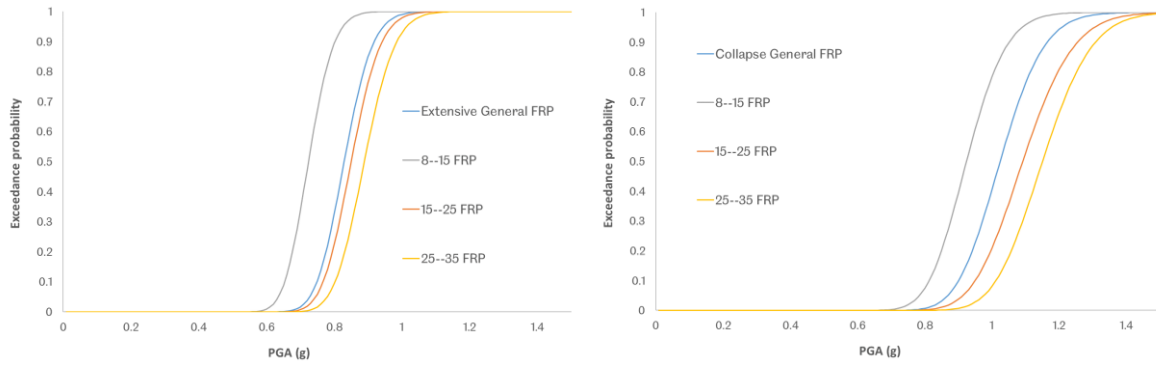


Figure 5-23: Dynamic upgraded fragility curves for the 4-storey substandard RC building with S220 steel type based on concrete strength.

5.3.1.4 Adaptive vulnerability curves

After deriving the fragility functions for the 4-storey existing substandard building, the fragility functions are converted into vulnerability curves (section 4.3.6).

To convert the fragility functions to the vulnerability curves, the damage conversion matrix of Bal et al. (2008) (Table 4-9) was used; this matrix was specifically defined for the case study region. Figure 5-24 presents the comparison between the derived adaptive vulnerability curves, taking into account the longitudinal steel type (S220, S420) with the general vulnerability curve for the existing 4-storey building.

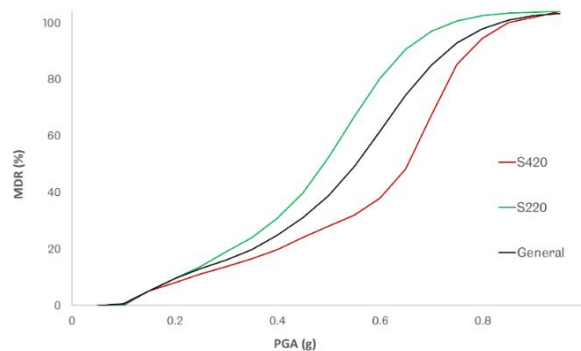


Figure 5-24: Comparison of the adaptive vulnerability curves based on steel type.

The effect of steel grade on the vulnerability assessment results was found to be extremely high. For instance, the percentage difference between the mean damage ratio of S420 and S220 at the IM level of 0.6g is 52%. The mean damage ratio at 0.6g level is 80% for S220, 38% for S420 whilst the MDR for the general vulnerability curve

is 62%. At the same IM level, the percentage differences of S220 and S420 from the general curve are 23% and 38%, respectively.

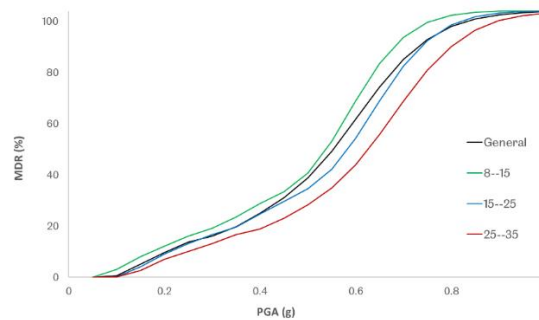


Figure 5-25: Adaptive vulnerability curves based on concrete strength.

By comparing the dynamic vulnerability curves based on concrete strength, it can be concluded that the effect of steel grade on the vulnerability assessment of the substandard building is the most significant (Figure 5-25). However, the effect of concrete strength on the vulnerability curves is still considerably high. For instance, the percentage differences of MDR between concrete adaptive vulnerability curves and the general vulnerability curve are -12%, +14% and +40%, for 8-15 MPa, 15-25 MPa and 25-35 MPa, respectively at 0.6g IM level. However, the difference between the two the MDR of 8-15 MPa and 25-35 MPa at PGA of 0.6g is 57%.

Since the vulnerability curves are the main inputs for damage calculation for a region during a seismic hazard assessment, the accuracy of the seismic hazard assessment output is directly affected (e.g. monetary or human loss, the number of the collapsed buildings, etc.). If the region of interest is located in a developing country like Turkey, there is the need to derive adaptive vulnerability curves to ensure an acceptable level of accuracy of damage.

Additionally to the results presented in section 5.3.1, a small study is performed to investigate the effect of yield strength of longitudinal rebar $f_y=220$ MPa instead of the experimental value of 320 MPa. For the analytical modelling procedure, the values considered for steel with S220 are taken from the 2018 Turkish Seismic Code (AFAD 2018) as follows: $f_y=220$ MPa, $\epsilon_{sy}=0.0011$, $\epsilon_{sh}=0.011$ and $\epsilon_{su}=0.12$. Fourteen extra samples

are collected and the fragility curves are derived and compared with $f_y=320$ MPa. Figure 5-26 presents the results for this comparison.

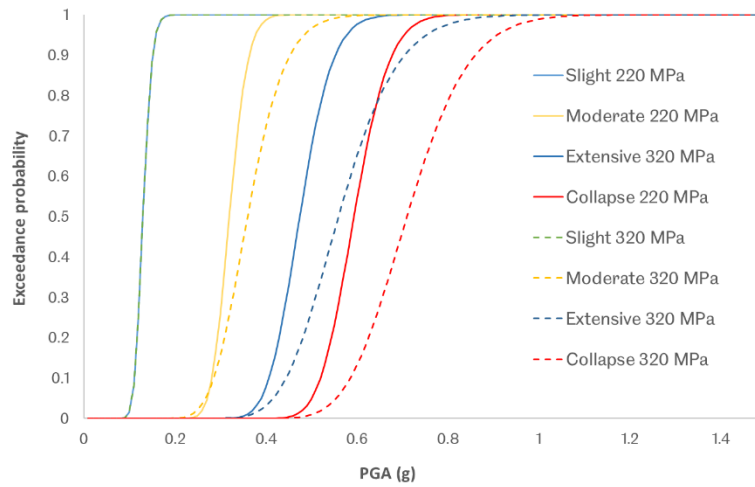


Figure 5-26: Comparison of fragility curves for $f_y=220$ MPa and $f_y=320$ MPa.

5.3.2 Comparison of fragility results with literature

Six well-known fragility functions with either PGA or PGV as IM found in the literature (suitable for the case study region: Turkey) are compared with the derived fragility functions (PhD²). While, the fragility curves considering PGA as IM are directly comparable with the derived general fragility curves of this study. To be able to compare the fragility curves with PGV as IM, PGA must be converted to PGV. For this, the EMS-98 intensity measure and peak ground motion parameters proposed by Zanini et al., (2019) are employed (Equation 5-2 and Equation 5-3).

$$I_{EMS-98} = 2.03 + 2.28 \log PGA \quad \text{Equation 5-2}$$

$$I_{EMS-98} = 4.16 + 1.62 \log PGV \quad \text{Equation 5-3}$$

² For this section only, in order to distinguish the fragility curves developed in this PhD with the ones derived by the examined authors, the abbreviation PhD will be used as clarification

5.3.2.1 Ahmad et al., 2010

The first study is by Ahmad et al. (2010) which developed fragility functions for regular and irregular low-rise, mid-rise and high-rise RC frames using accelerograms from the USA and IBC (2006) rock spectra. However, the authors mentioned that their fragility curves are suitable to be used for Euro-Mediterranean regions as well (Greece, Italy and Turkey). Their derived fragility curves are based on lognormal distribution with mean and standard deviation (SD) parameters to define the fragility functions using PGA as the intensity measure. Table 5-7 presents the fragility functions for ductile and non-ductile regular mid-rise buildings.

Table 5-7: Fragility functions by Ahmad et al. (2010).

	Slight		Moderate		Extensive		Complete	
	Mean	SD	Mean	SD	Mean	SD	Mean	SD
ductile	0.085	0.028	0.121	0.052	0.185	0.075	0.328	0.123
Non-ductile	0.085	0.028	0.122	0.055	0.187	0.077	0.235	0.093

Figure 5-27 shows the comparison between the fragility curves (PhD) with the fragility functions produced by Ahmad et al. (2010). From the comparison, the fragility curves of Ahmad et al. (2010) for ductile and non-ductile RC buildings are almost identical for all damage states except collapse. However, the results of the dynamic fragility analysis for the 4-storey substandard RC building (see Figure 5-20) indicates that the ductility of the structure seriously affects the fragility of the building. This can be shown as a comparison between ductile and non-ductile cases where a noticeable difference can be observed (Figure 5-27). On the other hand, the fragility curves presented by Ahmad et al. (2010) overestimate the damage probability for all damage states. For example, the percentage difference for the PGA, which corresponds to the 50% probability of collapse for non-ductile and ductile cases with the general fragility curves (PhD), is ~250% and ~150%, respectively.

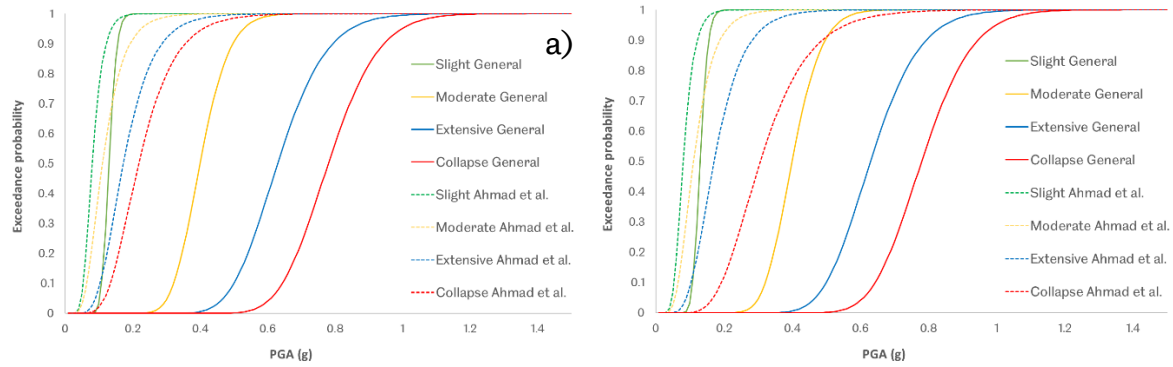


Figure 5-27: Comparison between the derived general fragility curves (PhD) and the fragility curves by Ahmad et al. (2010) for midrise a) ductile b) non-ductile RC buildings.

5.3.2.2 Akkar et al., 2005

The 2nd study is conducted by Akkar et al. (2005), which derived fragility functions for low-rise and mid-rise buildings in Turkey was based on an outdated low-level seismic design code (1975 Turkish Seismic Code). Table 5-8 presents the parameters for fragility functions (lognormal distribution) for the 4-storey RC building whilst PGV is considered as IM in this study. The damage states are considered to be light, moderate and severe.

Table 5-8: Fragility functions by (Akkar et al., 2005).

	Light		Moderate		Severe	
	Mean	SD	Mean	SD	Mean	SD
4-storey	14.212	8.027	59.589	23.642	75.670	19.151

The general fragility curves (PhD) are compared with the fragility curves presented by Akkar et al. (2005), (Figure 5-28: .

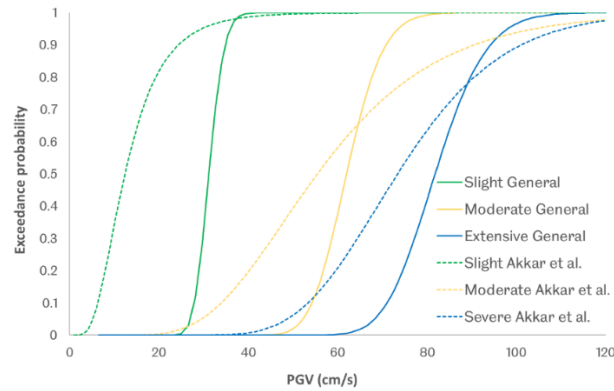


Figure 5-28: The comparison between general fragility curves (PhD) and fragility curves given by Akkar et al., (2005) for a 4-storey RC building.

Figure 5-28 shows that the fragility curve for slight damage states from Akkar et al. (2005) overestimates the probability of exceedance on each PGV value and approximately +150% for PGA corresponding to 50% probability of exceedance. On the other hand, the fragility curves for moderate and severe damage states underpredict the probability of exceedance at higher PGV values and overestimate at lower PGV values. Also, the probability of exceedance for severe damage reaches 100% at $PGV=200$ cm/s ($PGA=2.78$ g) for Akkar et al. (2005) fragility curves while $PVG=88$ cm/s ($PGA=0.94$ g) is the correspondence PGA when the probability reaches 100% for extensive damage from the PhD fragility curves. For extensive and moderate damage, it is obvious that especially for high probability of exceedance values over 70%, Akkar et al. (2005) fragility curves underestimate the damage.

The main focus of Akkar et al. (2005) was to consider the uncertainties which come from hazard by considering a large number of accelerograms from Turkey and the USA. This work considered the effect of deficiencies (longitudinal bar buckling, bond-slip behaviour, material and geometric uncertainties, etc.) in a structure on the fragility analysis by modelling the degrading behaviour of the building. The experimental study was used for validation, while dealing with the demand (hazard) deterministically to be able to focus on the real behaviour. The other main difference is in the damage limit state definition and the damage index used in these studies.

Akkar et al. (2005) used simple inter-storey drift limits for the damage index, whilst for this PhD study, a more realistic damage index is used based on the change of the structural period.

5.3.2.3 Erberik, 2008

The 3rd study is performed by Erberik (2008), which is a fragility analysis for low-rise and mid-rise RC buildings representing the structures constructed between 1973 and 1999 in the Duzce region, Turkey. The fragility functions are based on lognormal distribution with PGV as IM, considering serviceability (LS1), damage control (LS2) and collapse prevention (LS3) as damage states. Table 5-9 presents the fragility function for mid-rise bare frames (MR-BR).

Table 5-9: Fragility functions by Erberik (2008).

	LS1		LS2		LS3	
	Mean	SD	Mean	SD	Mean	SD
MR-BR	17.122	9.376	54.095	20.987	79.831	22.877

Figure 5-29 shows the comparison between general fragility curves (PhD) and Erberik (2008) fragility curves for the mid-rise bare frame building category.

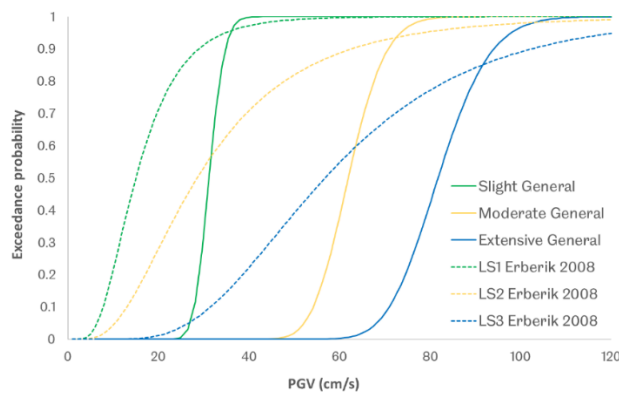


Figure 5-29: Comparison between general fragility curves (PhD) and Erberik's fragility curves for an RC mid-rise bare frame.

Figure 5-29 shows that for slight or serviceability damage states, Erberik overestimates the probability of exceedance, however, the exceedance probability is overestimated

at lower PGV and underestimated at higher PGV for limit states of damage control and collapse prevention.

The probability of exceedance for LS3 reaches 100% at PGV=200 cm/s (PGA= 2.78 g) for Erberik (2008) fragility curves, while PVG=88 cm/s (PGA=0.94 g) is the correspondent PGA when probability reaches 100% for extensive damage from the PhD fragility curves. Although Erberik fragility curves are produced for mid-rise buildings built in 1973-1999, when compared with LS3 fragility curves, it is obvious that Erberik's fragility curves underestimate damage for IM values above 80% probability of exceedance and overestimate for ranges below 80%.

5.3.2.4 Kirçil and Polat, 2006

The 4th study is performed by Kirçil and Polat (2006), focusing on the development of fragility curves for mid-rise RC structures (3, 5 and 7 storeys) designed according to the 1975 Turkish seismic design code. The fragility functions use a lognormal distribution considering two damage states of yielding and collapse with IM PGA, Sa and Sd. Table 5-10 gives the fragility function for 3 and 5 storeys structures with IM as PGA.

Table 5-10: Fragility functions by Kirçil and Polat (2006).

	Yielding		Collapse	
	Mean	SD	Mean	SD
3-storeys	0.093	0.029	0.799	0.165
5-storeys	0.073	0.016	0.701	0.166

Figure 5-30 presents the general fragility curves (PhD) compared with the fragility curves given by Kirçil and Polat (2006) for 3 and 5-storey RC buildings.

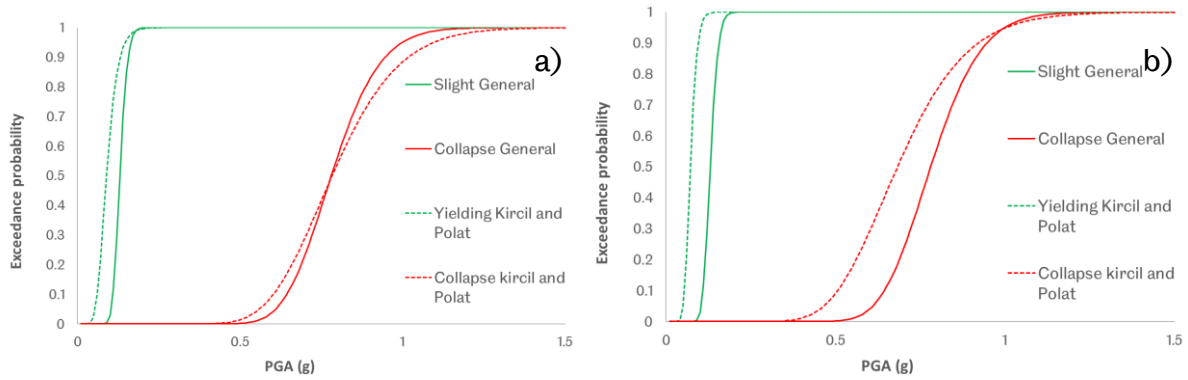


Figure 5-30: Comparison between general fragility curves (PhD) and fragility curves given by Kirçil and Polat (2006) for a) 3-storey b) 5-storey substandard RC building.

There is a good agreement between the slight and collapse damage limit states of the general fragility curves (PhD) with the fragility curves given by Kirçil and Polat (2006) for 3 storey substandard RC buildings.

5.3.2.5 Ozmen et al., 2010

The 5th study is conducted by Ozmen et al. (2010). The fragility functions for low-rise and mid-rise RC buildings are based on the pre-modern code (TEC-1975) and modern code (TEC-1998). The fragility functions for 4-storey RC buildings follow the pre-modern code, using a concrete strength of 16 MPa. The IM is PGA and the considered damage states are the immediate occupancy (IO), life safety (LS) and collapse prevention (CP), (Table 5-11). The fragility functions are based on lognormal distribution.

Table 5-11: Fragility functions by Ozmen et al. (2010).

	LS1		LS2		LS3	
	Mean	SD	Mean	SD	Mean	SD
4-storey	0.392	0.241	0.572	0.257	0.619	0.239

Figure 5-31 presents the general fragility curves (PhD) compared with fragility curves given for a 4-storey RC building by Ozmen et al. (2010).

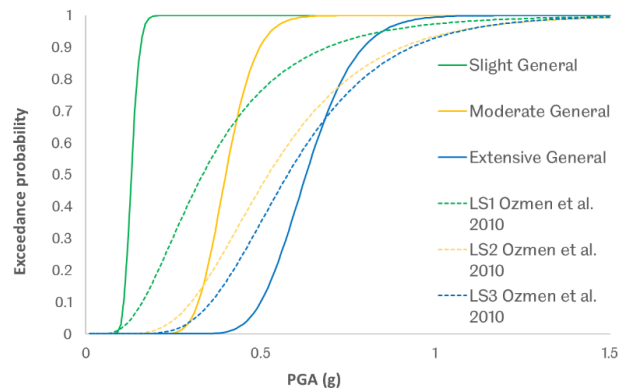


Figure 5-31: Comparison between the general fragility curves (PhD) and the fragility curves given by Ozmen et al. (2010) for a 4-storey RC building.

From the comparison, it is observed that the fragility curves given by Ozmen et al. (2010) underestimate the exceedance probability for damage states LS1 and LS2. On the other hand, for damage state LS3, the probability of exceedance is overestimated at lower PGA values and underestimated at higher PGAs.

5.3.2.6 Tsionis et al., 2011

The 6th study is conducted by (Tsionis et al., 2011) in which, fragility functions for low, mid and high rise RC buildings in the Euro-Mediterranean region are presented, considering as the main parameters the load-bearing system type, ductility level, design code and infill walls. Table 5-12 gives the fragility functions for mid-rise moment-resisting frame buildings designed according to pre-modern code (TEC-1975) for ductile and non-ductile cases. The fragility functions use a lognormal distribution with two damage states of yielding and collapse with PGA as IM.

Table 5-12: Fragility functions by Tsionis et al. (2011).

	Yielding		Collapse	
	Mean	SD	Mean	SD
Ductile	0.245	0.101	0.667	0.174
Non-Ductile	0.170	0.072	1.129	5.025

The general fragility curves (PhD) derived for the substandard 4-storey RC building was compared to the fragility curves given by Tsionis et al. (2011) ().

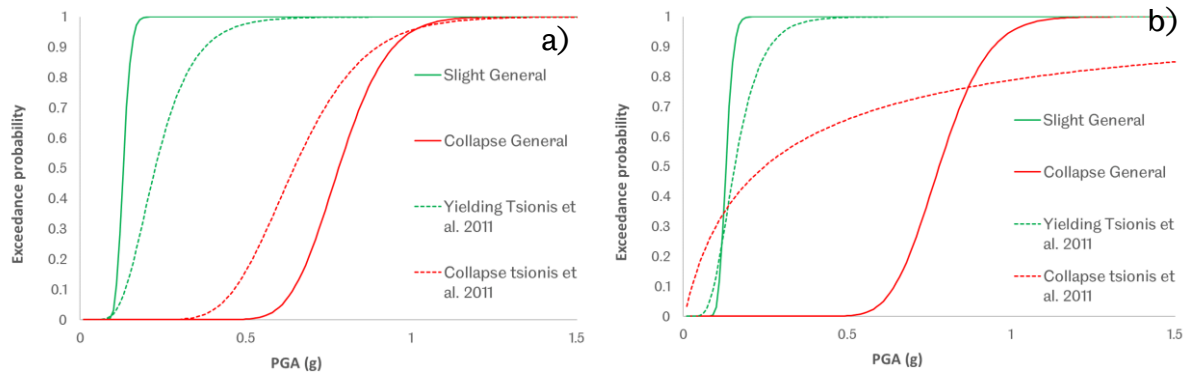


Figure 5-32: Comparison between the general fragility curves and fragility curves by (Tsionis et al., 2011) for a) ductile mid-rise low code b) non-ductile mid-rise low code.

The fragility curves given by Tsionis et al. (2011) for ductile mid-rise low-code RC buildings, underestimate the exceedance probability for yielding damage states and overestimate the exceedance probability for collapse damage state. In comparison to the fragility curves developed in this research, the fragility curve for the non-ductile case for the collapse limit state does not make meaningful sense since it reaches 96% damage at PGA of 5g.

5.3.2.7 Conclusions

It can be concluded that the examined analytical fragility functions show differences between each other in IM level, damage state and damage index consideration, variable parameters considered in analytical modelling, material quality, uncertainties considered in probabilistic analysis, statistical function fitting to the data, etc. This brings a high level of unreliability to risk calculations which use the results of fragility analysis as their input to calculate damage, collapsed buildings and estimated number of casualties during an earthquake event.

The framework introduced in this PhD is a simple, yet very effective solution to tackle this problem: the advanced adaptive fragility curves increase the accuracy of the damage calculations in the risk analysis by capturing the behaviour of these types of

substandard RC buildings. They can also provide the flexibility of choice between adaptive fragility curves according to the material quality and detailing of the buildings.

5.4 Proposed Vulnerability assessment framework

This framework is capable of deriving advanced adaptive vulnerability curves for any RC building class. It takes into account the flexural dominant failure mode considering:

- a. Longitudinal rebar buckling and the imposed pinching effect
- b. Longitudinal rebar slippage in column-to-joint and column-to-foundation
- c. Low quality of materials (Cyclic behaviour)

The user can choose the most accurate fragility function for different damage limit states according to material quality and detailing.

The analytical modelling procedure proposed for substandard RC columns/buildings using OpenSees, is validated against elemental and frame-level experimental data as the main input for the framework. Figure 5-33 presents the flowchart explaining the details of the developed framework. The main steps are:

- 1- Preparation of analytical 3D/2D mode of substandard (1)/upgraded RC (2) element/building using the proposed analytical procedure (Section 4.2).
- 2- Selection of scenario earthquake (site-specific design spectrum/record specific spectrum).
- 3- Generating LH samples based on variable parameters of the capacity.
- 4- Performing NRCPA for each sample.
- 5- Performing analytical vulnerability analysis using modified CSM.
- 6- Collection of all damage statistical data from all samples.
- 7- Performing statistical analysis (curve fitting) on the collected data.
- 8- Derivation of adaptive/general fragility curves.
- 9- Converting the fragility curves to vulnerability curves using a conversion matrix.

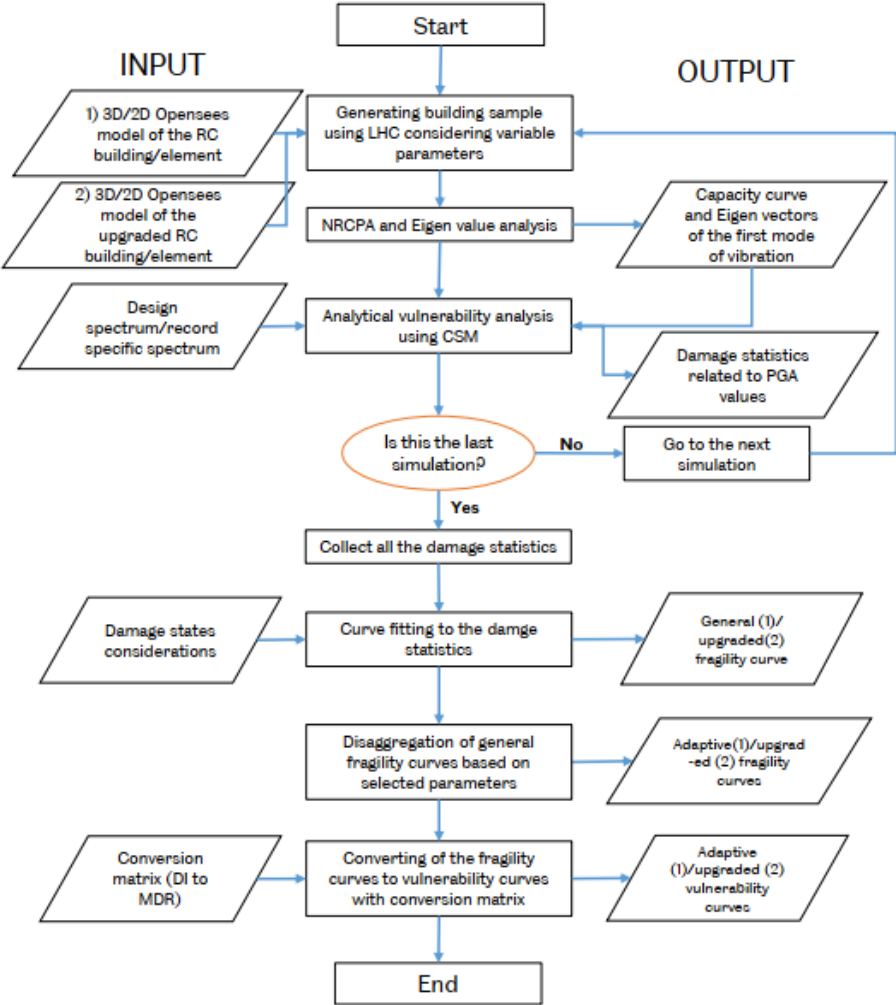


Figure 5-33: Flowchart of the developed framework.

CHAPTER 6 CONCLUSIONS AND FUTURE WORK

6.1 Introduction

This chapter presents the main conclusions/observations of this PhD research and recommendations for future work. The conclusions are grouped in main headings according to their thematic content. At the end of this chapter, further recommendations are given for future work.

The overall aim of this study is to develop an analytical probabilistic seismic fragility assessment framework applicable for substandard RC elements/buildings in developing countries. The proposed framework is a simple yet very effective solution to derive advanced adaptive fragility curves which can increase the accuracy of the damage calculations in risk analysis by capturing the actual behaviour of substandard RC buildings. They can also provide the flexibility of choice between adaptive (parameter specific) fragility curves according to the material quality and detailing of the buildings.

6.2 Conclusions and observations

6.2.1 Analytical FE modelling practices using OpenSees

- Lumped-plasticity element models are not suitable for element-based fragility analysis. The reason is the behaviour of the rotational springs is empirically

derived, and as a result, the element behaviour has to be known as a-priory. But it can be useful to determine overall structural level behaviour.

- DBE is not suitable for nonlinear seismic assessment of structures because the DB approach unrealistically overestimates the stiffness and the strength of the element compared to the FB formulation.
- To model the common deficiencies for substandard RC columns/buildings in OpenSees, a combination of “ZeroLengthSection” and “forceBeamColumn” elements was employed. For the “forceBeamColumn” element, separate fibre sections for the mid-part and the hinge-part were used.

6.2.2 Comparing local and global damage indices

- The comparison between three damage index methods (inter-storey drift-based, change of structural period and rotation-based) with experimental observations, indicates that the most suitable damage index is based on the change of structural period for both elemental and structural fragility analysis.

6.2.3 Performing adaptive probabilistic seismic fragility analysis on substandard RC column/building:

- Improved CSM with RCPA can be employed in seismic vulnerability assessment to account for cyclic degradation of material behaviour and the pinching effect originated by buckling.
- The comparison between NTHA results and the performance point from RCPA using improved CSM, indicates that CSM is suitable to be used for seismic assessment of substandard RC buildings.
- The percentage difference for PGA values corresponding to 50% probability of exceedance between S220 and S420 rebar types for the column under 20% axial load are: 17%, 30% for slight and moderate while 25% for extensive and collapse damage limit states. However, for probability of exceedance above 70%, the values are even more severe.

- For rebar type S220, increasing axial load from 20% to 50% can adversely affect the fragility curves by approximately 55% for slight, moderate and extensive damage limit states and 46% for collapse damage limit state.
- The differences between the concrete class 8-15 adaptive fragility curves and general fragility curves are -18%, -11%, -5% and -7% for slight, moderate, extensive and collapse LSs. While, the differences between the concrete class 25-35 adaptive fragility curves and general fragility curves are +15%, +18%, +11% and 9% for slight, moderate, extensive and collapse LSs.

6.2.4 Upgraded fragility curves for substandard RC column/building:

- Comparison between the PGA values of fragility curves of the case study RC building (bare and retrofitted) with rebar type of S220 (corresponding to 50% probability of exceedance) for slight, moderate, extensive and collapse limits, shows 85%, 56%, 48% and 44% improvement, respectively.
- The upgraded fragility curve for the ITU column (hypothetically strengthened with 1 layer of CFRP), shows promising improvement. The collapse damage limit state fragility curve for the column with S220 rebar type and 180 mm of stirrup spacing, improved approximately 55% comparing the PGA values corresponding to 50% probability of exceedance.

6.2.5 Vulnerability analysis of substandard RC building:

- Vulnerability curves are highly sensitive to the grade of the reinforcing steel. The MDR at 0.6g PGA level is 80% for S220, 38% for S420 whilst the MDR for the general vulnerability curve is 62%. The percentage differences of S220 and S420 from the general vulnerability curve are 23% and 38%, respectively.
- The effect of concrete strength on the vulnerability curves is also considerably high. At PGA level 0.6g, the percentage differences of MDR between concrete adaptive vulnerability curves and the general vulnerability curve are -12%, +14%

and +40% for 8-15 MPa, 15-25 MPa and 25-35 MPa, respectively. However, the percentage difference between the two MDR of 8-15 MPa and 25-35 MPa at PGA of 0.6g, is 57%.

6.2.6 Comparison of derived general fragility curves (4-storey substandard RC building) with fragility curves available in the literature:

6.2.6.1 Ahmad et al. (2010)

- For all damage states except collapse, the fragility curves of Ahmad et al. (2010) for ductile and non-ductile RC buildings are almost identical to each other. This contradicts the adaptive fragility analysis results (4-storey substandard RC building) which show that brittle structures affect fragility more critically.
- Ahmad et al. (2010) fragility curves overestimate damage probability for all damage states when compared with PhD fragility curves. For example, for non-ductile and ductile cases, the percentage difference of PGA corresponding to 50% probability of collapse, with the general fragility curves (PhD) is ~250% and ~150%, respectively.

6.2.6.2 Akkar et al. (2005)

- For the slight damage states, the fragility curve proposed by Akkar et al. (2005) overestimates the probability of exceedance values across all PGV values in comparison to the fragility curves (PhD) and approximately +150% at PGA corresponding to 50% probability of exceedance.
- In comparison to PhD fragility curves, Akkar et al. (2005) fragility curves underestimate the probability of exceedance for moderate and severe damage limit states, at higher PGV values. While, they overestimate at the lower PGV values.

- The probability of exceedance for severe damage LS reaches 100% at PGV=200 cm/s (PGA= 2.78 g) for Akkar et al. (2005). For the PhD fragility curves, PVG=88 cm/s (PGA=0.94 g) is for probability of 100% for the same damage LS.

6.2.6.3 Erberik, 2008

- Erberik (2008) fragility curves overestimates the probability of exceedance for slight/serviceability damage LSs, however, the exceedance probability is overestimated at lower PGV and underestimated at higher PGV, for damage control and collapse prevention LSs.
- The PGV, which the probability of exceedance reaches 100%, is 88 cm/s (PGA=0.94 g) and 200 cm/s (PGA= 2.78 g) for extensive damage LS (PhD) and the equivalent LS3 (Erberik, 2008), respectively.
- From comparing LS3 fragility curves with extensive damage LS (PhD), Erberik (2008) fragility curves, underestimate damage at PGV values above 80% probability of exceedance and overestimate below 80%.

6.2.6.4 Kirçil and Polat (2006)

- For slight and collapse damage LSs, Kirçil and Polat (2006) fragility curves show good agreement with the general fragility curves (PhD) for 3 and 5-storey substandard RC buildings.

6.2.6.5 Ozmen et al. (2010)

- Ozmen et al. (2010) fragility curves underestimate the exceedance probability for damage states LS1 and LS2. For damage state LS3, the probability of exceedance is overestimated at lower PGA values and underestimated at higher PGAs.

6.2.6.6 Tsionis et al., 2011

- Tsionis et al. (2011) ductile-fragility curves underestimate the exceedance probability for yielding damage LS while, overestimate for collapse damage LS in comparison to, the PhD fragility curves.
- The non-ductile-fragility curves for the collapse LS proposed by Tsionis et al. (2011) does not give a meaningful result, since it reaches 96% damage at PGA of 5g.

6.3 Recommendations for Future Work

Whilst the aim and objectives of this study were successfully achieved, additional areas for future work are identified as:

- The applicability of the PhD framework can be extended to cover other types of failure mechanisms of substandard RC buildings (shear failure, impact or pounding failure, foundation settlement, etc.).
- The effect of infill-walls, soil-structure interaction, etc. could be taken into account in the analytical model after validation against experimental results.
- More variables related to the capacity (e.g. ageing effect on the corrosion of the rebars, etc.) can be considered and added to the framework.
- The demand can be considered probabilistically either by taking several record specific spectra or by randomising the corner periods of the design spectrum for various soil types.
- Adaptive fragility curves can be derived using the developed framework to cover a wide range of building categories (e.g. low rise, midrise, etc.) in developing countries.
- The analytical modelling procedure can be enhanced by considering other failure mechanisms such as shear failure, short columns, irregularities in plan and height of the building, etc.

- The developed framework could be implemented into the existing earthquake risk assessment (ERA) framework developed at the University of Sheffield. Also, any available ERA framework for developing countries which has the feature of accepting fragility curves as an input (e.g. ELER (Hancilar et al., 2010)).
- The damage state definition based on the change of structural period requires further validation with the existing substandard RC building of the Marmara region and Turkish seismic codes.
- Increasing the sampling size and considering all the variabilities of longitudinal rebars could increase the accuracy of general fragility curves for substandard RC buildings.
- The conversion matrix used to convert fragility curves to vulnerability curves needs to be updated for the case study region.
- The analytical modelling procedure for upgraded substandard RC buildings/columns needs further validation with additional full-scale experimental data.

APPENDIX A LITERATURE REVIEW ON SEISMIC VULNERABILITY ASSESSMENT OF RC BUILDINGS.

SEISMIC VULNERABILITY ASSESSMENT METHODOLOGIES

Vulnerability curves graphically represent seismic risk and relate the probability of exceedance at various performance levels (damage limit states) to ground motion parameters of specific excitations. Strength or displacement-based damage limit states need to be defined for producing vulnerability curves.

A.1 Rapid Seismic Vulnerability Assessments:

A simple method for assessing the vulnerability from a most probable hazard, involves Rapid Visual Screening (RVS) following the provisions of FEMA154 (2002), an updated version of ATC-21 (1988). This procedure involves exterior inspection by trained inspectors following a sidewalk procedure. The surveyed buildings are classified into two groups according to the procedure specified in the handbook. One group contains buildings that are declared as no risk-to-life safety and the other group includes buildings that are seismically vulnerable, involve risk-to-life safety and thus, require more detailed assessments from professionals with experience in seismic design. To tag post-earthquake damaged buildings and declare their occupancy status (safe or unsafe), ATC-20 (1989) suggests that decisions must be made on the spot. Three

different cards are displayed on each building; “green” for safe, “yellow” for limited entry and “red” for unsafe.

A study performed by Hassan and Sozen, (1997), used the Turkish building inventory to develop a vulnerability function. The building information inventory was based on the floor area, structural elements (dimensions and reinforcement details) as well as infill walls. Using this information, the wall (ratio of the effective area of the infill and shear walls to the total floor area) and column (ratio of effective area of columns normalised to the total floor area) indices, are calculated. It was concluded that buildings with wall or column area of 0.5%, are safe, whilst with less than 0.25% are vulnerable.

A similar approach was adopted by Gulkan and Sozen, (1999), who related drift demand at the ground floor to wall area. One of the main drawbacks of these methods is that they assume the construction quality and material properties of the structures to be uniform, which is not the case for countries where building codes are not enforced.

Yakut, (2004) proposed a procedure for preliminary assessments on seismic vulnerability of moderate ductility, low to mid-rise RC buildings in Turkey. The procedure relies on the orientation, size and concrete strength of vertical load resisting components. It accounts for the contribution of effective filler wall areas and architectural features. A key strength of the procedure is its capability to incorporate the effects of regional seismicity and soil conditions through Vcode, which is directly computed from the seismic code.

A.2 Empirical Methods

Empirical methods are based on the statistical evaluation of past earthquake damage, therefore; these methods are suitable where extensive earthquake damage survey regional data are available. Unfortunately, post-seismic damage surveys and recording damage were not performed for many developing countries, hence, using empirical

seismic vulnerability assessment methods are limited and non-applicable. Although realistic vulnerability functions can be derived using this information, the generated vulnerability curves are highly specific/applicable to the built environment of a certain region. If used to predict damage in a different region, unsatisfactory damage predictions may be obtained (Palacios, 2004). This is due to different regional construction practices, traditions and characteristics of the earthquake. The quality and quantity of the observed data is of prime importance for the reliability of this method and requires a large number of observations over a wide range of ground motions to generate these curves with a high degree of certainty. Damage data from a single event may not be sufficient to efficiently define the vulnerability curve, since they are required at various ground motion levels.

Various types of empirical vulnerability assessment methods have been used widely for a variety of structural systems in different regions. These curves are based on observational data and are considered to be accurate since they include necessary information of the building stock exposed to an earthquake. This information is related to the structural system, construction year, number of stories and other deficiencies related to building configuration along with the building damage data. In addition, seismo-tectonics, geological and geotechnical information related to the exposed building stock is also included.

Two main types of empirical methods are: damage probability matrices (DPM) and vulnerability functions. DPMs can be developed using two approaches:

- a. using collected observation data from actual earthquakes. In this case, damage directly related to measured ground motion intensity.
- b. predicting the structural response and related damage using theoretical dynamic analysis.

A.2.1 Existing empirical vulnerability assessment studies

A.2.1.1 Damage Probability Matrices

To estimate the damage to a structure, damage probability matrices (DPM) can be used to express the relationship between damage probability levels and ground intensity levels. Empirical DPM were firstly proposed Whitman et al. (1973), based on compiled damage survey data collected from approximately 1600 buildings (5 to 19 stories), after the 1971 San Fernando earthquake (see Table 1). In this method and for a specific seismic event, buildings with the same structural system, are considered to perform similarly. In which, for building type T, the intensity of seismic event I and damage level D, are discretely related.

Table 1 Damage Probability Matrix by Whitman et al. (1973)

Damage State	Structural Damage	Non-structural Damage	Damage Ratio (%)	Intensity of earthquake				
				V	VI	VII	VIII	IX
0	None	None	0-0.05	10.4	-	-	-	-
1	None	Minor	0.05-0.3	16.4	0.5	-	-	-
2	None	Localised	0.3-1.25	40.0	22.5	-	-	-
3	Not noticeable	Widespread	1.25-3.5	20.0	30.0	2.7	-	-
4	Minor	Substantial	3.5-4.5	13.2	47.1	92.3	58.8	14.7
5	Substantial	Extensive	7.5-20	-	0.2	5.0	41.2	83.0
6	Major	Nearly total	20-65	-	-	-	-	2.3
7	Building condemned		100	-	-	-	-	-
8	Collapse		100	-	-	-	-	-

Whitman et al. (1973) introduced, for the first time, the damage level on a building to be quantified as the damage ratio (DR) (ratio of repair cost to replacement value), currently used by insurance companies as the most common economic indicator. This approach was frequently used by several researchers by adopting different intensity scales (i.e. Braga et al., 1982, Dolce et al., 2003, Di Pasquale et al., 2005) for various building classes in Europe.

Rota et al., (2008), developed empirical vulnerability curves for seismically designed structures in Italy from a database of 90000 buildings by establishing DPM. The PGA was defined using the event magnitude, a suitable attenuation relationship and site to

source distance. The DPM was further processed to define cumulative lognormal fragility curves by considering the probability of reaching or exceeding a damage limit state at a certain PGA level.

A.2.1.2 Vulnerability functions (Continuous vulnerability curves)

Many seismic vulnerability assessment studies were undertaken by gathering damage data for a type of structure from different earthquake events and regions. These datasets have been used to derive continuous vulnerability curves through regression analysis (Spence et al., 1992, Rossetto and Elnashai, 2003, Orsini, 1999).

Spence et al. (1992) derived empirical vulnerability curves using regression analysis by analysing data of 70000 buildings surveyed after 13 earthquakes. A high confident dataset with 20 to 100 damage survey data points was used for proposing vulnerability functions for common building types. To define the ground motion severity, the parameter-less Scale of Intensity (PSI) was used, since macroseismic intensity is not a continuous variable. To define damage state and vulnerability curves the MSK intensity scale and normal cumulative distribution were used, respectively.

Orsini (1999) developed empirical vulnerability curves by using damage data for apartment buildings from a single earthquake event in Italy. A total of 50,000 apartments from 41 different sites were used for deriving the vulnerability curves (Figure 1).

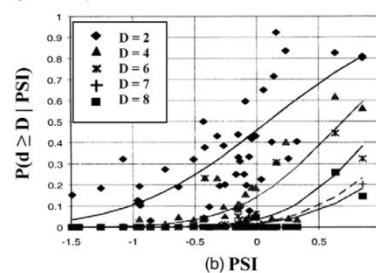


Figure 1: Empirical vulnerability curve developed by Orsini, (1999).

Similarly to Spence et al., (1992), PSI and MSK were used to define ground motion parameter and damage, respectively. PSI was converted to PGA using an empirical

correlation function so that the ground motion and damage were not defined in the form of intensity. However, the derived curves are of limited use since they were generated from a single earthquake. Also, a single building type (apartments) cannot be considered as representative sample of damaged buildings in a building stock where diverse structural systems exist. The scatter related to the derived curves was high and low R² values of 0.41 and 0.49 were reported, due to poorly defined damage states taken during the survey.

Yamazaki and Murao (2000) derived empirical vulnerability curves based on damage data gathered after the Kobe earthquake which was categorised according to the building age, material and height. For RC buildings, the data from 16 different locations were used including 3814 buildings. Peak ground velocity was used as a ground motion parameter and the vulnerability curves were generated based on different design codes, but no specific lateral load resisting system was considered. Only two damage states (moderate and heavy) were used, which is not enough for defining the overall structural performance.

Rossetto and Elnashai, (2003), developed a new damage scale, called homogenised reinforced concrete (HRC) damage scale, by using heterogeneous empirical damage data from several post-earthquake damage databanks. The limit states were defined in an HRC damage index (DIHRC), experimentally calibrated to the maximum inter-storey drift ratio (ISD_{max}%) using published dynamic test results conducted on RC bare, infilled and shear wall structural systems. Then, 99 existing post-earthquake damage databanks (340,000 RC buildings) were re-interpreted using the developed HRC scale. Correlation tables between the HRC and other existing damage scales for different structural systems were prepared using the authors interpretation of the relative limit state damage descriptions (Table 2).

Table 2. The equivalence between existing damage scales and HRC-Scale for general RC structures (Rossetto and Elnashai, 2003).

DI _{HRC}	DAMAGE STATE	DUCTILE MRF	NON-DUCTILE MRF	INFILLED MRF	SHEAR-WALL
0	None	No damage	No damage	No damage	No damage
10	Slight	Fine cracks in plaster partitions/infills	Fine cracks in plaster partitions/infills	Fine cracks in plaster partitions/infills	Fine cracks in plaster partitions/infills
20	Light	Start of structural damage	Start of structural damage	Cracking at wall-frame interfaces	Start of structural damage
30		Hairline cracking in beams and columns near joints (<1mm)	Hairline cracking in beams and columns near joints (<1mm)	Cracking initiates from corners of openings	Hairline cracking on shear-wall surfaces & coupling beams
40				Diagonal cracking of walls. Limited crushing of bricks at b/c connections	Onset of concrete spalling at a few locations
50	Moderate	Cracking in most beams & columns	Flexural & shear cracking in most beams & columns	Increased brick crushing at b/c connections	Most shear walls exhibit cracks
60		Some yielding in a limited number	Some yielding in a limited number	Start of structural damage	Some walls reach yield capacity
70		Larger flexural cracks & start of concrete spalling	Shear cracking & spalling is limited	Some diagonal shear cracking in members especially for exterior frames	Increased diagonal cracking & spalling at wall corners
80	Extensive	Ultimate capacity reached in some elements – large flexural cracking, concrete spalling & re-bar buckling	Loss of bond at lap-splices, bar pull-out, broken ties	Extensive cracking of infills, falling bricks, out-of-plane bulging	Most shear walls have exceeded yield, some reach ultimate capacity, boundary element distress seen.
90		Short column failure	Main re-bar may buckle or elements fail in shear	Partial failure of many infills, heavier damage in frame members, some fail in shear	Re-bar buckling, extensive cracking & through-wall cracks. Shear failure of some frame members
100	Partial Collapse	Collapse of a few columns, a building wing or single upper floor	Shear failure of many columns or impending soft-storey failure	Beams &/or columns fail in shear causing partial collapse. Near total infill failure	Coupling beams shattered and some shear walls fail
	Collapse	Complete or impending building collapse	Complete or isoft-storey failure at ground floor	Complete or impending building collapse	Complete or impending building collapse

Then, damage state vs proportion of the population of buildings were plotted for each dataset. The DI_{HRC} values were assigned to each damage state of every dataset using correlation tables for each defined structural system. To describe the relationship between DI_{HRC} and ISD_{max}%, the developed equations were used and DI_{HRC} values were converted to ISD_{max}% values. Then, the proportion of the population of the buildings was converted to cumulative form for each discrete ISD_{max}% values and

continuous probability distribution functions were attributed. Using the $ISD_{max\%}$ values, the HRC damage state exceedance probabilities were determined from the fitted cumulative distributions. For each HRC damage state, there are 99 exceedance probabilities. Vulnerability is obtained by plotting these exceedance probabilities along with the corresponding seismic ground motion parameters, which are defined in terms of peak ground acceleration, spectral acceleration/displacement for 5% damping, or inelastic spectral displacement for a displacement-based damping value. For each ground motion severity, damage state exceedance probabilities derived from each dataset were combined either using an equal weighting or using weighting factors based on the sample of the surveyed buildings. Nonlinear regression analyses were carried out to derive the vulnerability curves. Ground motion parameters were obtained from available ground motion records or attenuation relationships. In addition to class-specific curves, 'homogenous' or 'general' vulnerability relationships, which apply to all lateral-load resisting systems, were also developed (Figure 2).

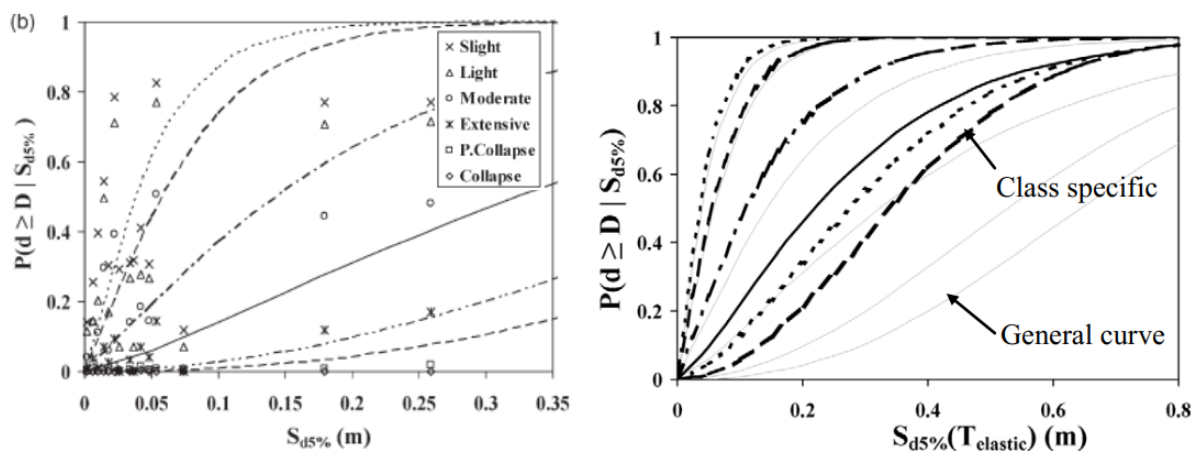


Figure 2: a) General empirical vulnerability curve compared with the weighted damages data b) fragility curve for pre-seismic building class (class-specific (Rossetto and Elnashai, 2003))

Rossetto and Elnashai (2003) also reported that the derived general curves underestimated the damages of the RC building stock after the 2001 Bhuj earthquake (India), because of its poor construction practices which led to brittle failures. Their

analysis was based on a database taken after the 1999 Kocaeli earthquake (Turkey), which had similar characteristics with the examined building stock.

The disadvantages of empirical methods can be summarised as (Ahmad, 2011):

1-Heterogeneity of the building damage data in a combined dataset arise due to the use of different damage scales in different countries and can result in inconsistent damage classification for a building class. This is the main error found in empirical vulnerability curves derived from a composite dataset.

2-Skewness of the damage data at lower ground motion intensity also arises due to the occurrence of very few strong earthquakes in areas with large populations causing uncertainty in the damage predictions at higher ground motion intensities.

3-Errors can be introduced due to inconsistent surveys performed by engineers with different experience and knowledge, and not well defined damage scales.

A.3 Existing judgmental vulnerability assessment studies

ATC-13 (Council, 1985) used this approach to develop Damage Probability Matrices (DPM) to evaluate the seismic risk in California, USA. A Damage Factor (DF) was included for intensities from VI to XII on the MMI scale, for 36 types of buildings. The DF values were suggested by 70 experts who were asked to provide three values of damage (mean, low and high). This technique has no scientific basis and has a lot of limitations, since the experience level of each expert can affect the outcome. For example, the DPM developed for typical building classes in California in ATC-13 (Council, 1985), cannot be applied to other regions such as Europe or Asia, due to differences in construction and design practices. Since the behaviour of NERC structures is not very well known, it can be difficult for an expert to assess the NERC building performance of a specific class in a specific region at various ground motion levels.

Schnabel (W.E., 1987) developed vulnerability curves for Cyprus using the building damage data of similar seismo-tectonic environments and also by considering expert opinions. Vulnerability curves were defined for two different classes of structures which included superior and substandard construction. Figure 3 shows the upper and lower bound curves for the buildings with a superior and substandard construction quality.

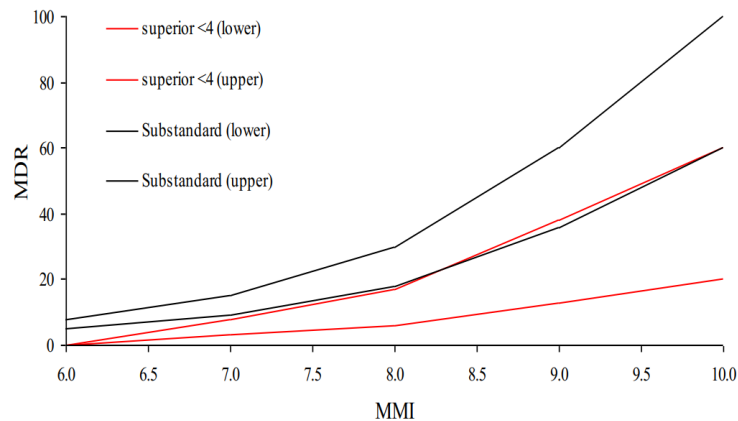


Figure 3: Judgemental curves developed by Schnabel for RC structures of Cyprus

Kyriakides (2007) compared these curves (Figure 3) with new analytical curves developed for buildings having pre-seismic design category. It was found that the curves showed a good correlation up to the MDR=50% but after that, they could not predict well the abrupt increase in damage.

A.4 Analytical/Mechanical Methods

In the recent years, analytical procedures were extensively used to derive vulnerability curves. In this method, Finite Element Analysis (FEA) of structural models is performed to determine the damage distributions. This involves the use of simulated response parameters corresponding to different building performance levels with increasing demand. The accuracy of these curves is governed by the ground motion parameter, material models, response parameter, analysis type, damage index and structural idealisation. This approach was used by several researchers to develop vulnerability curves (e.g. Mosalam et al., 1997, Calvi, 1999, Lang, 2002, Kyriakides, 2007).

Various versatile inelastic elements in FEA programmes such as Drain 3dx, ZEUS-NL or OpenSees, have empowered analytical techniques and enabled users to include response features such as shear-flexural-axial interaction, re-bar buckling, bond and shear failures. The improvements in different material models and the increase in computational speed has further enhanced their popularity. The non-linear static analytical techniques have simplified the procedure to generate damage data for a large number of structures in a swift manner and with good accuracy. Despite all the above-mentioned advantages, limitations in the current modelling techniques still exist and simulating brittle failure modes are still a challenge. Experimental data of low-strength structural elements (or entire frames) are also required to validate the existing analytical tools and can be used for calibration purposes. Material and hysteretic models in the existing analytical tools need to be improved to simulate more realistically the behaviour of engineered and NERC structures. To apply an analytical vulnerability assessment technique to a particular building stock in a region, uncertainties related to different demand and capacity parameters must also be accounted.

A.4.1 Displacement based vulnerability assessment studies

A.4.1.1 Mosalam et al., (1997)

Mosalam et al., (1997) developed analytical vulnerability curves for both bare and infilled 2-storey 2-bay GLD RC structures in Memphis, USA. Typical detailing deficiencies were considered in the analysis. For characterising the dynamic characteristics of the equivalent single degree of freedom system (SDOF), pushover analysis was conducted. 200 SDOF models with varying dynamic characteristics were defined to account for material characteristics variability. As a ground motion parameter, PGA was adopted and two sets of artificial time history records were used to perform NLTHA (to account for demand uncertainty). Inter-storey drift (ISD_{max}) was used as a response parameter and the threshold values for each limit state were judgementsally estimated. For the infilled frame, these values were considered to be

one-tenth of the values of the bare frame. For the derived curves, a considerable scatter was observed for each limit state POE around the regression curves and this was attributed to the uncertainty in the capacity and demand parameters.

A.4.1.2 Singhal and Kiremidjian, 1997

Singhal and Kiremidjian (1997), developed analytical vulnerability curves for low, medium and high-rise bare RC building structures seismically designed in California. RC buildings with 2, 5 and 12 stories and 5 bays were considered and the damage statistics were generated by carrying out a series of NLTHA. The damage index by Park and Ang (1985) was used. To represent the ground motion for each type of RC structure, average spectral accelerations between the range of periods 0.1-0.5 sec, 0.5-0.9 sec and 0.9-2.5 sec were used. 100 artificial time histories were generated to carry out NLTHA for the selected category of structures. The ground motion records were scaled following the average spectral acceleration values for each building defined period range. Uncertainties related to both demand and capacity were introduced stochastically through Monte Carlo simulations. These vulnerability curves were described with lognormal cumulative distribution and considered to be very reliable compared to existing vulnerability curves. Singhal and Kiremidjian (Singhal and Kiremidjian, 1997) updated the previously developed curves for low-rise RC buildings by adopting a Bayesian approach and by using the observed building damage data from the Northridge earthquake. This updating process helped in defining the confidence bounds on the fragility curves using the observed data.

A.4.1.3 Calvi, 1999

A deformation based simple analytical vulnerability method was proposed by Calvi* (1999) for RC frames failing in column-sway and beam-sway mechanisms. The structures were modelled as equivalent SDOF. The structural capacity of each structure was defined by yield and ultimate strength points estimated using simplified equations. In this method, the ratio of the building capacity over demand (from the displacement response spectrum) was calculated at various damage states. The

minimum and maximum drift values were predicted at four different damage states as well as their corresponding secant periods (periods were estimated using the established relationship based on the secant stiffness of a particular damage state). The minimum and maximum values of displacements and their corresponding periods were plotted (as horizontal and vertical lines) in the displacement demand spectrum which resulted in the formation of a rectangle which represents the capacity area (see Figure 4). This capacity area can be compared with the demand spectrum, and the area under the spectrum shows the building proportion failing or exceeding damage state.

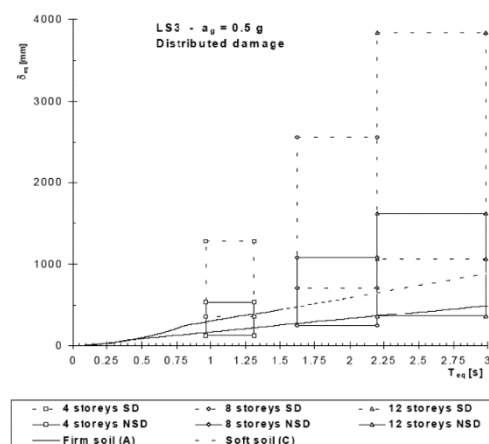


Figure 4: Example of the Calvi (Calvi*, 1999) method for the limit state (L.S.3 at 0.5g) with demand spectrum intersecting capacity

A.4.1.4 Cornell et al., 2002

Cornell et al. (2002) developed a probabilistic framework for structural assessment using a capacity and demand format. Various sets of ground motion records with different intensity levels were used to evaluate the seismic demand of the structures. Unlike Singhal and Kiremidjian (1997) who used stripe analysis, a cloud analysis was performed using seismic demand data. By carrying out cloud analysis, the demand model was defined as the median seismic demand presented by a log-linear function of a ground motion parameter. It was assumed that about the median, the structural demand is log-normally distributed having a constant logarithmic standard deviation.

Cornell et al. (Cornell et al., 2002) using a capacity and demand format developed a probabilistic framework for structural assessment. Various sets of ground motions record having different intensity levels were used to evaluate the seismic demand on the structures. Unlike Singhal and Kiremidjian (Singhal and Kiremidjian, 1997) who used stripe analysis, a cloud analysis was carried out using all the seismic demand data. By carrying out cloud analysis, the demand model was defined as having median seismic demand which was presented as a log-linear function of a ground motion parameter. It was assumed that about the median, the structural demand is log-normally distributed having a constant logarithmic standard deviation.

A.4.1.5 Erberik, 2008

Erberik (2008) developed the analytical vulnerability curves for mid-rise flat slab RC structures with infill panels. Each of the structural models generated using random data of various capacity parameters matched separately with every ground motion record, unlike in the other methods where the structural models were matched randomly with accelerograms. Apart from this, the same procedure was adopted by Singhal and Kiremidjian (1997). Pushover analysis of the structural model was used to define the performance limits for the generation of the vulnerability curves.

A.4.1.6 Rossetto and Elnashai, 2005

Rossetto and Elnashai (2005) developed analytical vulnerability curves for low-rise infilled RC frame structures representative of the Italian building stock which was designed according to a 1982 Italian building code. Target spectra for three different return periods corresponding to three different damage states were generated. These target spectra were used to select the performance specific earthquake records (10 natural records), for defining the mean spectra. To evaluate the seismic demand by considering the ground motion characteristics with less computational effort as compared to NLTHA, an adaptive pushover technique was adopted which updates the applied lateral load at each increment by incorporating the instantaneous stiffness,

modal characteristics and demand. A modified capacity spectrum method (CSM) was used for evaluating seismic demand in terms of ISD_{max} for each structure. The uncertainty in the capacity was considered by randomly generating different material parameters using the Latinhyper cube method, which results in several structural models with a random combination of the generated parameters. The seismic demand and the ground motion intensity data was used to fit the response surface equation. Using a re-sampling technique, the damage statistics corresponding to different ground motion intensities were generated from the response surface. This re-sampled data was used to develop the fragility curves for each damage state. The response surface equation used to develop each curve was defined according to the hazard level linked with the certainty that a certain performance objective will be acquired. These curves were also called performance consistent curves. For the generated fragility curves using the response surface equations, confidence bounds were also introduced. The analytical vulnerability curves after comparison with the observed data (Rossetto and Elnashai, 2003)) were found to be more conservative. Figure 5 shows the vulnerability curves for the low-rise infilled RC structures.

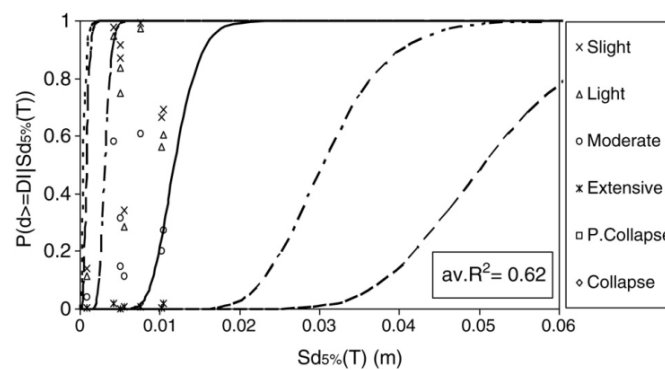


Figure 5: Analytical vulnerability curve of low-rise buildings by (Rossetto and Elnashai, 2005).

A.4.1.7 Kwon and Elnashai, 2006

More recently, analytical vulnerability curves were derived by Kwon and Elnashai (2006) for low-rise RC structures. The use of full combination of stochastic material parameters in the structural models was found to give a biased sample. Detailing

deficiencies related to the lack of ties in the joint causing reduced shear capacity and short anchorages in the bottom rebar of beams were not addressed. The uncertainty associated with the ground motion was considered to be significantly higher than the uncertainty related to the various capacity (material) parameters. The developed fragility curves were found to be dependent on the choice of earthquake dataset in a fragility assessment study of low rise RC building by Ramamoorthy et al. (2006). A cloud analysis was carried out using seismic demand data and a bilinear relationship (instead of linear as used by Cornell et al. (2002)) was established for median seismic demand. A Bayesian relationship was used to evaluate the regression parameters of the demand model.

A.4.2 Vulnerability assessment studies with detailed modelling consideration

A.4.2.1 Erberik, 2008

Erberik (Erberik, 2008) evaluated the fragility of low and mid-rise RC structures (bare and infilled) in Turkey by selecting characteristics of RC structures available in the Duzce field damage database. Each building in the database was considered as an equivalent SDOF and characterised with parameters such as period (T), strength ratio (R) and post-elastic stiffness ratio (α). Peak ground velocity (PGV) was used as the ground motion parameter. The reference fragility curves (Figure 2.8, dark lines) were generated by evaluating seismic demand from time history analysis of inelastic SDOF systems having variable T and R characteristics and a deterministic α value. Different factors affecting the fragility curves were investigated such as α , sampling technique and size of sample, limit state definition and influence of degrading behaviour. Based on the results Mid-rise buildings are more vulnerable compared to low-rise and bare frames are more vulnerable compared to infilled frames. It was found that α , sample size and sampling technique do not significantly affect the fragility estimations. Uncertainty in the limit state definition and the degrading behaviour were found to greatly affect the fragility curves. To incorporate the degrading behaviour in this study,

an energy-based hysteretic model that accounts for a low cycle fatigue model was used with two parameters controlling the behaviour. One parameter controls the level of degradation and the other one controls the degradation rate. Three types of building degradation levels were considered ranging from theoretically no degradation to very high degradation of brittle structures. The comparison of the reference fragility curves with curves for moderate and severe levels of degradation behaviour can be seen in Figure 6. This clearly shows the importance of realistically incorporating degradations from different sources in the analytical models.

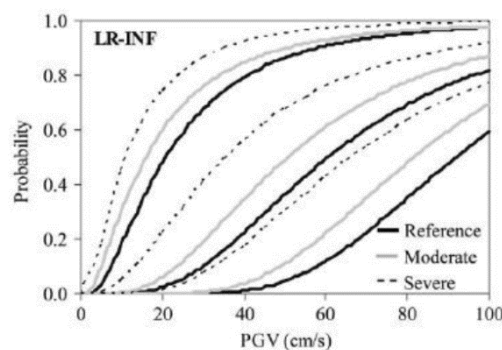


Figure 6: Analytical vulnerability curves for low-rise infilled RC structures of Turkey, Erberik (Erberik, 2008).

A.4.2.2 Celik and Ellingwood, 2008

Celik and Ellingwood (2008) studied the importance of modelling shear and bond-slip behaviour of beam-column joints for fragility analysis of GLD RC frame structures typical found in mid-American region. In this study, the full-scale beam-column joints data from existing research were used to select an appropriate joint model to attain a joint shear stress-strain relationship. Various existing joint models were examined and one more realistically replicating the experimental behaviour was selected and used in the fragility assessment. The rigid joint model was found to be unsuitable in simulating the highly pinched cyclic behaviour. The defined joint shear stress-strain relationship was used for simulating cyclic behaviour for the joint panel zone in the GLD building. A three-storey GLD building was used to evaluate the effect of the new joint model. The building had weak columns and strong beams and failed as a soft storey. Since

significant earthquake records were not available for the studied region, artificial earthquake records were used having earthquakes ranging from small to large return periods. Large inter-storey drift (ISD) occurred at the first storey when the rigid joint was used. When the new joint model was used, large deformation also occurred at the first storey, but the roof drifts at the upper stories were higher as compared to the roof drifts when the rigid joint was used. This indicated that the new model captured the flexibility due to joint shear deformation and bond degradation. On the other hand, ISD_{max} for the case building was less when the new joint model was used. This shows that the use of rigid joint models ruled out joint damage and overestimated the soft storey behaviour. For the case structure with strong columns and weak beams, ISD_{max} was higher. The rigid joint model was proposed for structures that are designed for earthquake loading according to modern codes. The derived fragility curves for 3 storey GLD bare RC building are shown in Figure 7.

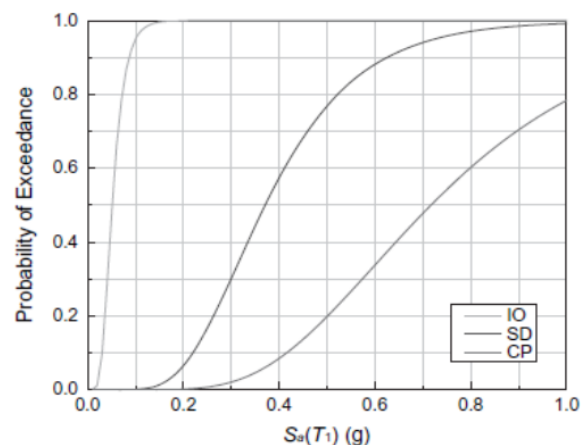


Figure 7: Analytical vulnerability curves for bare GLD low-rise building in Mid-America (Celik and Ellingwood, 2008).

A.4.2.3 Kyriakides, 2007

Kyriakides N (2007) developed a framework for analytical vulnerability assessment of low and mid-rise RC structures in Cyprus. The technique was based on improved modelling assumptions, improved performance evaluation method and probabilistically addressing capacity related uncertainties. For simplicity and

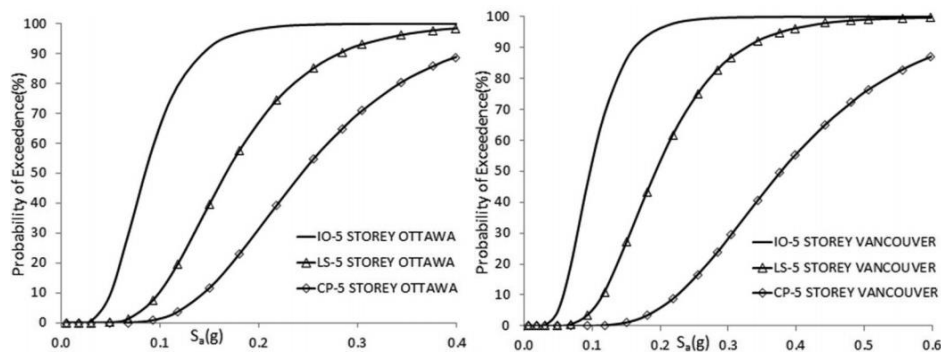
efficiency of the framework, the improved non-linear static method (NSM) was used proposed by FEMA440 (2005). Several equivalent elastic perfectly plastic (EEPP) systems at every point of the capacity curve were assumed and each point was considered to be the performance point. This assumption led to a set of secant periods, which were associated with the different level of ductility. For modelling the complex behaviour of degrading systems using selected NSM the unrecoverable energy was not included in the energy balance. The brittle failure modes were successfully captured for the pre seismic code structures using a damage index having a secant period as a response parameter. Vulnerability curves were derived as a function of PGA. Since existing capacity models for different failure mechanisms were used to simulate the degrading behaviour, the results may be conservative for LSC structures and new models in particular for concrete, bond and shear are required.

A.4.2.4 Al Mamun and Saatcioglu, 2017

Al Mamun and Saatcioglu (Al Mamun and Saatcioglu, 2017) generated the seismic fragility curves for 2, 5 and 10-stories RC buildings designed based on NBCC 2010 for average and high ductility levels, representing RC buildings at Eastern and Western Canada, respectively. A 3D model of the bare frames was developed and incremental dynamic analysis was conducted using Perform 3D to generate fragility curves. Beam and column elements modelled containing two symmetrical segments each has an elastic beam and a plastic hinge (energy degradation factor introduced to capture the stiffness degradation) with stiff end zone. In the model flexural behaviour was assumed to be dominant failure mode consequently, linear behaviour was used for elements. Synthetic earthquake records developed with a 2% probability of exceedance in 50 years with various epicentral distances and magnitudes for each region considering soil type C and compatible with NBCC (2010). Magnification of records for performing IDA was done using two spectral values design period provided by code (T_d) and effective period (T_e) observed after Eigenvalue analysis of 3D models using PRISM (2011). In this study, inter-storey drift was used as a damage indicator and the limits for performance levels assumed to be 2% for life safety (LS). For the immediate

occupancy (IO), softening index is used assuming the effective period at immediate spectral accelerations will be equal to 1.25 times of T_e . For collapse prevention (CP), the median of the maximum inter-story drift ratio attained on the IDA curve is used. In this work, uncertainty and randomness in member capacity and damage indicator (failure criteria) were not explicitly considered. Instead, dispersion for limit states and analytical modelling was taken into account in the calculation of fragility relations. Uncertainties in seismic input were considered by using several records from actual earthquakes representative of different hazard scenarios involving different magnitude-distance combinations. The conditional probability of exceeding a limit state at a given intensity, $S_a(T_e)$ or $S_a(T_d)$ calculated using Eq. 1 where D_c is median drift capacity for a limit state, D_m is conditional median of drift demand which is calculated using Cornell et al. (2002) method and assumption that demand has a lognormal probability distribution, σ_{TOT} is total uncertainty. It was found that at design period spectral acceleration the Ottawa (Eastern Canada) buildings showed less probability of exceeding limit state performance levels than Vancouver (Western Canada). The derived fragility curves for 5 storey buildings are shown in Fig.8 as a sample.

$$P_{LS} = 1 - \Phi\left(\frac{\ln D_C - \ln D_M}{\sigma_{TOT}}\right) \tag{Eq.1}$$



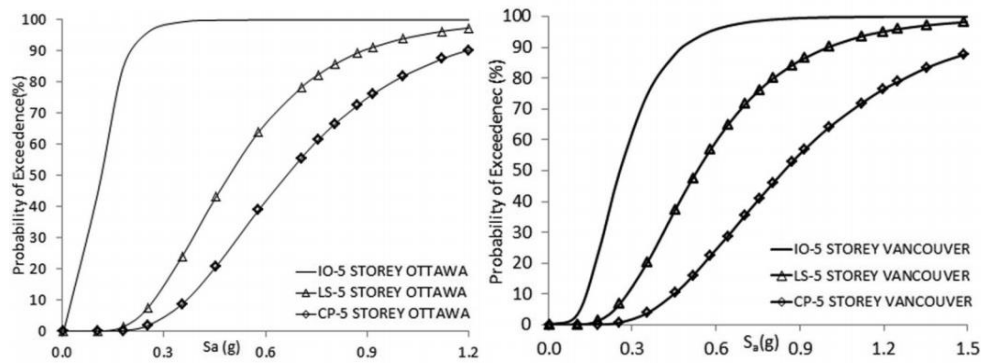


Figure 8: (a) and (b) Fragility response of 5-storey structure developed with amplified seismic records based on $S_a(T_e)$ in Eastern and Western Canada respectively. (c) (d) Fragility response of 5-storey structure developed with amplified seismic records based on $S_a(T_d)$ in Eastern and Western Canada respectively (Al Mamun and Saatcioglu, 2017).

• HAZUS

HAZUS software (HAZUS99 (1999)) developed by FEMA/NIBS (1997) has been used widely for assessing seismic risk and for seismic mitigation purposes of different cities and regions. Thirty different building types were considered. The buildings were categorised in terms of their height, structural system, level of seismic design, usage, seismic hazard zone and design. Four damage states are defined for each building class: slight, moderate, extensive and complete collapse. HAZUS adopted the capacity spectrum method (CSM) by ATC-40 (Council, 1996), to evaluate the performance point of a structure at the intersection of the capacity and the demand spectrum in Acceleration-Displacement Response Spectrum format (ADRS) as shown in figure 9a. The capacity curves for prototype structures of US were defined in HAZUS through nonlinear static pushover analysis and the variability in this curve was defined through expert opinion, earthquake damage data, and structural performance data. The seismic demand corresponding to a particular hazard scenario was included through the demand spectrum. Spectral displacement (S_d) was used for defining threshold

values and the variation of damage grade based on expert opinion. The capacity of the structures was defined by yield and ultimate points evaluated using the equations shown in figure 9b. The PP was used to evaluate the percentage of the buildings exceeding a threshold of a particular damage state. A lognormal distribution was used to develop the fragility curves. The limitation of the HAZUS approach is that it does not allow modifications of its different components. HAZUS gives the mean values of damage prediction and to get input parameter variation, a tedious sensitivity analysis is required by changing the value of the input parameter each time and rerunning HAZUS each time.

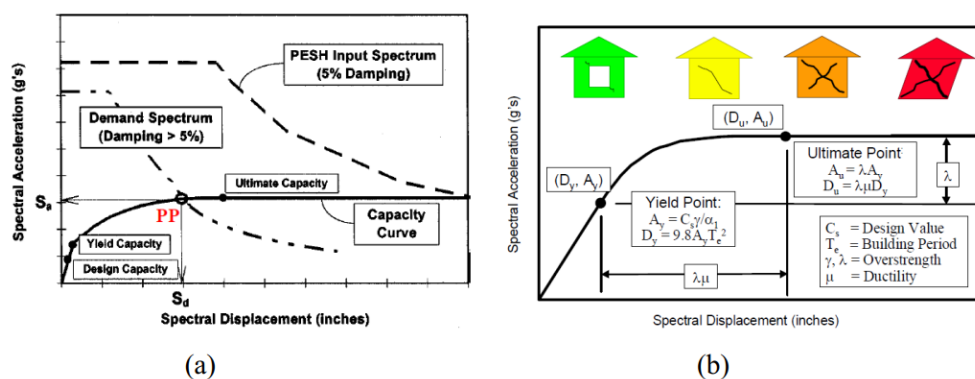


Figure 9: ATC-40 CSM for PP evaluation in HAZUS b) Capacity Spectrum with the yield and ultimate strength points

• DBELA

The Displacement Based Earthquake Loss Assessment (DBELA) framework was developed by Crowley et al. (Crowley et al., 2004) for the analytical vulnerability assessment of RC structures using the methodology of Calvi (Calvi*, 1999). Two types of failure mechanisms were considered: the column-sway mechanism and the beam sway mechanism. These mechanisms were differentiated for buildings based on the year of construction and ground storey weakness. In this method, the capacity curves were not generated using the pushover analysis, but instead the displacement capacity and the period of the equivalent single degree of freedom system calculated at different damage states. Equations derived based on simple mechanics were used to

calculate displacement capacities corresponding to three limit states by considering the steel and concrete section strains at 1) yield, 2) significant damage and 3) collapse. A random set of structures were generated having different material and geometrical properties and for each building, the displacement capacity and period at each limit state were calculated. A comparison was made between displacement capacity and displacement demand predictions at limit state periods for each building from a random sample as shown in figure 10.

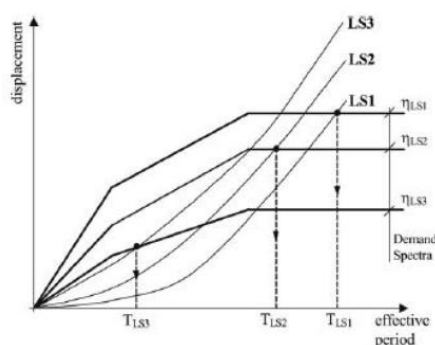


Figure 10: Comparison of the displacement demand with the evaluated displacement capacity (Crowley et al., 2004).

The probability of a damage state to be exceeded was evaluated by counting the buildings which had displacement capacity less than the demand and are divided by the total number of buildings. Capacity PDF in DBELA is modelled by a joint probability density function (JPDF) of displacement capacities and period.

COSENZA et al. (2005) presented a general method for seismic assessment of building classes which are defined based on the number of story and construction time. For each building class three level of class specifications defined as; low, medium and high order based on, knowledge level of input parameters. Simplified frame models were generated and the capacity of these frames was calculated using pre-defined failure mechanisms according to (MAZZOLANI and PILUSO, 1997) Fig.11 only concerning flexural behaviour. By using simplified frame models, it was not possible to evaluate the effect of moment redistribution cause by element nonlinearity, brittle failure, etc. Base shear was calculated by equilibrium equations whereas, ultimate roof displacement

was determined as a function of ultimate rotation of structural elements. Buildings seismic capacity was represented by the lowest base shear coefficient (base shear over seismic weight) among all mechanisms and corresponding drift. The effect of input variables and level specification was investigated based on engineering judgement consequently; knowledge level of building stock has a significant influence on the evaluation process of seismic capacity for a building class. The probability of exceedance of a fixed threshold limit was derived using Monte Carlo simulations with a simple probabilistic formula accounting for the number of simulations in which their analytical response was less than the fixed threshold over the total number of simulations. Finally, capacity curves were derived for 3 and 6 story buildings with different information level as illustrated in Fig. 12.

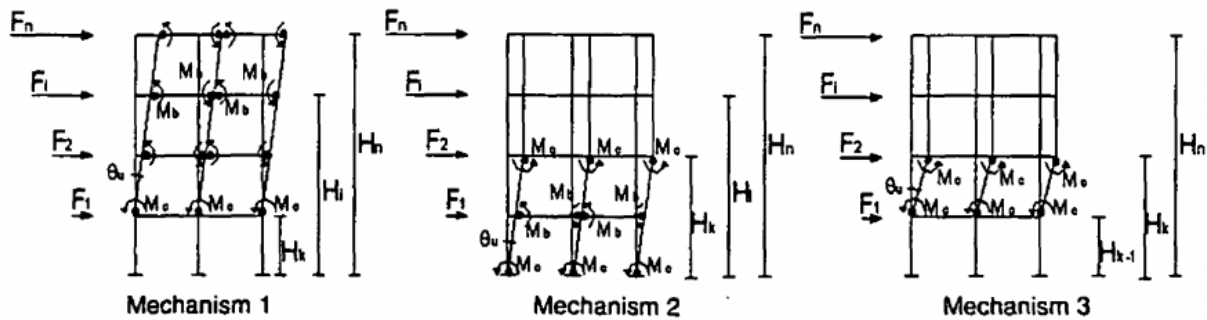
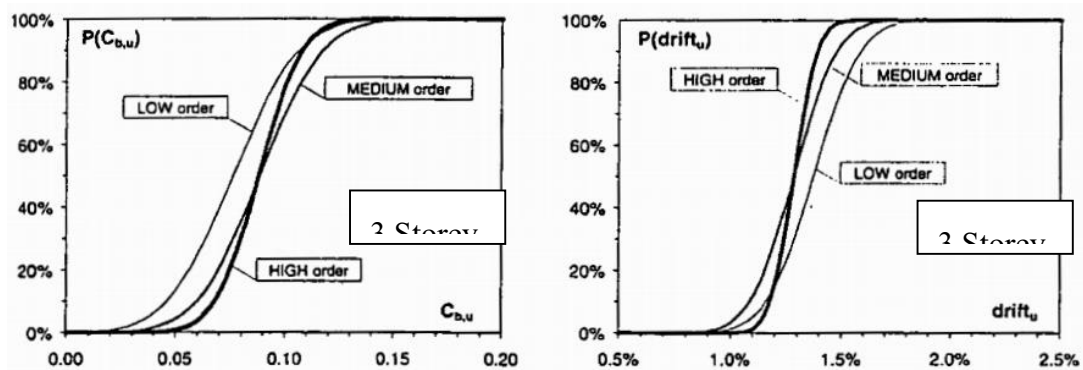


Figure 11: Analysed collapse mechanism types (COSENZA et al., 2005)



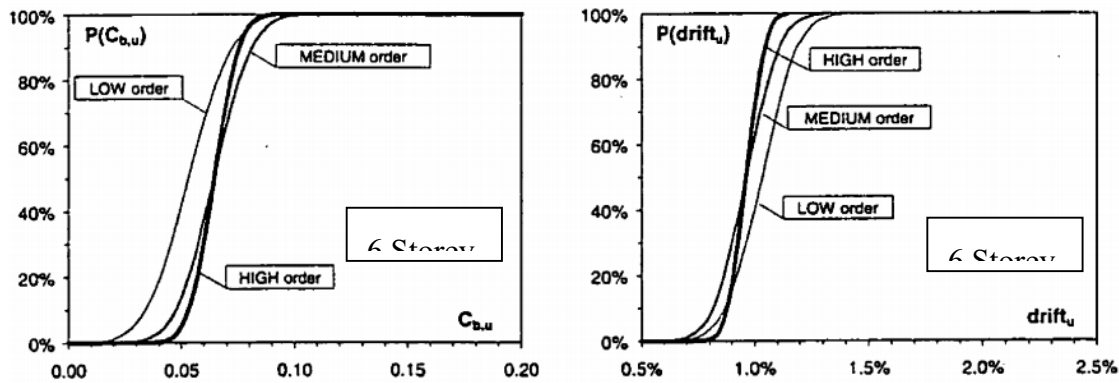


Figure 12: Capacity corresponding to low, medium and high order knowledge level for 3 and 6 storey buildings (COSENZA et al., 2005)

• SP-BELA

Borzi et al. (2008) extended the displacement-based vulnerability assessment methodology (DBELA) developed by Crowley et al. (2004). In DBELA, an assumption, in priority, should be made on the failure mode (column-sway or beam-sway) of the structure to derive vulnerability curves. In SPBELA (Simplified Pushover Based Earthquake Loss Assessment), an algorithm was added to the DBELA methodology to predict the failure mode of the structure. The details of the SPBELA procedure is shown on a flowchart in Fig 13. In SPBELA, to define the base shear capacity of buildings, a capacity curve was defined using a mechanics-based simple methodology, as proposed by COSENZA et al. (2005). A collapse multiplier was introduced based on the shear capacity of each storey taking into account the maximum shear force that a column can withstand for shear and flexural failure mechanisms and only flexural mechanism in beams. The final collapse multiplier of the building was considered the smallest multiplier calculated for each storey. Three collapse mechanisms were introduced: 1- Shear failure, 2-column-sway mechanism and 3-beam-sway mechanism. In the storey with the smallest collapse multiplier, if there are some columns stronger than beams or some beam stronger than columns in the storey with the smallest collapse multiplier, the collapse mechanism cannot be identified. In SPBELA, damage indicators are based on chord rotations, which was calculated using empirical equations based on sectional strains in steel and concrete. Four limit states were

considered: non-structural light damage, light damage, significant damage and collapse damage states. For non-structural light, damage limit state, inter-storey rotation capacity between 0.1% and 0.3% for drift-sensitive partition walls. For light, significant and collapse limit states the rotation capacity is limited by yield, $\frac{3}{4}$ of ultimate and ultimate chord rotations respectively. The displacement capacity of the structure is calculated at the height of equivalent SDOF system was calculated based on Priestley (1997) and assuming linear deformed shape for light damage and multilinear displacement profile beyond the elastic limit. For non-structural light damage elastic period of vibration calculated using the formula from Eurocode 8 while, for structural limit states the vibration period of the equivalent SDOF system correspond to the secant period was used. Monte Carlo simulation with a normal distribution using the Latin Hypercube algorithm was used to randomise structural parameters such as geometrical parameters (only span length), material properties and design loads while the section dimensions and reinforcement of the structural elements and inter-storey height were assumed to be deterministic. For displacement demand, the acceleration spectrum defined according to Italian regulations based on PGA values and 5% damping. Furthermore, to overcome the linearization effect of the structural model on the energy dissipation capacity overdamped elastic response spectra was used in the way that, the equivalent viscous damping when each limit state is achieved was calculated using the expression proposed by (Calvi*, 1999) then, the spectra reduction factor expressed as a function of the equivalent viscous damping. Uncertainties in displacement demand were considered by randomising the corner periods with a uniform distribution between the maximum and minimum values moreover, the spectral amplification factor was taken as a random variable with the logarithmic distribution. Finally, the demand and capacity of buildings were compared for limit conditions. The derived vulnerability curves are shown in Fig.14.

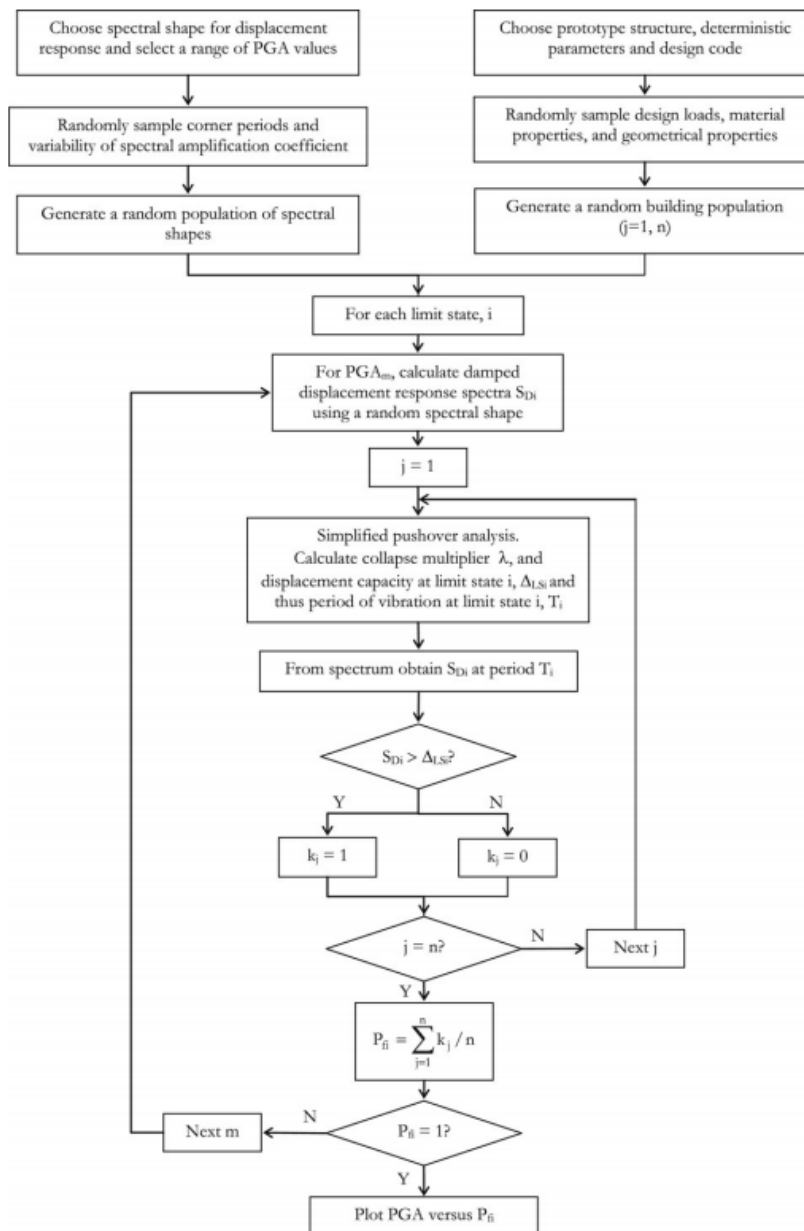


Figure 13: Flowchart of the SP-BELA methodology for the derivation of vulnerability curves for RC buildings (Borzi et al., 2008).

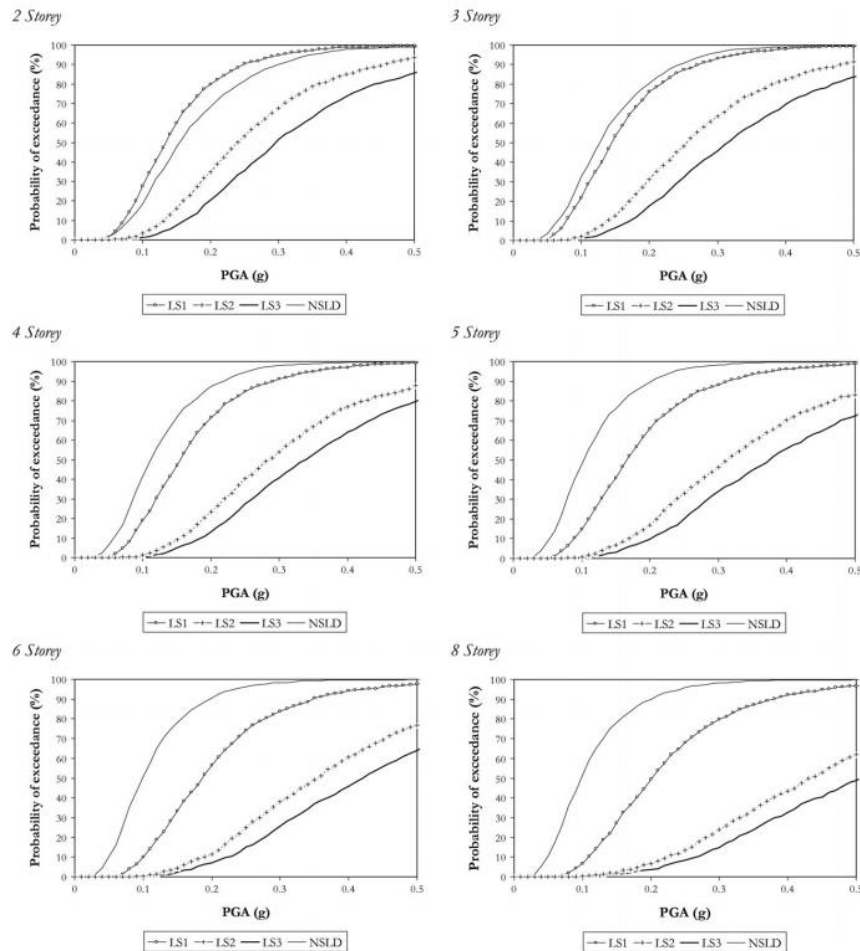


Figure 14. vulnerability curves derived with SP-BELA (Borzi et al., 2008).

A.5 Hybrid methods

This method is a combination of post-earthquake damage statistics and analytical damage statistics from a mathematical model. Various types of uncertainties exist in the vulnerability curves derived from the above-mentioned techniques due to limited post-earthquake damage data, judgemental data subjectivity and modelling issues in analytical vulnerability. To reduce these uncertainties in curves, hybrid vulnerability curves have been derived by researchers ((Jalalian, Kappos et al., 1998)) which use data from various sources.

(Jalalian) et al. derived hybrid vulnerability curves for different building categories of Iran by combining elements from both the empirical and judgemental techniques. Singhal and Kiremidjian (1997) used this approach to update the previously developed analytical vulnerability curves for low rise RC buildings adopting a Bayesian approach by using the observed building damage data from the Northridge earthquake.

If data from a single source are used, there is a possibility that the model may end up with more uncertainty than it started, since data from one event do not necessarily include a large range of ground motion values. So, multiple data sources are required for more efficient hybrid vulnerability curves.

In hybrid curves, the deficiency of the observational data at a particular intensity level can be covered by carrying out nonlinear static or time history analysis, and the judgemental or analytical curves can be modified by utilising observational data. Experimental test data can also be used to reduce the deficiencies in observational, judgemental or analytical vulnerability curves. So, another way of carrying out vulnerability assessment is by using laboratory testing ((Pinho and Elnashai, 2000)). The benefit of this method is the freedom provided by testing any building type for which data are needed. The limitations are due to the scale of model, loading type and laboratory equipment capacity. Experimental data are expensive and allow few parameters to be investigated at a time, so they are mostly used for verification purposes rather than as an additional source. In the loss or vulnerability assessment process the building stock needs to be categorized in different damage categories according to its performance in a seismic event. This categorization is done using various suitable damage scales having different damage states and mostly associated with certain threshold values of a physical parameter.

APPENDIX B TEST RESULTS

B.1 RC columns

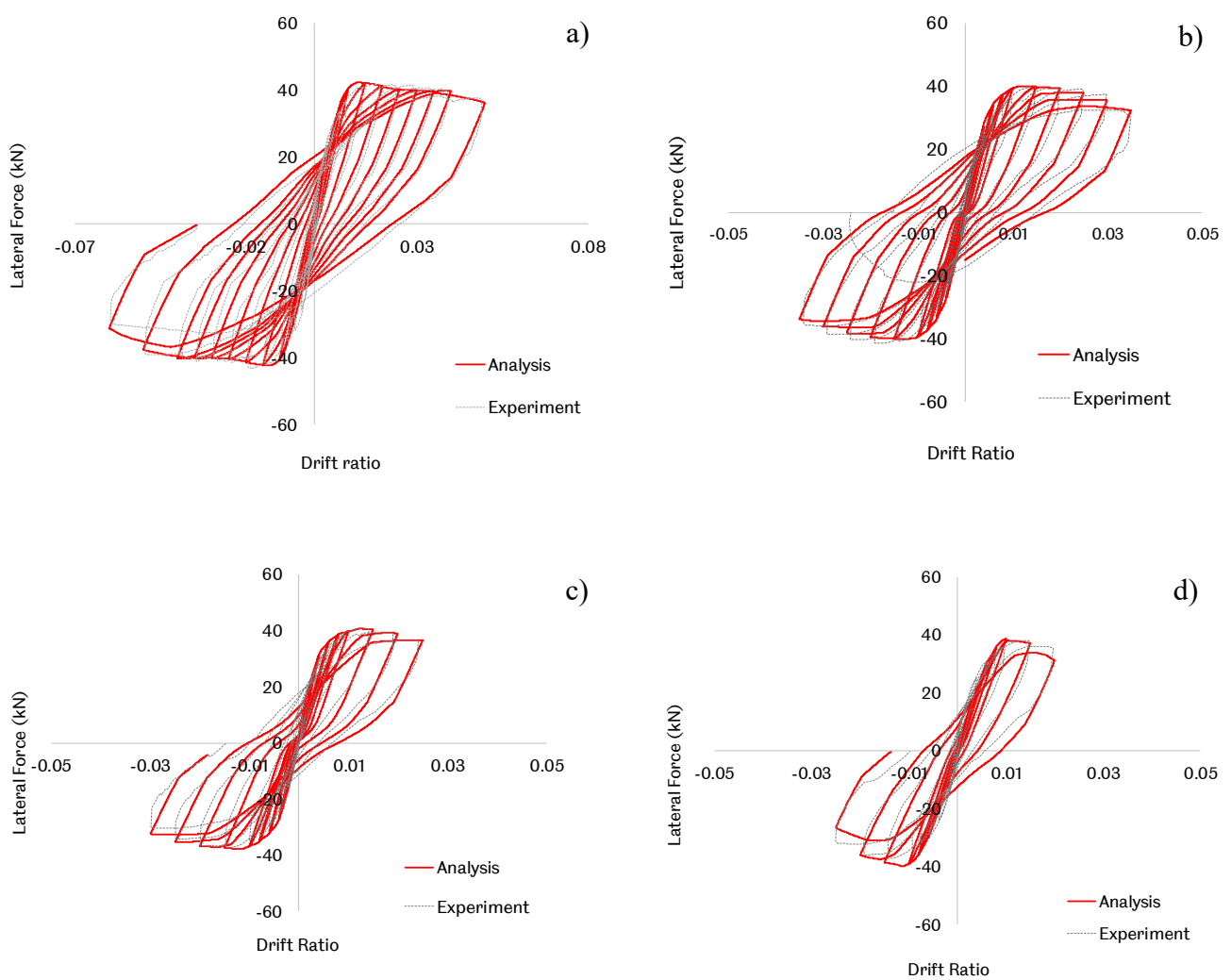


Figure 6-1: Comparison of analytical versus experimental results for RCPC of columns with a) S=60 mm, b) S=90 mm, c) S=120 mm and d) S=180 mm.

B.2 ECOLEADER frame

This section presents the comparison between experimental and analytical results for ECOLEADER substandard RC frame in terms of storey time history displacement (mm).

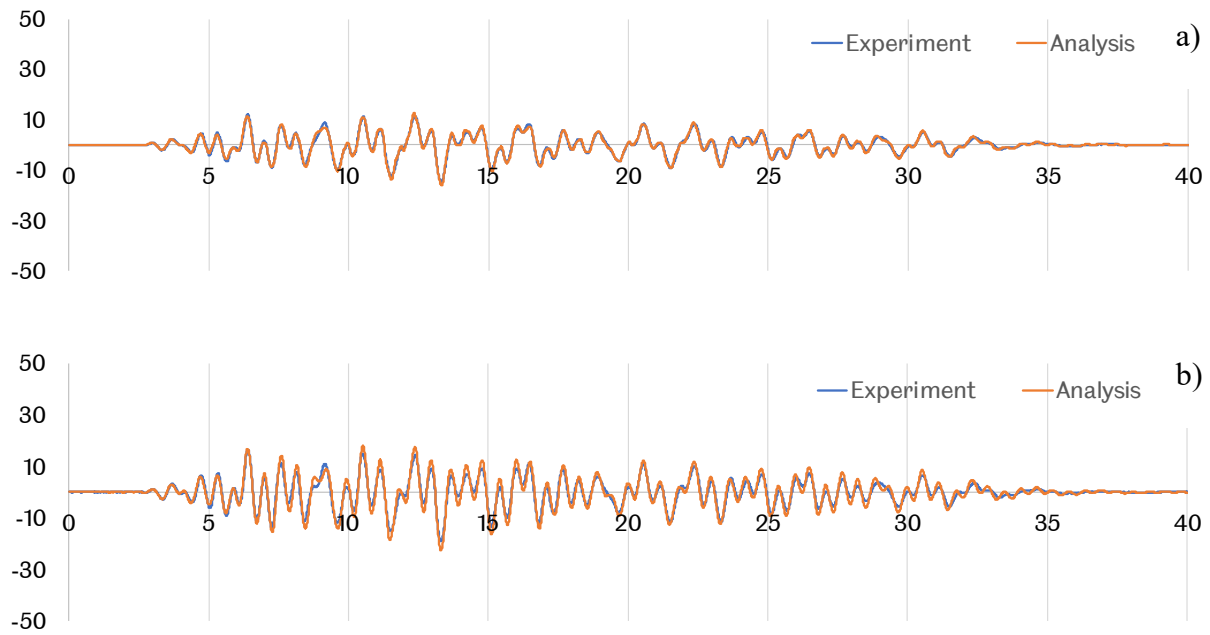


Figure 6-2: Comparison between experimental and analytical results of THA with PGA=0.05 g for a) 1st floor and b) 2nd floor.

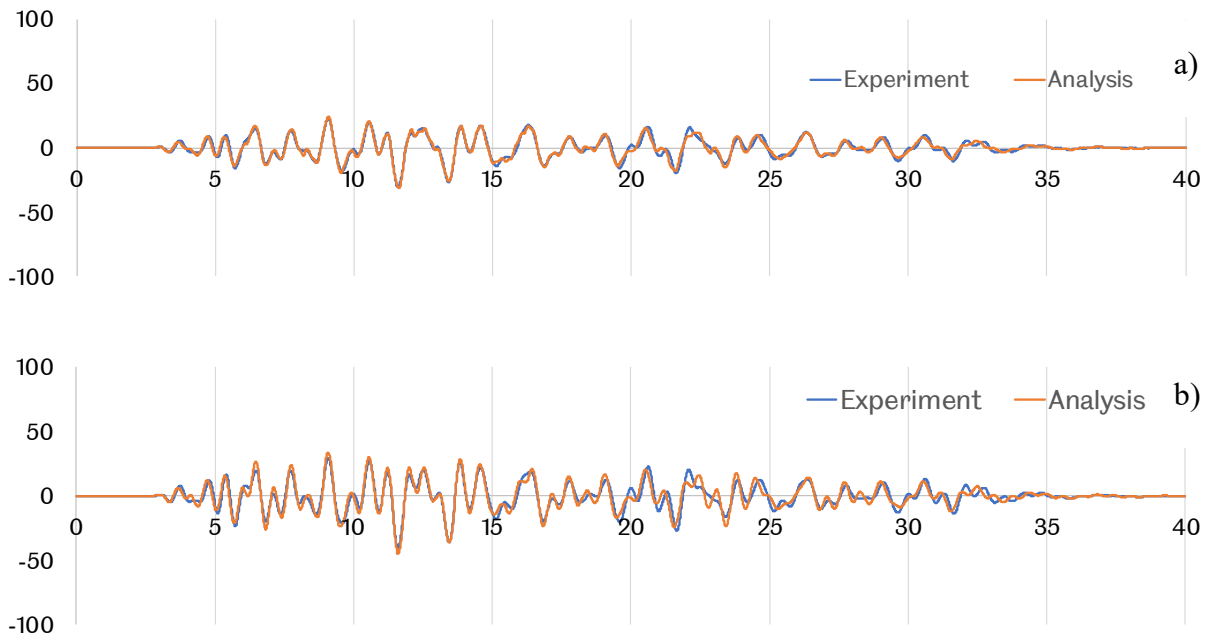


Figure 6-3: Comparison between experimental and analytical results of THA with PGA=0.1 g for a) 1st floor and b) 2nd floor.

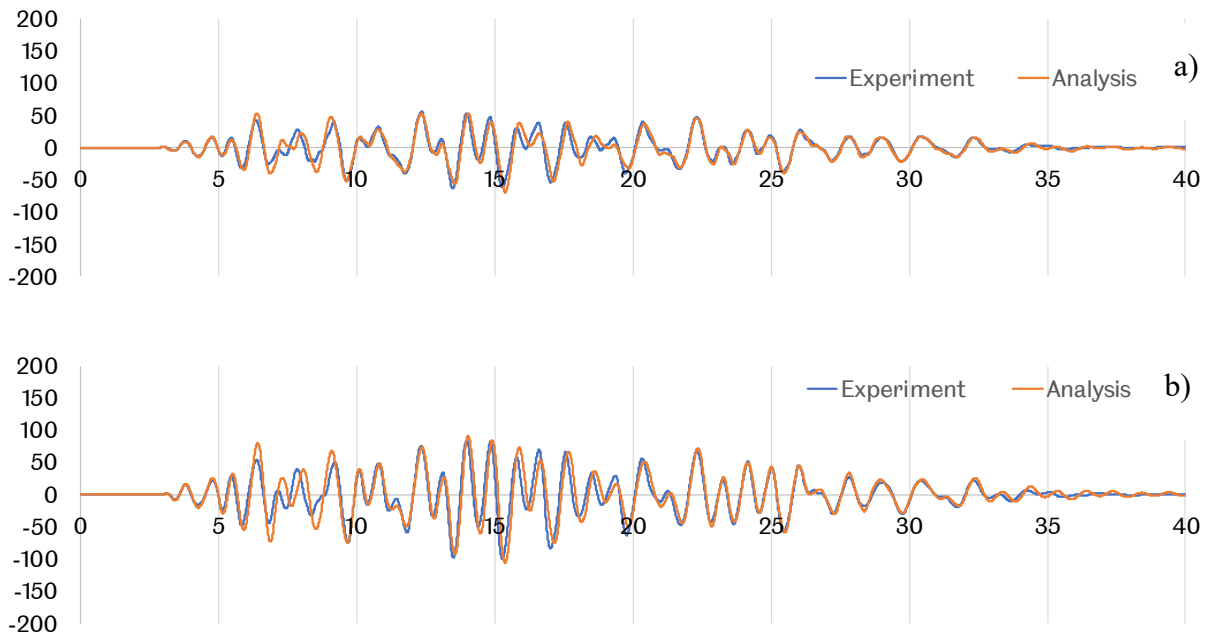


Figure 6-4: Comparison between experimental and analytical results of THA with PGA=0.2 g for a) 1st floor and b) 2nd floor.

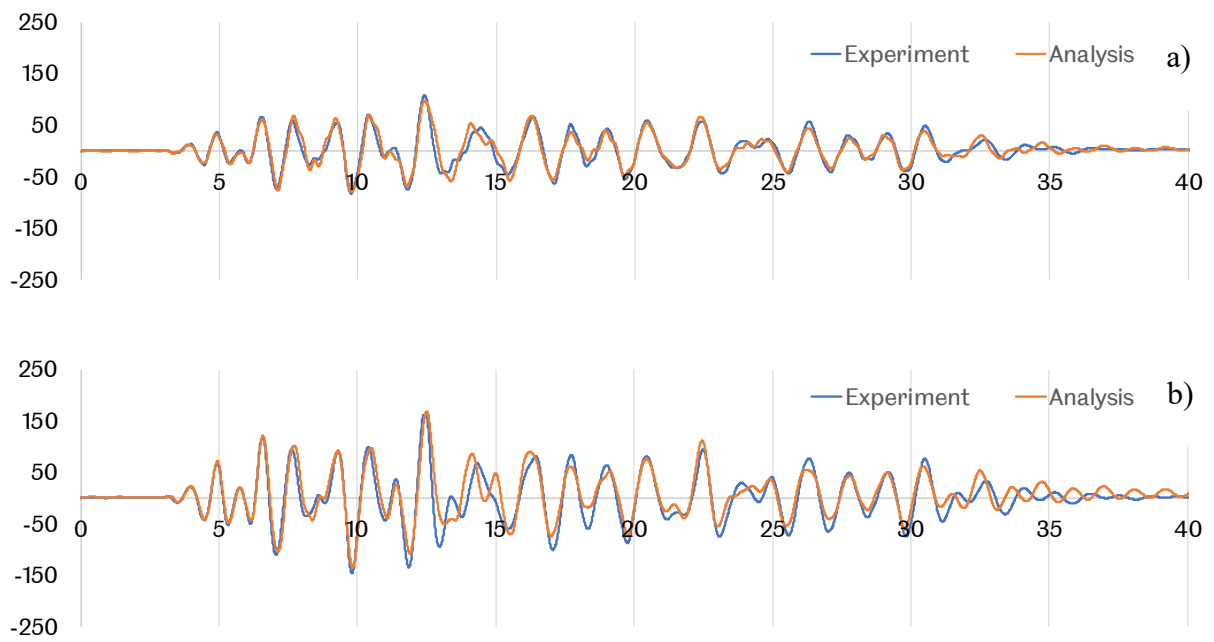


Figure 6-5: Comparison between experimental and analytical results of THA with PGA=0.3 g for a) 1st floor and b) 2nd floor.

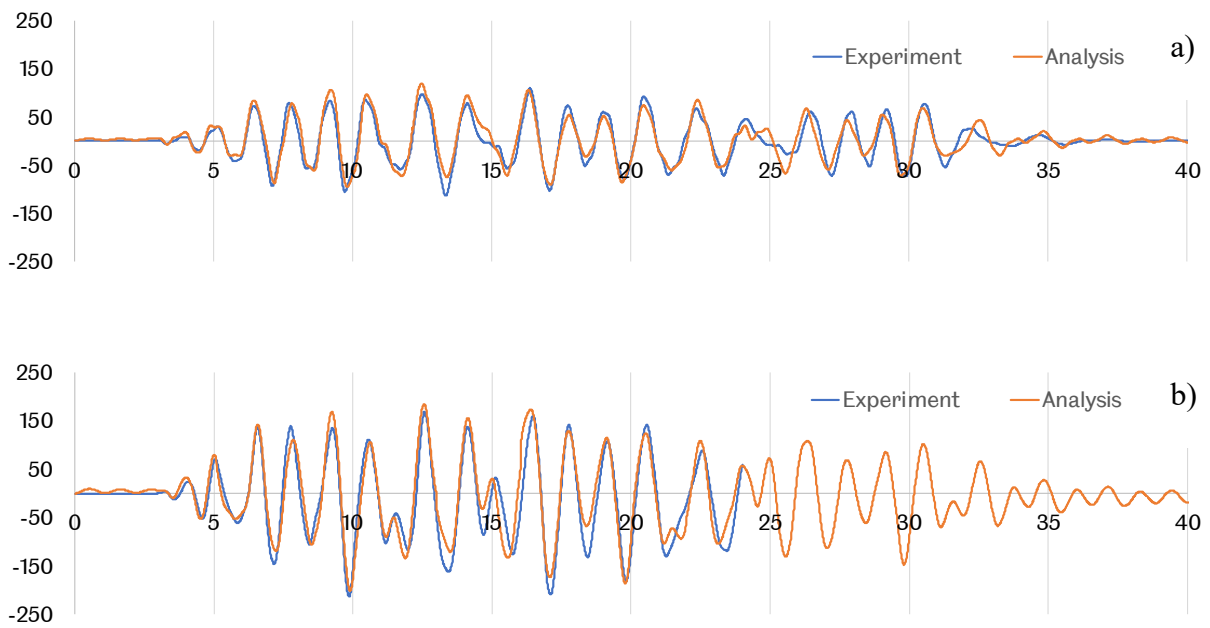


Figure 6-6: Comparison between experimental and analytical results of THA with PGA=0.4 g for a) 1st floor and b) 2nd floor.

Table B-1: Comparison between experimental and analytical 1st mode of vibration's period form THA.

Tests	Experimental 1st Period	Analytical 1st Period
Undamaged	0.53	0.52
0.05g	0.60	0.58
0.1g	0.74	0.70
0.2g	0.93	0.92
0.3g	1.14	1.10
0.4g	1.47	1.40

B.3 BANDIT frame

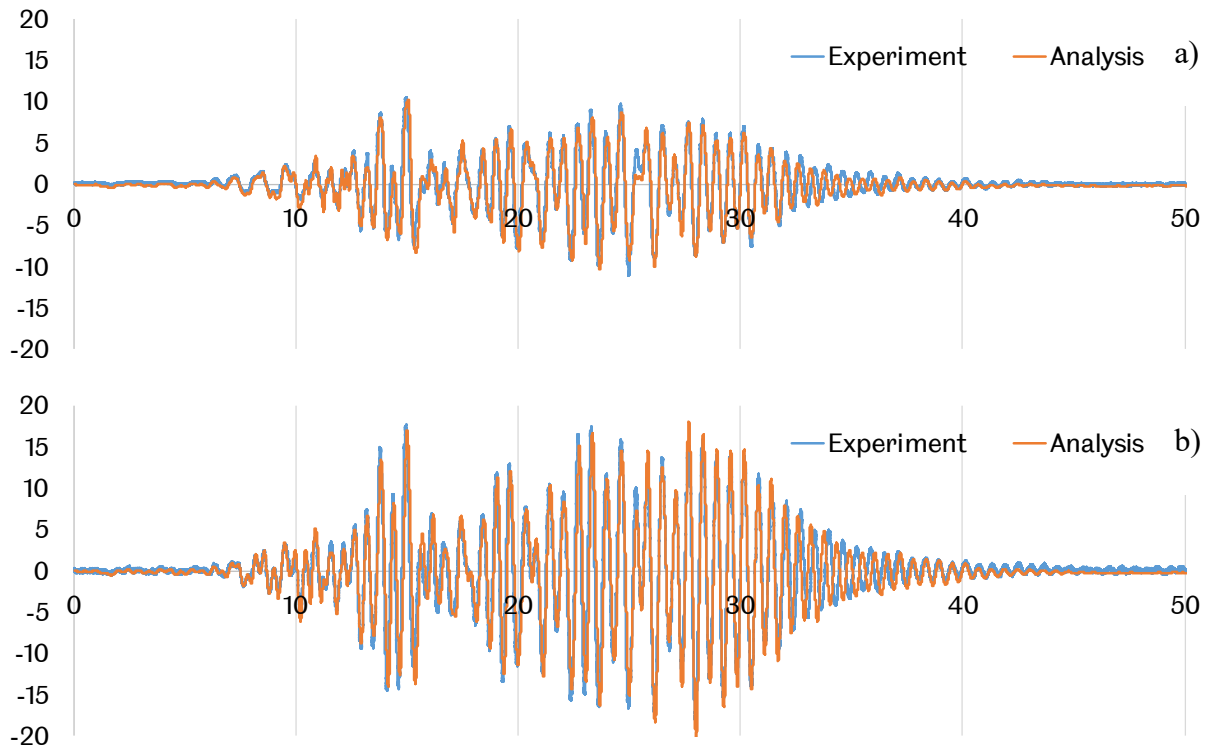


Figure 6-7: Comparison between experimental and analytical results of THA with PGA=0.05 g for a) 1st floor and b) 2nd floor.

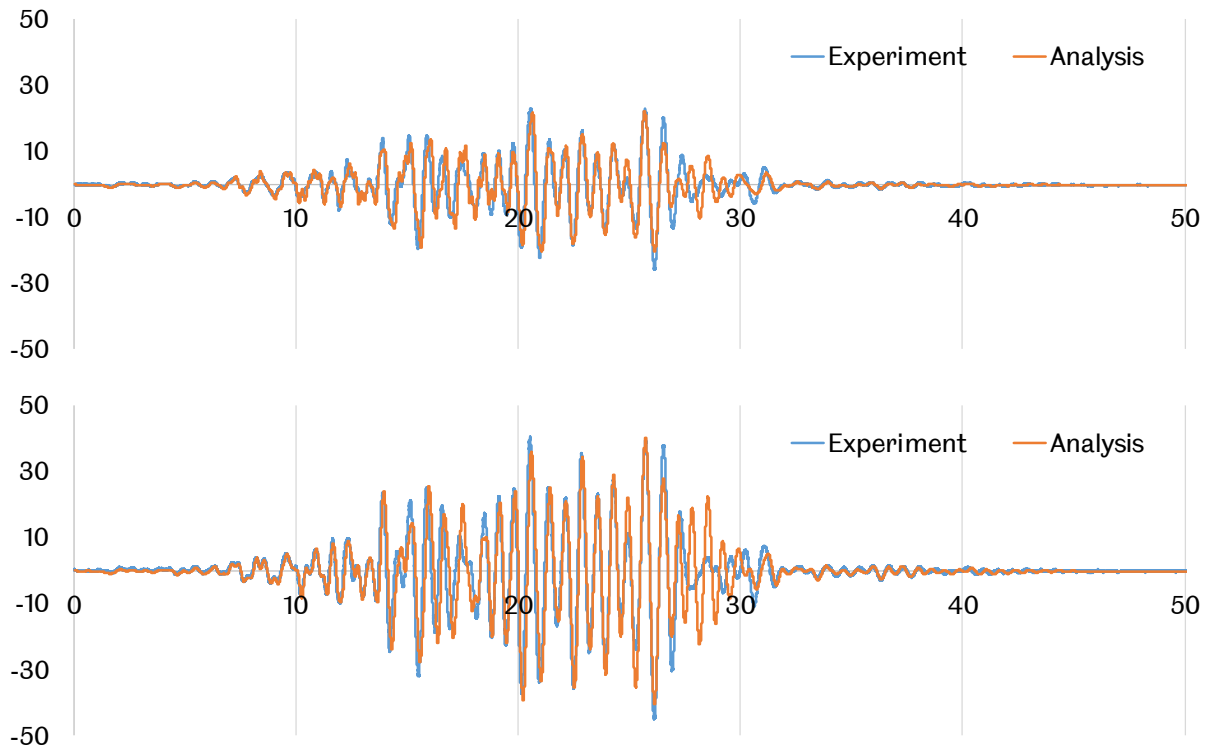


Figure 6-8: Comparison between experimental and analytical results of THA with $PGA=0.1\text{ g}$ for a) 1st floor and b) 2nd floor.

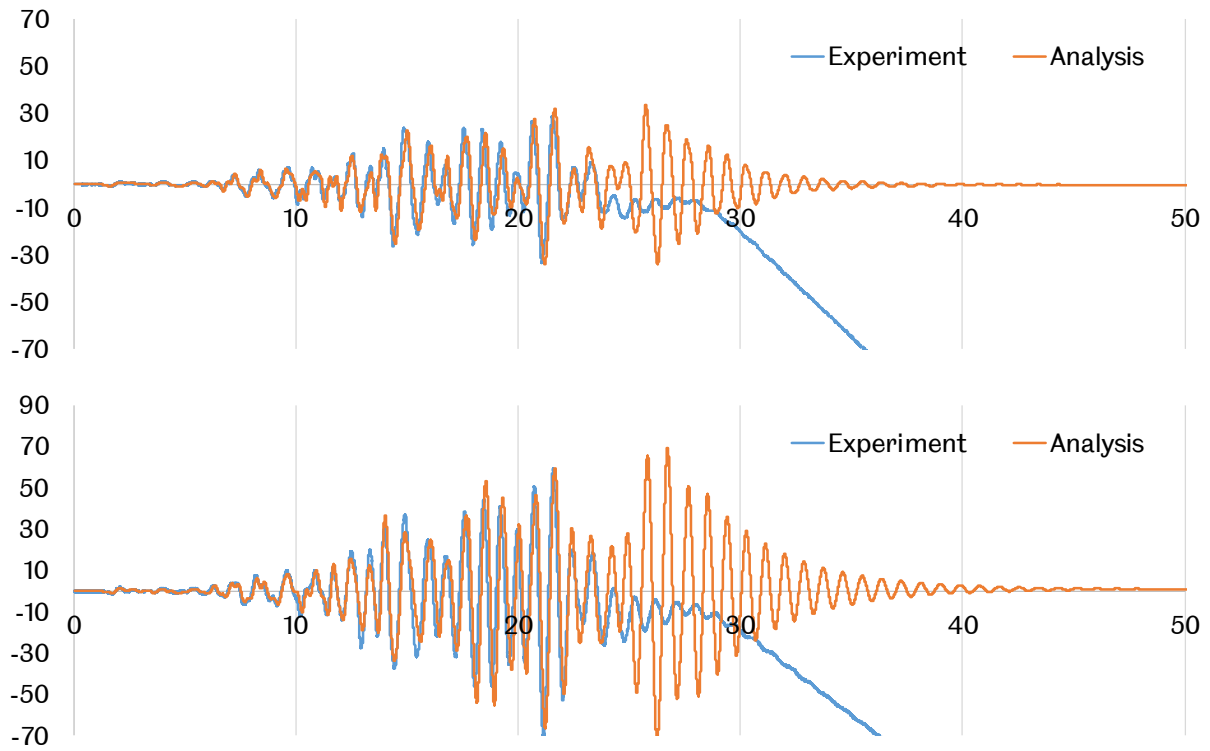


Figure 6-9: Comparison between experimental and analytical results of THA with PGA=0.15 g for a) 1st floor and b) 2nd floor.

Table B-2: Comparison between experimental and analytical 1st mode of vibration's period from THA.

Tests	Experimental 1 st Period	Analytical 1 st Period
Undamaged	0.48	0.50
0.050	0.60	0.61
0.100	0.68	0.70
0.150	0.88	0.89

REFERENCES

- 154–ATC-21, F. 1988. Rapid Visual Screening of Buildings for Potential Seismic Hazards: A Handbook. Federal Emergency Management Agency Washington, DC, USA.
- 310, F. 1998. Handbook for the seismic evaluation of buildings—A prestandard. Federal Emergency Management Agency Washington, DC, USA.
- AFAD 2018. Turkish Seismic Hazard Map ,Disaster Management and Natural Disaster Statistics in Turkey, Turkey.
- AGENCY, F. E. M. 2003. HAZUS-MH Technical Manual. Federal Emergency Management Agency Washington, DC, USA.
- AGENCY, F. E. M. 2008. Recommended methodology for quantification of building system performance and response parameters.
- AHMAD, N., CROWLEY, H. & PINHO, R. 2010. Analytical fragility functions for reinforced concrete and masonry buildings and building aggregates. UPAV-Internal Report.
- AHMAD, S. 2011. *Seismic Vulnerability of Non-Ductile Reinforced Concrete Structures in Developing Countries*. PhD, Department of Civil & Structural Engineering, The University of Sheffield.
- AKKAR, S., SUCUOĞLU, H. & YAKUT, A. 2005. Displacement-based fragility functions for low-and mid-rise ordinary concrete buildings. *Earthquake Spectra*, 21, 901-927.
- AL-SALLOUM, Y. A., SIDDIQUI, N. A., ELSANADEDY, H. M., ABADEL, A. A. & AQEL, M. A. 2011. Textile-reinforced mortar versus FRP as strengthening material for seismically deficient RC beam-column joints. *Journal of Composites for Construction*, 15, 920-933.
- AL MAMUN, A. & SAATCIOGLU, M. 2017. Seismic fragility curves for reinforced concrete frame buildings in Canada designed after 1985. *Canadian Journal of Civil Engineering*, 44, 558-568.
- ALCOCER, S. M. & JIRSA, J. O. 1993. Strength of reinforced concrete frame connections rehabilitated by jacketing. *ACI structural journal*, 90.
- ANBARCI, N., ESCALERAS, M. & REGISTER, C. A. 2005. Earthquake fatalities: the interaction of nature and political economy. *Journal of Public Economics*, 89, 1907-1933.

- ATC-13 1985. Earthquake damage evaluation data for California. Palo Alto. *Applied Technology Council Report*
- ATC-24 1992. "Guidelines for cyclic seismic testing of components of steel structures". ATC-24, Redwood City, CA. .
- ATC-40. Seismic evaluation and retrofit of concrete buildings. 2. Appendices. 1996. ATC.
- ATC-58 2009. Guidelines for seismic performance assessment of buildings. ATC-58 50% Draft, Applied Technology Council Redwood City, CA.
- BAE, S. & BAYRAK, O. 2008. Plastic hinge length of reinforced concrete columns. *ACI Structural Journal*, 105, 290.
- BAE, S., MIESES, A. M. & BAYRAK, O. 2005. Inelastic buckling of reinforcing bars. *Journal of Structural Engineering*, 131, 314-321.
- BAKER, J. W. 2015. Efficient analytical fragility function fitting using dynamic structural analysis. *Earthquake Spectra*, 31, 579-599.
- BAL, İ. E., CROWLEY, H., PINHO, R. & GÜLAY, F. G. 2008. Detailed assessment of structural characteristics of Turkish RC building stock for loss assessment models. *Soil Dynamics and Earthquake Engineering*, 28, 914-932.
- BASOZ, N. I., KIREMIDJIAN, A. S., KING, S. A. & LAW, K. H. 1999. Statistical analysis of bridge damage data from the 1994 Northridge, CA, earthquake. *Earthquake Spectra*, 15, 25-54.
- BERRY, M. P. & EBERHARD, M. O. 2006. *Performance modeling strategies for modern reinforced concrete bridge columns*.
- BIDDAH, A., GHOBARAH, A. & AZIZ, T. S. 1997. Upgrading of nonductile reinforced concrete frame connections. *Journal of Structural Engineering*, 123, 1001-1010.
- BINICI, B. & MOSALAM, K. M. 2007. Analysis of reinforced concrete columns retrofitted with fiber reinforced polymer lamina. *Composites Part B: Engineering*, 38, 265-276.
- BIRD, J. F. & BOMMER, J. J. 2004. Earthquake losses due to ground failure. *Engineering Geology*, 75, 147-179.
- BISKINIS, D. & FARDIS, M. N. 2013. Models for FRP-wrapped rectangular RC columns with continuous or lap-spliced bars under cyclic lateral loading. *Engineering Structures*, 57, 199-212.
- BORZI, B., PINHO, R. & CROWLEY, H. 2008. Simplified pushover-based vulnerability analysis for large-scale assessment of RC buildings. *Engineering Structures*, 30, 804-820.
- BRADLEY, B. A. & DHAKAL, R. P. 2008. Error estimation of closed-form solution for annual rate of structural collapse. *Earthquake Engineering & Structural Dynamics*, 37, 1721-1737.
- BRAGA, F., DOLCE, M. & LIBERATORE, D. A statistical study on damaged buildings and an ensuing review of the MSK-76 scale. Proceedings of the seventh European conference on earthquake engineering, Athens, Greece, 1982. 431-450.

- CALABRESE, A., ALMEIDA, J. P. & PINHO, R. 2010. Numerical issues in distributed inelasticity modeling of RC frame elements for seismic analysis. *Journal of Earthquake Engineering*, 14, 38-68.
- CALVI, G. M., PINHO, R., MAGENES, G., BOMMER, J. J., RESTREPO-VÉLEZ, L. F. & CROWLEY, H. 2006. Development of seismic vulnerability assessment methodologies over the past 30 years. *ISET journal of Earthquake Technology*, 43, 75-104.
- CALVI*, G. M. 1999. A DISPLACEMENT-BASED APPROACH FOR VULNERABILITY EVALUATION OF CLASSES OF BUILDINGS. *Journal of Earthquake Engineering*, 3, 411-438.
- CARDONA, O. D. 2013. The need for rethinking the concepts of vulnerability and risk from a holistic perspective: a necessary review and criticism for effective risk management. *Mapping vulnerability*. Routledge.
- CARDONE, D. 2016. Fragility curves and loss functions for RC structural components with smooth rebars. *Earthquakes and Structures*, 10, 1181-1212.
- CEB-FIP, M. C. 1993. Design Code, Comité Euro-International du Béton. Thomas Telford Services Ltd, London.
- CELIK, O. C. & ELLINGWOOD, B. R. 2008. Modeling beam-column joints in fragility assessment of gravity load designed reinforced concrete frames. *Journal of Earthquake Engineering*, 12, 357-381.
- CHADWELL, C. B., AND IMBSEN, R. A 2002. (2002). "XTRACT-cross section analysis software for structural and earthquake engineering." " TRC, Rancho Cordova, CA, (<http://www.imbsen.com/xtract.htm>) (Aug. 30, 2011).
- CHANG, G. & MANDER, J. B. 1994. *Seismic energy based fatigue damage analysis of bridge columns: Part I-Evaluation of seismic capacity*, National Center for Earthquake Engineering Research Buffalo, NY.
- CHAUDAT, T., GARNIER, C., CVEJIC, S., POUPIN, S., LE CORRE, M. & MAHE, M. 2005. ECOLEADER Project No. 2: Seismic tests on a reinforced concrete bare frame with FRP retrofitting-Tests Report. *Report SEMT/EMSI/RT/05-006/A*.
- COLEMAN, J. & SPACONE, E. 2001. Localization issues in force-based frame elements. *Journal of Structural Engineering*, 127, 1257-1265.
- COLOMBI, M., BORZI, B., CROWLEY, H., ONIDA, M., MERONI, F. & PINHO, R. 2008. Deriving vulnerability curves using Italian earthquake damage data. *Bulletin of Earthquake Engineering*, 6, 485-504.
- CORAZAO, M. & DURRANI, A. J. 1989. *Repair and strengthening of beam-to-column connections subjected to earthquake loading*, National Center for Earthquake Engineering Research.
- CORNELL, C. A., JALAYER, F., HAMBURGER, R. O. & FOUTCH, D. A. 2002. Probabilistic Basis for 2000 SAC Federal Emergency Management Agency Steel Moment Frame Guidelines. *Journal of Structural Engineering*, 128, 526-533.

- COSENZA, E., MANFREDI, G., POLESE, M. & VERDERAME, G. M. 2005. A MULTILEVEL APPROACH TO THE CAPACITY ASSESSMENT OF EXISTING RC BUILDINGS. *Journal of Earthquake Engineering*, 09, 1-22.
- COUNCIL, A. T. 1985. *Earthquake damage evaluation data for California*, Applied technology council.
- COUNCIL, A. T. Seismic evaluation and retrofit of concrete buildings. 2. Appendices. 1996. ATC.
- CROWLEY, H., PINHO, R. & BOMMER, J. J. 2004. A Probabilistic Displacement-based Vulnerability Assessment Procedure for Earthquake Loss Estimation. *Bulletin of Earthquake Engineering*, 2, 173-219.
- D'AYALA, D., MESLEM, A., VAMVATSIKOS, D., PORTER, K., ROSSETTO, T., CROWLEY, H. & SILVA, V. 2014. Guidelines for analytical vulnerability assessment of low/mid-rise Buildings—Methodology. Vulnerability Global Component project. DOI.
- DEL GAUDIO, C., DI LUDOVICO, M., POLESE, M., MANFREDI, G., PROTA, A., RICCI, P. & VERDERAME, G. M. 2020. Seismic fragility for Italian RC buildings based on damage data of the last 50 years. *Bulletin of earthquake engineering*, 18, 2023-2059.
- DHAKAL, R. P. & MAEKAWA, K. 2002. Modeling for postyield buckling of reinforcement. *Journal of structural engineering*, 128, 1139-1147.
- DIZAJ, E. A., MADANDOUST, R. & KASHANI, M. M. 2018. Probabilistic seismic vulnerability analysis of corroded reinforced concrete frames including spatial variability of pitting corrosion. *Soil Dynamics and Earthquake Engineering*, 114, 97-112.
- DUMOVA-JOVANOSKA, E. Fragility curves for RC structures in Skopje region. Proceedings of the 13th World Conference on Earthquake Engineering, 2004.
- DURUKAL, E. 2002. Critical evaluation of strong motion in Kocaeli and Düzce (Turkey) earthquakes. *Soil Dynamics and Earthquake Engineering*, 22, 589-609.
- EADS, L., MIRANDA, E., KRAWINKLER, H. & LIGNOS, D. G. 2013. An efficient method for estimating the collapse risk of structures in seismic regions. *Earthquake Engineering & Structural Dynamics*, 42, 25-41.
- ERBERIK, M. A. 2008. Fragility-based assessment of typical mid-rise and low-rise RC buildings in Turkey. *Engineering Structures*, 30, 1360-1374.
- ESCALERAS, M., ANBARCI, N. & REGISTER, C. A. 2007. Public sector corruption and major earthquakes: a potentially deadly interaction. *Public Choice*, 132, 209-230.
- ESTRADA, M., MATSUOKA, M. & YAMAZAKI, F. 2000. Spectral Analysis of Optical Remote Sensing Images for the Detection of Damage due to The 1999 Kocaeli, Turkey Earthquake. *SEISAN KENKYU*, 52, 586-589.
- FAJFAR, P. 2000. A nonlinear analysis method for performance-based seismic design. *Earthquake spectra*, 16, 573-592.

- FEMA 356, P. 2000. Commentary for the seismic rehabilitation of buildings. *FEMA-356, Federal Emergency Management Agency, Washington, DC.*
- FEMA 440, A. 2005. 440, Improvement of nonlinear static seismic analysis procedures. *FEMA-440, Redwood City, 7, 11.*
- FILIPPOU, F. C., POPOV, E. P. & BERTERO, V. V. 1983. Effects of bond deterioration on hysteretic behavior of reinforced concrete joints.
- FRANGOU, M., PILAKOUTAS, K. & DRITSOS, S. 1995. Structural repair/strengthening of RC columns. *Construction and building materials, 9, 259-266.*
- FRASER, S., JONGMAN, B., BALOG, S., SIMPSON, A., SAITO, K. & HIMMELFARB, A. 2016. *The making of a riskier future: How our decisions are shaping future disaster risk*, Global Facility for Disaster Reduction and Recovery.
- GARCIA, R., HAJIRASOULIHA, I., GUADAGNINI, M., HELAL, Y., JEMAA, Y., PILAKOUTAS, K., MONGABURE, P., CHRYSOSTOMOU, C., KYRIAKIDES, N. & ILKI, A. 2014. Full-scale shaking table tests on a substandard RC building repaired and strengthened with Post-Tensioned Metal Straps. *Journal of Earthquake Engineering, 18, 187-213.*
- GARCIA, R., HAJIRASOULIHA, I. & PILAKOUTAS, K. 2010. Seismic behaviour of deficient RC frames strengthened with CFRP composites. *Engineering Structures, 32, 3075-3085.*
- GARCIA, R., PILAKOUTAS, K., GUADAGNINI, M., HELAL, Y., JEMAA, Y., HAJIRASOULIHA, I. & MONGABURE, P. 2012. Seismic strengthening of deficient RC buildings using post-tensioned metal straps: an experimental investigation. *Proceedings of the 15WCEE, Lisbon, Portugal.*
- GARCIA, R., PILAKOUTAS, K., HAJIRASOULIHA, I., GUADAGNINI, M., KYRIAKIDES, N. & CIUPALA, M. A. 2017. Seismic retrofitting of RC buildings using CFRP and post-tensioned metal straps: shake table tests. *Bulletin of Earthquake Engineering, 15, 3321-3347.*
- GHAFOREY-ASHTIANY, M., MOUSAVI, M. & AZARBAKHT, A. 2011. Strong ground motion record selection for the reliable prediction of the mean seismic collapse capacity of a structure group. *Earthquake Engineering & Structural Dynamics, 40, 691-708.*
- GHASEMI, H., COOPER, J. D., IMBSEN, R. A., PISKIN, H., INAL, F. & TIRAS, A. 2000. The November 1999 Duzce earthquake: post-earthquake investigation of the structures on the Tem. United States. Federal Highway Administration.
- GHOBARAH, A., AZIZ, T. S. & BIDDAR, A. 1996. Seismic rehabilitation of reinforced concrete beam-column connections. *Earthquake Spectra, 12, 761-780.*
- GHODRATI AMIRI, G., JALALIAN, M. & RAZAVIAN AMREI, S. Derivation of vulnerability functions based on observational data for Iran. *Proceedings of the International Symposium on Innovation & Sustainability of Structures in Civil Engineering, 2007. 28-30.*
- GILKAN, P., SUCUOGLU, H. & ERGIINAY, O. 1992. Earthquake vulnerability, loss and risk assessment in Turkey.

- GOKSU, C. 2021. Fragility functions for reinforced concrete columns incorporating recycled aggregates. *Engineering Structures*, 233, 111908.
- GRAMMATIKOU, S., FARDIS, M. N. & BISKINIS, D. 2018. Models of the flexure-controlled strength, stiffness and cyclic deformation capacity of rectangular RC columns with smooth bars, including lap-splicing and FRP jackets. *Bulletin of Earthquake Engineering*, 16, 341-375.
- HANCILAR, U., TAUCER, F. & CORBANE, C. 2012. Empirical fragility assessment after the January 12, 2010 Haiti earthquake. *WIT Transactions on Information and Communication Technologies*, 44, 353-365.
- HANCILAR, U., TUZUN, C., YENIDOGAN, C. & ERDIK, M. 2010. ELER software—a new tool for urban earthquake loss assessment. *Natural Hazards and Earth System Sciences*, 10, 2677-2696.
- HAZUS 2003. HAZUS-MH Technical Manual. *Developed by the Department of Homeland Security, Federal Emergency Management Agency. Washington DC: Mitigation Division.*
- IBARRA, L. F. & KRAWINKLER, H. 2005. *Global collapse of frame structures under seismic excitations*, Pacific Earthquake Engineering Research Center Berkeley, CA.
- ILKI, A., PEKER, O., KARAMUK, E., DEMIR, C. & KUMBASAR, N. 2008. FRP retrofit of low and medium strength circular and rectangular reinforced concrete columns. *Journal of Materials in Civil Engineering*, 20, 169-188.
- IMJAI, T., CHAISAKULKIET, U., GARCIA, R. & PILAKOUTAS, K. 2018. Strengthening of RC members using Post-Tensioned Metal Straps: state of the research. *Lowland Technology International*, 20, 109-118.
- IOANNOU, I., ROSSETTO, T. & GRANT, D. Use of regression analysis for the construction of empirical fragility curves. *Proceedings of the 15th world conference on earthquake engineering*, September, 2012.
- JAIN, S. K. 2005. The Indian earthquake problem. *Current Science*, 89, 1464-1466.
- JALALIAN, M. DERIVATION OF HYBRID VULNERABILITY FUNCTIONS BASED ON OBSERVATIONAL DATA FOR IRAN.
- KAPPOS, A., STYLIANIDIS, K. & PITILAKIS, K. 1998. Development of seismic risk scenarios based on a hybrid method of vulnerability assessment. *Natural Hazards*, 17, 177-192.
- KARABABA, F. S. & POMONIS, A. 2011. Damage data analysis and vulnerability estimation following the August 14, 2003 Lefkada Island, Greece, Earthquake. *Bulletin of Earthquake Engineering*, 9, 1015-1046.
- KARAYANNIS, C. G., CHALIORIS, C. E. & SIRKELIS, G. M. 2008. Local retrofit of exterior RC beam–column joints using thin RC jackets—An experimental study. *Earthquake Engineering & Structural Dynamics*, 37, 727-746.
- KASHANI, M. M., CREWE, A. J. & ALEXANDER, N. A. 2013. Nonlinear cyclic response of corrosion-damaged reinforcing bars with the effect of buckling. *Construction and Building Materials*, 41, 388-400.

- KASHANI, M. M., LOWES, L. N., CREWE, A. J. & ALEXANDER, N. A. 2016. Nonlinear fibre element modelling of RC bridge piers considering inelastic buckling of reinforcement. *Engineering Structures*, 116, 163-177.
- KENNY, C. 2009. Policy Research Working Paper 4823. *Policy*.
- KIRÇIL, M. S. & POLAT, Z. 2006. Fragility analysis of mid-rise R/C frame buildings. *Engineering Structures*, 28, 1335-1345.
- KWON, O.-S. & ELNASHAI, A. 2006. The effect of material and ground motion uncertainty on the seismic vulnerability curves of RC structure. *Engineering structures*, 28, 289-303.
- KYRIAKIDES N. 2007. *Seismic vulnerability assessment of RC structures*. PhD Thesis, UOS, UK.
- KYRIAKIDES, N., AHMAD, S., PILAKOUTAS, K., NEOCLEOUS, K. & CHRYSOSTOMOU, C. 2014. A probabilistic analytical seismic vulnerability assessment framework for substandard structures in developing countries. *Earthquakes and Structures*.
- LAGOMARSINO, S. & GIOVINAZZI, S. 2006. Macroseismic and mechanical models for the vulnerability and damage assessment of current buildings. *Bulletin of Earthquake Engineering*, 4, 415-443.
- LAM, L. & TENG, J. G. 2003. Design-oriented stress–strain model for FRP-confined concrete. *Construction and building materials*, 17, 471-489.
- LANG, K. 2002. *Seismic vulnerability of existing buildings*, vdf Hochschulverlag AG.
- LEE, C.-L. & FILIPPOU, F. C. 2009. Efficient beam-column element with variable inelastic end zones. *Journal of Structural Engineering*, 135, 1310-1319.
- LIEL, A. B. & LYNCH, K. P. 2012. Vulnerability of reinforced-concrete-frame buildings and their occupants in the 2009 L'Aquila, Italy, earthquake. *Natural hazards review*, 13, 11-23.
- LIN, Y.-Y. & LIN, Y.-S. 2009. Non-iterative equivalent linearization based on secant period for estimating maximum deformations of existing structures. *Journal of Earthquake Engineering*, 13, 170-192.
- MA, C. K., AWANG, A. Z., OMAR, W., LIANG, M., JAW, S. W. & AZIMI, M. 2016. Flexural capacity enhancement of rectangular high-strength concrete columns confined with post-tensioned steel straps: experimental investigation and analytical modelling. *Structural concrete*, 17, 668-676.
- MANDER, J. B., PRIESTLEY, M. J. & PARK, R. 1988. Theoretical stress-strain model for confined concrete. *Journal of structural engineering*, 114, 1804-1826.
- MAZZOLANI, F. M. & PILUSO, V. 1997. PLASTIC DESIGN OF SEISMIC RESISTANT STEEL FRAMES. *Earthquake Engineering & Structural Dynamics*, 26, 167-191.
- MAZZONI, S., MCKENNA, F., SCOTT, M. H., FENVES, G. & JEREMIC, B. 2007. OpenSees command language manual. Pacific Earthquake Engineering Research Center. *University of California, Berkeley*.

- MAZZONI, S., MCKENNA, F., SCOTT, M. H. & FENVES, G. L. 2006. OpenSees command language manual. *Pacific Earthquake Engineering Research (PEER) Center*, 264, 137-158.
- MOGHADDAM, H., SAMADI, M. & PILAKOUTAS, K. 2010a. Compressive behavior of concrete actively confined by metal strips, part B: analysis. *Materials and structures*, 43, 1383-1396.
- MOGHADDAM, H., SAMADI, M., PILAKOUTAS, K. & MOHEBBI, S. 2010b. Axial compressive behavior of concrete actively confined by metal strips; part A: experimental study. *Materials and Structures*, 43, 1369-1381.
- MOSALAM, K. M., AYALA, G., WHITE, R. N. & ROTH, C. 1997. SEISMIC FRAGILITY OF LRC FRAMES WITH AND WITHOUT MASONRY INFILL WALLS. *Journal of Earthquake Engineering*, 1, 693-720.
- MOSALLAM, A. S., BAYRAKTAR, A., ELMIKAWI, M., PUL, S. & ADANUR, S. 2014. Polymer Composites in Construction: An Overview. *SOJ Materials Science & Engineering*.
- MUKHERJEE, A. & JOSHI, M. 2005. FRPC reinforced concrete beam-column joints under cyclic excitation. *Composite structures*, 70, 185-199.
- MURRU, M., AKINCI, A., FALCONE, G., PUCCI, S., CONSOLE, R. & PARSONS, T. 2016. $M \geq 7$ earthquake rupture forecast and time-dependent probability for the Sea of Marmara region, Turkey. *Journal of Geophysical Research: Solid Earth*, 121, 2679-2707.
- NEUENHOFER, A. & FILIPPOU, F. C. 1997. Evaluation of nonlinear frame finite-element models. *Journal of structural engineering*, 123, 958-966.
- ORSINI, G. 1999. A model for buildings' vulnerability assessment using the parameterless scale of seismic intensity (PSI). *Earthquake Spectra*, 15, 463-483.
- ÖZERDEM, A. & BARAKAT, S. 2000. After the Marmara earthquake: Lessons for avoiding short cuts to disasters. *Third World Quarterly*, 21, 425-439.
- OZMEN, H., INEL, M., MERAL, E. & BUCAKLI, M. Vulnerability of low and mid-rise reinforced concrete buildings in Turkey. Proceedings of the 14th European conference on earthquake engineering, Ohrid, Macedonia, 2010.
- PARK, Y.-J. & ANG, A. H.-S. 1985. Mechanistic seismic damage model for reinforced concrete. *Journal of structural engineering*, 111, 722-739.
- PINHO, R. & ELNASHAI, A. 2000. Dynamic collapse testing of a full-scale four storey RC frame. *ISET Journal of earthquake Technology*, 37, 143-163.
- PORTER, K., KENNEDY, R. & BACHMAN, R. 2007. Creating fragility functions for performance-based earthquake engineering. *Earthquake Spectra*, 23, 471-489.
- PRIESTLEY, M. J. N. 1997. DISPLACEMENT-BASED SEISMIC ASSESSMENT OF REINFORCED CONCRETE BUILDINGS. *Journal of Earthquake Engineering*, 1, 157-192.

- RAMAMOORTHY, S. K., GARDONI, P. & BRACCI, J. M. 2006. Probabilistic demand models and fragility curves for reinforced concrete frames. *Journal of Structural Engineering*, 132, 1563-1572.
- RAZVI, S. & SAATCIOGLU, M. 1999. Confinement model for high-strength concrete. *Journal of Structural Engineering*, 125, 281-289.
- ROSSETTO, T., D'AYALA, D., IOANNOU, I. & MESLEM, A. 2014. Evaluation of existing fragility curves. *SYNER-G: Typology definition and fragility functions for physical elements at seismic risk*. Springer.
- ROSSETTO, T. & ELNASHAI, A. 2003. Derivation of vulnerability functions for European-type RC structures based on observational data. *Engineering Structures*, 25, 1241-1263.
- ROSSETTO, T. & ELNASHAI, A. 2005. A new analytical procedure for the derivation of displacement-based vulnerability curves for populations of RC structures. *Engineering Structures*, 27, 397-409.
- ROSSETTO, T., IOANNOU, I. & GRANT, D. 2013. Existing empirical fragility and vulnerability relationships: compendium and guide for selection. *Pavia, Italy: GEM Foundation*.
- ROSTI, A., ROTA, M. & PENNA, A. 2018. Damage classification and derivation of damage probability matrices from L'Aquila (2009) post-earthquake survey data. *Bulletin of Earthquake Engineering*, 16, 3687-3720.
- ROTA, M., PENNA, A. & STROBBIA, C. 2008. Processing Italian damage data to derive typological fragility curves. *Soil Dynamics and Earthquake Engineering*, 28, 933-947.
- SABETTA, F., GORETTI, A. & LUCANTONI, A. Empirical fragility curves from damage surveys and estimated strong ground motion. Proceedings of the 11th European conference on earthquake engineering, Paris, France, 1998. 1-11.
- SAMAAN, M., MIRMIRAN, A. & SHAHAWY, M. 1998. Model of concrete confined by fiber composites. *Journal of structural engineering*, 124, 1025-1031.
- SCOTT, M. & HAMUTÇUOĞLU, O. 2008. Numerically consistent regularization of force-based frame elements. *International journal for numerical methods in engineering*, 76, 1612-1631.
- SCOTT, M. H. & RYAN, K. L. 2013. Moment-Rotation Behavior of Force-Based Plastic Hinge Elements. *Earthquake Spectra*, 29, 597-607.
- SEISMO-ARTIF (2018 version). A program process strong-montion data, <http://www.seismosoft.com/seismoartif>.
- SHANNAG, M., BARAKAT, S. & ABDUL-KAREEM, M. 2002. Cyclic behavior of HPFRC-repaired reinforced concrete interior beam-column joints. *Materials and Structures*, 35, 348-356.
- SHINOZUKA, M., FENG, M. Q., LEE, J. & NAGANUMA, T. 2000. Statistical analysis of fragility curves. *Journal of engineering mechanics*, 126, 1224-1231.

- SINGHAL, A. & KIREMIDJIAN, A. S. 1997. *A method for earthquake motion-damage relationships with application to reinforced concrete frames*, National Center for Earthquake Engineering Research Buffalo, NY.
- SPENCE, R. J. S., COBURN, A. W., POMONIS, A., SAKAI, S. & INT ASSOC EARTHQUAKE, E. 1992. CORRELATION OF GROUND MOTION WITH BUILDING DAMAGE - THE DEFINITION OF A NEW DAMAGE-BASED SEISMIC INTENSITY SCALE. *Proceedings of the Tenth World Conference on Earthquake Engineering, Vols 1-10*, 551-556.
- STANDARDIZATION, E. C. F. 2005. Design of structures for earthquake resistance, part 3: Assessment and retrofitting of buildings. *EN 1998-3: 2005*.
- TBEC 2018. Turkish Building Earthquake Code. *Republic of Turkey Prime Ministry Disaster and Emergency Management Authority, Ankara, Turkey*.
- TSIONIS, G., PAPAILIA, A. & FARDIS, M. 2011. Analytical fragility functions for reinforced concrete buildings and buildings aggregates of Euro-Mediterranean regions—UPAT methodology. Internal report, SYNER-G project 2009/2012, SYNER-G Research.
- TSONOS, A.-D. G. 2010. Performance enhancement of R/C building columns and beam-column joints through shotcrete jacketing. *Engineering Structures*, 32, 726-740.
- VAMVATSIKOS, D. & CORNELL, C. A. 2002. Incremental dynamic analysis. *Earthquake Engineering & Structural Dynamics*, 31, 491-514.
- WHITMAN, R. V. 1973. Damage probability matrices for prototype buildings. *Structures Publication*, 380.
- YUSUF, Y., MATSUOKA, M. & YAMAZAKI, F. Detection of building damages due to the 2001 Gujarat, India, earthquake using satellite remote sensing. 7th US National Conf. on Earthquake Engineering, 2002.
- ZHAO, J. & SRITHARAN, S. 2007. Modeling of strain penetration effects in fiber-based analysis of reinforced concrete structures. *ACI Structural Journal*, 104, 133-141.